

# On the analysis tools of turbulent and financial time series

Von der Fakultät für Mathematik und Naturwissenschaften der Carl  
von Ossietzky Universität Oldenburg zur Erlangung des Grades und  
Titles eines Doktors der Naturwissenschaften (Dr. rer. nat.)  
angenommene Dissertation

Amjed Mohammed  
geboren am 6.5.1960 in Bagdad (IRAK)

Oldenburg, June 2007  
Revised, October 2007

Gutachter : Prof. Dr. Joachim Peinke  
Zweitgutachter: Prof. Dr. Alexander Rauh  
Tag der Disputation 18.12.2007

# Contents

<b>Contents</b>	<b>i</b>
<b>Preface</b>	<b>v</b>
<b>Abstract</b>	<b>vii</b>
<b>Zusammenfassung</b>	<b>viii</b>
<b>Acknowledgments</b>	<b>ix</b>
<b>List of Figures</b>	<b>xvi</b>
<b>List of Symbols</b>	<b>xvi</b>
<b>1 Introduction to turbulence</b>	<b>1</b>
1.1 Navier-Stokes equations and averaging . . . . .	1
1.2 Averaging . . . . .	2
1.3 The turbulent kinetic energy equation and the closure problem . . . . .	4
1.4 Direct numerical simulation (DNS) . . . . .	5
1.5 Reynolds-Averaged Navier-Stoke (RANS) Models . . . . .	5
1.6 Boussinesq's Eddy-Viscosity concept . . . . .	8
1.7 Prandtl's Mixing Length Model . . . . .	8
1.8 One Equation Model . . . . .	9
1.9 Discretization, Numerical Grids and Nodes . . . . .	9
1.10 Estimation of the Needed Number of Nodes . . . . .	11

1.11	Space-averaging and Filtering	13
1.12	Large Eddy Simulation (LES)	14
1.13	The LES equations	16
1.14	Subgrid Scales (SGS) Models	17
1.15	Detached-Eddy Simulation (DES)	18
<b>2</b>	<b>Diffusion and the Master Equation</b>	<b>19</b>
2.1	Diffusion	19
2.2	Fick's law	20
2.3	Non-Fickian diffusion and the $\tau$ approximation	23
2.4	The very basic master equation	25
2.4.1	The isotropic case	25
2.4.2	The nonisotropic case	26
2.5	The Kramers equation	28
2.6	Nonlinear Diffusion Equations	29
2.6.1	Burgers' equation	29
2.6.2	Kardar-Parisi-Zhang equation (KPZ)	30
2.6.3	Gravity Waves equation	32
2.7	Testing the programs for conservation	33
2.8	Physical significance and applications	33
<b>3</b>	<b>Dynamical Systems</b>	<b>36</b>
3.1	Time series and Intermittency	36
3.2	Lorenz and Rössler Models	38
3.3	Flare maps and Intermittency	40
3.4	Fractals, multifractals and dimensions	43
3.5	Embedding dimension (ED)	48
3.6	Dimensions reduction	49
<b>4</b>	<b>Statistical Turbulence</b>	<b>52</b>
4.1	Increments and structure functions	52

4.2	The scaling of the structure functions . . . . .	53
4.3	The Kolmogorov 1941 paper (K41) . . . . .	54
4.4	The autocorrelation and the structure function . . . . .	56
4.5	The spectrum regions and the length scales . . . . .	59
4.5.1	The integral length scale ( $L$ ) . . . . .	60
4.5.2	The Taylor microscale ( $\lambda$ ) . . . . .	61
4.5.3	The Kolmogorov scale ( $\eta$ ) . . . . .	63
4.6	The K62 and the intermittency . . . . .	63
4.7	Extended self-similarity (ESS) . . . . .	64
4.8	Dissipation . . . . .	65
4.9	Probability density functions (PDF's) . . . . .	69
<b>5</b>	<b>Financial Diffusion</b>	<b>73</b>
5.1	The DAX index data analysis . . . . .	73
5.2	The Wiener process as a model for financial Data . . . . .	75
5.3	The Karhunen-Lòve decomposition or PCA . . . . .	77
5.4	Itô's process . . . . .	77
5.5	Stationarity and non-stationarity . . . . .	78
5.6	Tools for non-stationary time series . . . . .	79
5.7	Short-Time Fourier Transform (STFT) . . . . .	79
5.8	The Wigner-Ville spectrum . . . . .	81
5.9	Wavelets . . . . .	82
<b>6</b>	<b>Backlook and Outlook</b>	<b>84</b>
<b>A</b>	<b>Exponential Time Differencing</b>	<b>90</b>
<b>B</b>	<b>Various declarations</b>	<b>91</b>
<b>C</b>	<b>Curriculum Vitae</b>	<b>92</b>
<b>D</b>	<b>Erklärung</b>	<b>93</b>

<b>Bibliography</b>	<b>94</b>
<b>Index</b>	<b>104</b>

# Preface

In this thesis we try to detail some methods of modelling the small scales that appear in the Navier-Stokes equations (NSE) which are used to describe the formidable problem of turbulence. This problem dominates the description of the unpredictable movements of many particles in contrast to the movement of one particle or even two or three particles which was already solved in Newtonian physics. The NS equations, which express basic principles of conservation of mass and momentum, were formulated towards the middle of the nineteenth century, and there is a general consensus that turbulence is described by these equations.

On the other hand, there are the Fokker-Planck equation and the Langevin equations which were formulated at the beginning of the twentieth century and they describe the probabilities of the movements of many particles. In short the later are a description of the statistics of turbulence.

Finding the long sought exact solution for the Navier-Stokes equations or even approximations to it means, for example bringing a great improvement in environmental sciences, or faster and more efficient transportation means, or even better predictions for the stokes exchange markets to name but a few. Sometimes turbulence should be avoided for the sake of good aerodynamics or for market stability other times it should be generated artificially for the sake of good mixing. For an exhaustive list see [1].

Examples for the non stationary time series are the global temperature register, which tends to rise year after year and thus the non-stationarity is due to the rising trend. Another important example is the financial markets which has a trend that is time dependent, because of inflation and other conflicting factors. These important family of series need other analysis tools than the ones used to analyze the stationary ones.

Chapter 1 lays down the main themes in turbulence namely the Navier-Stokes equation (NSE), its averaging, and at last finding a closure hypothesis for the modelling of the Reynolds stress tensor. The handling of turbulence here has more to do with high Reynolds number flows which could occur outside boundary layers which

are usually formed near solid surfaces. Also here the main models in turbulence, namely Reynolds-averaged Navier-Stokes (RANS) and large eddy simulation (LES), are analyzed. All the flows that are discussed in this thesis (except for the last chapter) are incompressible and stationary.

Chapter 2 discusses a simplified set of equations of a special case of NSE, the phenomenon underlying these equations is called diffusion. This special case happens when the convective (advective) forces are negligible which means that the viscous forces are important. So the flows take place in the boundary layer and across and are mainly laminar here. Moreover the pressure forces and buoyancy which are usually part of the NSE are neglected here. The main theme in this chapter is examining the connection between the different diffusion equations like Fick's law, Fokker-Planck equation, Burgers equation, just to name a few. A 3dimensional diffusion should actually give the same results that one gets from the Navier-Stokes equation.

Some researchers have connected turbulence to Chaos, but while chaos has few degrees of freedom, turbulence has too many degrees of freedom. Chapter 3 goes through such dynamical systems that exhibit chaotic structures and specifically flare (burst) attractors. The main tools in analyzing dynamical systems, like embedding, correlation dimensions and singular spectrum analysis, has been exhibited here in order to develop some measures that would be useful for later analysis and to understand the role of intermittency in turbulent stationary time series.

Since one is dealing with a huge amount of degrees of freedom in turbulence the need arises to develop an alternative treatment for turbulence based on statistical analysis rather than force-mass Newtonian equations. Thus chapter 4 is dedicated to the mission of examining some of the most important statistical tools for analyzing turbulence like multifractals, the correlation, the spectrum, the probability density function, ...etc.

In chapter 5, we analyze why the tools that were already used in analyzing stationary time series are not useful in analyzing non-stationary time series taking financial time series as the main example for this endeavor. The tools that were looked at were the time-frequency transforms, the Wigner-Ville spectrum and at last wavelets.

The last chapter, chapter 6, is a review of the whole work, discussing the most important results and an outlook at future studies that could be based on the results of this thesis.

# Abstract

The aim of this work is to give a review on some of the important tools used in analyzing time series. Since turbulence turned out to be a rather complex phenomenon, a variety of different models and analysis tools have been devised to simulate, analyze and address the different questions that are raised by the behaviour of these seemingly very erratic, highly chaotic time series that are gained from the natural phenomena or the models that are supposed to simulate these processes whether natural, financial, ... etc. The most part of the work was dedicated to the stationary time series which are gained from laboratory controlled turbulence experiments, for example, or the models that simulate them e.g. the direct numerical simulation. The main models that were dealt with are the large eddy simulation (LES) and the diffusion equation which is a simplified version of the Navier-Stokes equations (NSE). Then there are tools that are used to extract different information from the time series, like the dimensions, e.g. embedding, fractal, correlation, and the statistical tools like the spectrum, autocorrelation, scaling of the structure function. We have shown that these tools do not say a lot about non-stationary time series and that there are another set of tools e.g. the spectrogram, Wigner-Ville spectrum, wavelets, that define more clearly events that have a beginning and an end but the full interpretation of their results needs more research.

# Zusammenfassung

Das Ziel dieser Arbeit ist es, einen Überblick über einige der wichtigsten Instrumente zur Analyse von turbulenten Zeitreihen zu geben. Turbulenz erwies sich bisher als ein recht komplexes Phänomen. Daher sind eine Vielzahl von verschiedenen Modellen und Analysemethoden entwickelt worden. Mit ihrer Hilfe werden die verschiedenen Fragen bearbeitet, die sich aus dem Verhalten der scheinbar sehr sprunghaften, hoch chaotischen Zeitreihen stellen, die von natürlichen Phänomenen oder aus der Modellsimulation solcher Prozesse (natürliche Prozesse, Finanzdaten, usw.) stammen. Die vorliegende Arbeit widmet sich vor allem der Analyse stationärer Zeitreihen aus kontrollierten Turbulenzexperimenten im Labor bzw. den dazugehörigen Modellsimulationen (z.B. direkte numerische Simulation). Die wichtigsten Modelle welche behandelt werden sind die Large Eddy Simulation (LES) und die Diffusions-Gleichung, eine vereinfachte Version der Navier-Stokes-Gleichungen (NSE). Es werden außerdem Analysewerkzeuge vorgestellt, mit deren Hilfe man verschiedene Informationen aus den Zeitreihen extrahieren kann. Beispiele sind die Dimensionen, wie etwa Einbettung, Fraktale, und Korrelation oder statistische Datenanalyse wie Spektrum, Autokorrelation und Skalierung der Struktur-Funktion. In der Arbeit wird gezeigt, dass diese Methoden über instationäre Zeitreihen wenig aussagen, dass es jedoch eine Reihe anderer Methoden wie z.B. das Spektrogramm, das Wigner-Ville-Spektrum oder Wavelets gibt, welche Ereignisse, die einen Anfang und ein Ende haben, klarer beschreiben können. Die vollständige Interpretation ihrer Ergebnisse verlangt jedoch noch weitere Untersuchungen.

# Acknowledgments

The author wishes to thank Professor Peinke and Professor Rauh for their guidance throughout the years. Professor J. Peinke should be accredited for detailing the concepts for Chapter Four. More thanks for Prof. Axel Brandenburg for the very productive two months in NORDITA institute in Copenhagen, which were behind the development of Chapter Two. In addition special thanks for Dr. Malte Siefert, Dr. Stephan Barth, Dr. Matthias Wächter, Andreas Nawroth, Edgar Anahua, Anne Laupichler, Michael Hölling and the rest of the hydrodynamic group of Oldenburg University for their welcoming and their time for discussions. Thanks also to Benno Hubert from the Oldenburg University Computer center for all the support during these long years also Mohammed Ouadi from the computer sciences faculty, Dr. Younis Fathy from the mathematics faculty, and Udo Bonn from the economy faculty.

Many thanks to Prof. Mogens H. Jensen for his declarations on the GOY models which I should have received 3 - 4 years earlier, also to Dr. Horvath Denis, Prof. Joseph McCauley, Peter Toke H. Ahlgren, and all the other attendants of the Geilo 2007 school "Evolution from Cellular to Social Scales" for the interesting discussions which were behind the development of Chapter Five.

More thanks to my parents who telephoned me always from Baghdad to ask about my progress.

I should also thank the scholarships of "Hans-Böckler-Stiftung" from 1998-2002 and then from 2002-2005, "EWE AG" from 2006-2007, and "CeWe Color" from 2006-2007 for financing my study wholly or partially.

At last Almighty God was most generous and helpful to me.

# List of Figures

1.1	<i>A DNS simulation of the NS eq.(1.1) in addition to a diffusion equation of a passive scalar. The size of the grid is <math>256^3</math> and the initial condition is a top hat [33]. The yellow color here represents the passive scalar (the top hat) and the blue colour represents the medium where the passive scalar will disperse (see also appendix B).</i>	6
2.1	<i>1+1 dimensional Fickian diffusion simulation with a Gaussian initial condition according to eq.(2.5) (or equivalently according to eq.(2.15) with the parameter values taken as <math>a = 1</math> and <math>\tau = 6</math>). The interpretation of the colours starting from this figure until the end of the thesis is explained in appendix B. It should also be mentioned that the dependent variable called <math>x</math> in all the figures of this chapter could be a concentration, probability density function, height... etc., as it is defined in the context of the simulated equation.</i>	22
2.2	<i>(a) The non-Fickian diffusion according to eq.(2.12), taking <math>\tau = 10</math> and <math>u = 1</math>. (b) The wave equation according to eq.(2.13) with <math>c = 1</math>.</i>	24
2.3	<i>(a) The nonisotropic Fickian diffusion or simply Fokker-Planck diffusion according to eq.(2.20) with <math>a = 10</math> and <math>\tau = 10</math>. (b) The nonisotropic non-Fickian diffusion or a 2nd order in time Fokker-Planck according to eq.(2.21) with <math>a = 10</math> and <math>\tau = 10</math>.</i>	27
2.4	<i>The Krammers eq.(2.22) with a Gaussian initial condition. The parameters are taken as <math>\gamma = 0.2</math> and <math>\frac{\gamma kT}{m} = 0.2</math>. The vertical axis represents the magnitude of either <math>x</math> or <math>v</math>.</i>	28
2.5	<i>(1+1)dimensional Burgers equation (2.23) with a Gaussian initial condition and <math>c = 0.1</math>.</i>	29
2.6	<i>(1+1)dimensional Kuramoto-Sivashinsky equation (2.27) with a Gaussian initial condition and <math>\nu = \mu = \lambda = 1</math>.</i>	31

2.7	<i>Nonlinear and dispersive propagation of surface waves according to Eq.(2.28) with a Gaussian initial condition. All the parameters were taken equal to one. . . . .</i>	32
2.8	<i>Testing the conservation of the different previous diffusion processes, by calculating the area of the different sections shown on the top of each figure: (a) Fickian diffusion (eq.(2.5)). (b) Non-Fickian diffusion (eq.(2.12)). (c) Fokker-Planck (eq.(2.12)). (d) Nonlinear Fokker-Planck or Burger's (eq.(2.23)). (e) Kuramoto-Sivashinsky (eq.(2.27)). (f) Gravity waves (eq.(2.28)). . . . .</i>	34
3.1	<i>Time series of different signals: (a) Random time series produced from Pareto distribution as in eq. (3.1) (<math>a = 4.9</math>). (b) Flare from eq.(3.6) taking <math>a = 4</math>, <math>b = 1</math>, <math>c = .4</math> and <math>d = 0.6</math>. (c) Flare from eq.(3.7) taking <math>a = 1.5</math>, <math>b = 1.8</math>, <math>c = .9</math> and <math>d = 0.3</math>. (d) Iran Earthquake. (e) Oldenburg's air-tank free-jet experiment. (f) The pulsar GRO. In the inset we show a blowup for a shorter range for the same signal as in the main figure. . . . .</i>	37
3.2	<i>The time series and the phase space for (a) and (b) Lorenz attractor eq.(3.2) taking <math>Pr = 10</math>, <math>Ra = 28</math> and <math>b = 8/3</math>, and (c) and (d) for Rössler attractor eq.(3.3), taking <math>a = 0.2</math>, <math>b = 0.2</math> and <math>c = 10</math>, respectively. . . . .</i>	38
3.3	<i>Changing the initial condition from 1 to 1.0001 produces another orbit for the Lorenz attractor. One notices that a change in the initial condition of only 0.0001, makes the second orbit diverge from the first between 25-30. Using the same parameters as in fig.3.2 . . . . .</i>	40
3.4	<i>Intermittency route to chaos for eq.(3.7). . . . .</i>	41
3.5	<i>Some of the bifurcation diagrams for eq.(3.7) (figures (a) and (b)). Figures (figures (c) and (d)) are for eq. (3.6). . . . .</i>	42
3.6	<i>The time series and phase space of eq. (3.5) and eq. (3.6). In (a) and (b) the time series and the 3D phase space of eq. (3.5) are shown. As for (c), (d), (e), and (f) the time series and the 2D phase space of eq. (3.6) are shown, where in the first two figures the parameter <math>a</math> in the equation was chosen as 3.95 and in the last two figures (e and f) the parameter was equal to 4. The other parameters are of <math>O(1)</math>. . . . .</i>	44

3.7	(a) Koch curve with four stages. Where the first frame on the top LHS represents stage one and the last one on the bottom RHS represents stage four. (b) The development of a multifractal in a random way. Were we start with a rectangular mass with mass $10 \times 1$ and redistribute it according to $n^{\text{stage}}$ . On the top LHS we start with stage zero and end on the RHS with stage 8 where $n=2$ . . . . .	45
3.8	(a) Henon attractor and (b) its correlation dimension. (c) and (d) are the correlation dimension for Lorenz attractor (see eq. (3.2) and fig. 3.2b) for 20,000 points and 60,000 points respectively. . . . .	46
3.9	The correlation dimension of (a) Gaussian distributed data (60k points), (b) Pareto distributed data 60k points ( $ED=1$ ), (c) Pareto distributed data 60k points ( $ED=3$ ), (d) Blamforth attractor (3.5) 20k points on the $r$ -axis ( $ED=3$ ), (e) Blamforth attractor 20k points on the $w$ -axis ( $ED=3$ ), (f) Blamforth attractor 200k points on the $x$ -axis ( $ED=3$ ), (g) Flare eq. (3.6) 60k points on the $x$ -axis ( $ED=3$ ), (h) Flare eq.(3.6) 60k points this time on the $w$ -axis ( $ED=3$ ). . . . .	47
3.10	The embedding of (a) Rössler system eq.(3.3), (b) Blamforth eq.(3.5), (c) and (d) are for Oldenburg's airtank data [118] with the embedding dimensions equal to 3 and 10 respectively. There are no dramatic changes upon increasing the embedding dimension to more than 10. . . . .	49
3.11	PCA for Oldenburg university foto (2-d matrix) showing from (a)-(c) the rank of the matrix used in the approximation. . . . .	50
3.12	Singular spectrum analysis (SSA) for the incremented turbulence data produced in Oldenburg's university airtank. . . . .	51
4.1	A temperature time series showing in (a) a global warming trend. In (b) the time series has been detrended and in (c) the structure function of the same time series in (a) is shown. . . . .	53
4.2	The spectrum of experimental data (the Oldenburg airtank). In the main figure a simple averaging filter was used to filter the original signal (in blue). The filtered signal is in red. Whereas in the inset a convolution was used for the same purpose i.e. filtering and also to show that both filtering techniques give the same result in the inertial range. In both figures the parallel line to the spectrum has $-5/3$ slope. The figure shows also four distinct regions. . . . .	55

4.3	<i>Spectra of different signals. The red represents the filtered signal: (a) Random signal from a Pareto distribution as in eq. (3.1). (b) Flare from eq.(3.7). (c) Flare from eq.(3.6). (d) Iran Earthquake. (e) Wiener process signal. (f) The pulsar GRO. In figures (c, d, e) there are two lines to approximate the spectrum. The upper has a <math>-5/3</math> slope and the one under the spectrum has a slope of <math>-2</math>. The y-axes in these figures is the energy spectrum <math>E(f)</math> and the x-axis is the frequency <math>f</math>.</i>	57
4.4	<i>The autocorrelation function (ACF) (in blue color) of two data sets are shown: (a)the Oldenburg University wind canal dataset [118], and (b) the Grenoble dataset [105]. The inset shows the parabola intersection (the red line) with the x-axis which defines the Taylor microscale. The units of the lags are the tact of the measurements and the ACF is normalized.</i>	61
4.5	<i>Scatter plots showing how the correlation deteriorates until the data becomes zero correlated (random, heat) when the ACF crosses the zero. In fig. (a) the crossing happens at 619 and shows the Oldenburg data [118] and for the RHS fig.(b) the crossing happens at 5542 and it shows Grenoble data [105]. Here the joint PDFs was used instead of the scatter plot and to the same effect.</i>	62
4.6	<i>The scaling of the structure functions of the Oldenburg data. In (a) the y-axis represents the the structure functions from <math>S_1</math> until <math>S_{15}</math> and the x-axis are the increments <math>r</math> as in eq. (4.3). (b) Shows the exponents <math>\zeta_p</math> vs. the orders <math>p = 15</math>.</i>	63
4.7	<i>(a) Shows the ESS for 15 structure functions exponents (for Oldenburg data 125,000 points) with a least square fitted slope (in red color) on a logarithmic scale. (b) The scaling of the structure functions for the ESS case. Shown also the linear K41 (red) and the lognormal (continuous blue).</i>	65
4.8	<i>The ESS scaling until the 20 exponent for 8 million points from Grenoble data showing all scaling models just like before.</i>	66
4.9	<i>The spectrum of (a)the Oldenburg data [118] and (b) Grenoble data [105]. On both one could see the energy spectrum (compare with fig. 4.2) in blue dashed line, which scales as <math>-5/3</math>, and the dissipation spectrum gained from the energy spectrum multiplied by <math>k^2</math> in dark green dotted line and its scaling is <math>1/3</math>. For each figure there are two y-axis the left one belongs to the energy spectrum and the right one to the dissipation spectrum. The x-axis in both figures is the wave number.</i>	67

4.10	<i>The scaling of the dissipative structure functions of the Grenoble data (8 million points) [105]. In (a) the scaling was compared with the lognormal model eq. (4.24) and taking <math>\mu = 0.24</math>. In (b) the dissipation was compared with the <math>\beta</math> model eq. (4.25) and taking <math>\mu = 0.35</math>.</i> . . . . .	69
4.11	<i>The PDF's of (a)the Oldenburg data [118] and (b) Grenoble data [105].</i> . . . . .	70
4.12	<i>PDF's of the Grenoble data [105] and its correlation. The first PDF was taken at the first zero crossing i.e. <math>r_1 = 4197</math>, and the other PDF's are taken at each further crossing. This shows that the PDF's keep its Gaussian distribution (the fact that they fall on each other) as long as the first zero-crossing has been passed.</i> . . . . .	71
4.13	<i>The PDF's of (a) Blamforth's attractor eq.(3.5) which seems that it has a uniform distribution after incrementing. (b) is the PDF of eq. (3.6).</i> . . . . .	72
5.1	<i>(a) Time series of the DAX 16.02-31.12 of the year 2001 [122]. (b) the autocorrelation function (ACF) of the DAX data. (c) Its spectrum and dissipation spectrum. (d) Its PDFs.</i> . . . . .	74
5.2	<i>(a) Time series of a Wiener process (see eq.(5.2)) (b) the autocorrelation function (ACF) of the Wiener time series. (c) Its spectrum. (d) Its PDFs.</i> . . . . .	76
5.3	<i>Singular spectrum analysis (SSA) for the DAX returns data showing the return data and two components.</i> . . . . .	78
5.4	<i>(a) This figure shows an intermittent detrended signal showing random activity in the middle of a sinusoid signal of two frequencies 50 and 100 Hz. (b) The logarithmic Fourier spectrum of the signal (just like in figs. 4.3) and in the inset the normal spectrum showing two peaks at 50 and 100 HZ. (c) The contour of the STFT of the signal. The x-axis represents the time and the y-axis the frequency. (d) 3-Dimensional STFT spectrum. Here again the horizontal-axis represents the time and the axis going into the page the frequency, while the vertical axis represents the amplitude. (e) The logarithmic STFT of the DAX (fig.5.1(a)). The axes are just like in figure (d) above. (f) The STFT of the Wiener process (fig.5.2(a)) and the axis are again just like in figs. (d) and (e).</i> . . . . .	80

5.5	(a) <i>The Wigner-Ville spectrum for a noisy sinusoid of 300 Hz frequency. The vertical axis is the amplitude of the signal and <math>f</math> is the frequency. (b) The contour of the Wigner-Ville spectrum for the same signal. Here too <math>f</math> is the frequency.</i> . . . . .	82
5.6	(a) and (b) <i>An intermittent signal of 30 Hz frequency and its scalogram. (c) and (d) An intermittent signal with 2 frequencies 30 and 300 and its scalogram. (e) and (f) The previous non-stationary signal of the temperature (fig.4.1) and its scalogram. (g) and (h) The DAX index signal and its scalogram. In all the scalograms the x-axis represents time and the y-axis the scaling of the frequency.</i> . . . . .	83

# List of Symbols

$\tilde{u}$	the measured velocity. All quantities with a tilde are measured quantities
$\tilde{p}$	the measured pressure
$\rho$	the density
$\nu$	the kinematic viscosity
$\varphi(x_j, t)$	a measured passive scalar vector
$\overline{\varphi(x_j)}$	the above vector averaged
$\varphi(x_j, t)$	
$\mathcal{W}(\epsilon, \lambda)$	kernel, weighting function and in the last chapter the wavelet
$\otimes$	the convolution
$k$	the turbulent kinetic energy
$s_{ij}$	
<i>DNS</i>	direct numerical simulation
<i>RANS</i>	Reynolds Averaged Navier-Stoke
<i>FDM</i>	Finite Difference Methods
<i>FVM</i>	Finite Volume Methods
<i>FEM</i>	Finite Element Methods
<i>Re</i>	Reynolds number
$\mathcal{G}(x)$	space filter, kernel or weighting function
<i>LES</i>	Large-eddy tensor
<i>DES</i>	detached-eddy simulation
$L_{ij}$	Leonard stress tensor
$c$	concentration
$l_m$	the mean free path
$F$	the flux
$D$	the diffusion constant but is also used as the substansive operator
$\kappa$	the diffusion constant
$P$	the probability
$\gamma$	the friction constant
$k$	Boltzmann's constant and also the wavenumber
<i>KPZ</i>	Kardar-Parisi-Zhang equation

$h$	the fluctuation of the height of the surface
$\lambda$	the growth velocity
$\eta$	white noise
$Pr$	Prandtl number
$Ra$	Rayleigh number
$r$	sensitivity parameter and also as the distance
$d$	the dimension
$RHS$	right-hand-side
$LHS$	left-hand-side
$CD$	the correlation dimension
$ED$	the embedding dimension
$PCA$	principle component analysis
$SSA$	singular spectrum analysis
$SVD$	singular value decomposition
$S_p(r)$	the structure function raised to the power $p$
$E(k)$	energy spectrum
$R_{ij}$	the autocorrelation. Sometimes $R$ is also used as ACF
$ACF$	the autocorrelation function i.e. the normalized autocorrelation
$\omega$	the frequency
$L$	the integral length scale
$\lambda$	Taylor microscale
$\eta$	Kolmogorov microscale
$\epsilon$	the dissipation
$D(k)$	the dissipation spectrum
$W_t$	wiener process
$\mu$	drift
$\sigma$	variance, volatility
$WV_t$	Wigner-Ville spectrum
$w_x$	the wavelet transform

# Chapter 1

## Introduction to turbulence

Some of the characteristics of turbulence are its randomness, nonlinearity, diffusivity, and dissipation, just to name a few.

Saying that turbulence is a random movement does not mean that its distribution is Gaussian, as we will see in later chapters, but rather it is a description of the face of hyperchaos that controls the movements of particles. Its nonlinearity exhibits itself with the eruptions of new motions and structures as long as the movement is sustained and this fact is an indication that the equations that describes turbulence must contain a nonlinear term. Turbulent diffusivity is much more efficient than molecular diffusivity in mixing the constituents of the turbulent object be it velocities, temperatures, chemicals, ...etc. All these velocities, temperatures, chemicals are dissipated as heat or distributed randomly and not any more in big aggregations, swirls (eddies) or whatever, at the end of the process. This indicates that the equations must contain diffusive dissipative terms including the viscosity of the medium.

### 1.1 Navier-Stokes equations and averaging

The Navier-Stokes equation which are assumed to reflect the instantaneous state of a turbulent flow are usually written as

$$\frac{\partial \tilde{u}_i}{\partial t} + \tilde{u}_j \frac{\partial \tilde{u}_i}{\partial x_j} = -\frac{1}{\rho} \frac{\partial \tilde{p}}{\partial x_j} + \nu \frac{\partial^2 \tilde{u}_i}{\partial x_j \partial x_j} , \quad (1.1)$$

and the *continuity* equation

$$\frac{\partial \rho}{\partial t} + \frac{\partial \rho \tilde{u}_i}{\partial x_i} = 0 , \quad (1.2)$$

where  $\tilde{u}$  is the fluid velocity,  $x_j$  is its direction,  $\rho$  the density, and  $\nu$  is the viscosity. The First equation represents the sum of all the forces that could influence the movement of a bulk of fluid while the second one describes the *compressibility* conditions of the fluid.

The usual practice used to reduce the time and length scales to a number that could be dealt with with the existing computers consists of two steps:

- Substituting the Reynolds decomposition in our dynamic equations

$$\tilde{\varphi}(x_j, t) = \bar{\varphi}(x_j) + \varphi(x_j, t) \quad , \quad (1.3)$$

where  $\tilde{\varphi}(x_j, t)$  is used to represent all possible instantaneous quantities whether be it velocity, temperature, concentration, stock-market prices and indexes ...etc,  $\bar{\varphi}(x_j)$  is the mean in time of  $\varphi$  and is defined by

$$\bar{\varphi}(x_j) = \lim_{T \rightarrow \infty} \frac{1}{T} \int_0^T \tilde{\varphi}(x_j, t) dt. \quad (1.4)$$

and at last the quantity  $\varphi(x_j, t)$  represents the fluctuations of the averaged quantity (for a detailed discussion see [9]).

- Averaging: to obtain the equations

$$\frac{\partial \bar{u}_i}{\partial t} + \frac{\partial (\bar{u}_i \bar{u}_j)}{\partial x_j} = -\frac{1}{\rho} \frac{\partial \bar{p}}{\partial x_i} + \nu \frac{\partial^2 \bar{u}_i}{\partial x_j \partial x_i} - \frac{\partial}{\partial x_j} (\overline{u_i u_j}) \quad , \quad (1.5)$$

$$\frac{\partial \bar{u}_i}{\partial x_i} = 0 \quad . \quad (1.6)$$

So upon using the Reynolds decomposition and time averaging we have now an extra term in the equations which is the *correlation*  $\overline{u_i u_j}$ . This extra term is called the Reynolds tensor or stress.

## 1.2 Averaging

An average over the entire volume of fluid gives a space average which is only a function of time. If, on the other hand, we average over all time only, the resulting function depends only upon the position coordinates [5].

In a statistically steady flow, every variable can be written as the sum of an average value and a fluctuation about that value [6] as we have seen in eq.(1.3) and the definition eq.(1.4).

If the flow is unsteady, time averaging cannot be used and must be replaced by ensemble averaging:

$$\bar{\varphi}(x_j) = \lim_{N \rightarrow \infty} \frac{1}{N} \sum_{n=1}^N \varphi(x_j, t) \quad , \quad (1.7)$$

where  $N$  is the number of the members of the ensemble which must be large enough to eliminate the effects of the fluctuations. Whether we use (1.4) or (1.7), it follows that  $\overline{\varphi(x_j)} = 0$ . In the Reynolds-Averaged Navier-Stoke (RANS) models one uses either the time or the ensemble averaging procedures depending on the flow.

If  $f(x_i, t)$  is a function that describes a flow variable with irregular variations from point-to-point and from time-to-time then a more general process is the *convolution* (which will be looked at later):

$$\bar{f}(\lambda, t) = \int_{\epsilon=-\infty}^{\epsilon=+\infty} W(\epsilon, \lambda) f(t - \epsilon) d\epsilon = (W \otimes f) = (f \otimes W) \quad (1.8)$$

where  $\epsilon$  is a parameter of integration with units of time and  $W(\epsilon)$  is a weighting function (called also kernel) with parameter  $\lambda$ . The only restrictions on  $W(\epsilon)$  are that it should be a real function which satisfies the normalization condition:

$$\int_{-\infty}^{+\infty} W(\epsilon, \lambda) d\epsilon \equiv 1. \quad (1.9)$$

The parameter  $\lambda$  is defined by

$$\lambda = \int_{-\infty}^{+\infty} [W(\epsilon)]^2 d\epsilon. \quad (1.10)$$

One could see that equation (1.4) is only a special case of (1.8). A known kernel  $W(\epsilon) = 1/T$  is called the *top hat* function:

$$W(\epsilon) = \begin{cases} \frac{1}{T} & , \quad |\epsilon| \leq \frac{T}{2} \\ 0 & , \quad |\epsilon| > \frac{T}{2} \end{cases} \quad (1.11)$$

For time *smoothing* or filtering (which will be used later) we let  $\epsilon = t - t'$  and we have:

$$\bar{f} = \int_{-\infty}^{\infty} W(t - t') f(t') dt' \quad (1.12)$$

### 1.3 The turbulent kinetic energy equation and the closure problem

Observing Reynolds tensor  $\overline{u_i u_j}$  closely we notice that it is the averaged product of the fluctuations, so it is the averaged turbulent kinetic energy. To get an equation for that first we must subtract eq.(1.5) from eq.(1.1) and then average. We start with substituting the Reynolds composition in eq.(1.1) and then subtract from it eq.(1.5) to get

$$\frac{\partial u_i}{\partial t} + \overline{u_j} \frac{\partial u_i}{\partial x_j} + u_j \frac{\partial \overline{u_i}}{\partial x_j} + u_j \frac{\partial u_i}{\partial x_j} - \frac{\partial}{\partial x_j} (\overline{u_i u_j}) = -\frac{1}{\rho} \frac{\partial p}{\partial x_i} + \nu \frac{\partial^2 u_i}{\partial x_j \partial x_j} . \quad (1.13)$$

This equation describes the development of the small scales dynamics. Multiplying it (eq. (1.13)) by  $u_i$  and averaging one gets

$$\frac{\partial k}{\partial t} + \overline{u_j} \frac{\partial k}{\partial x_j} + \overline{u_i u_j} \frac{\partial \overline{u_i}}{\partial x_j} + \overline{u_i u_j} \frac{\partial u_i}{\partial x_j} - \overline{u_i \frac{\partial}{\partial x_j} (\overline{u_i u_j})} = -\overline{u_i} \frac{1}{\rho} \frac{\partial p}{\partial x_i} + \nu \overline{u_i \frac{\partial^2 u_i}{\partial x_j \partial x_j}} , \quad (1.14)$$

where  $k = \frac{1}{2} \overline{u_i^2}$  is the turbulent kinetic energy. After some simplifications using eqs. (1.2) and eq.(1.6), where the fifth term on the LHS vanishes, and also writing the last term on the RHS as

$$\nu \overline{u_i \frac{\partial^2 u_i}{\partial x_j \partial x_j}} = 2\nu (\overline{\partial x_j (u_i s_{ij})} - \overline{s_{ij} s_{ij}}) , \quad (1.15)$$

where  $s_{ij} = \frac{1}{2} (\frac{\partial u_i}{\partial x_j} + \frac{\partial u_j}{\partial x_i})$  is the fluctuating strain rate [2]. Implementing the above in eq.(1.14) we get

$$\underbrace{\frac{\partial k}{\partial t}}_A + \underbrace{\overline{u_j} \frac{\partial k}{\partial x_j}}_B = - \underbrace{\frac{\partial}{\partial x_j} \left( \frac{1}{\rho} \overline{u_j p} + \frac{1}{2} \overline{u_i u_i u_j} - 2\nu \overline{u_i s_{ij}} \right)}_C - \underbrace{\overline{u_i u_j} \frac{\partial \overline{u_i}}{\partial x_j}}_D - \underbrace{2\nu \overline{s_{ij} s_{ij}}}_E \quad (1.16)$$

where (see [27]):

$A$  is the rate of change of the turbulent (fluctuating) kinetic energy,

$B$  its convective transport,

$C$  the divergence of the transport of turbulent kinetic energy, where we could see here the triple correlation  $\overline{u_i u_i u_j}$  which one gets when one tries to find an extra equation for the Reynolds stresses (*closure problem*) ,

$D$  the production of Reynolds stresses by shear, since it is negative then it represents a loss of mean kinetic energy, in addition to that one could see that it is an interaction term between the Reynolds stress with the mean shear,

$E$  the viscous dissipation [20] [2]. Here too we have a closure problem .

The above procedure will be used again for the diffusion equation.

## 1.4 Direct numerical simulation (DNS)

The DNS is the most exact approach to turbulence. In this method one solves the NS equations without averaging or approximation other than the necessary numerical discretization whose errors can be estimated and controlled. In the DNS the domain on which the computation is performed must be at least as large as the largest turbulent eddy and must also capture all of the kinetic energy dissipation. One can control the external variables in a way that is difficult or impossible to implement in the laboratory. There are several cases in which the results of DNS disagreed with those of experiments and in which the former turned out to be more correct [6].

Fig. 1.1 shows instants of a passive scalar DNS simulation (the whole simulations are found on [31]) of an NSE with the continuity and a diffusion equation for a passive scalar (see next chapter) ([30] and [33]) with the size of  $256^3$  grid points. The simulation was done using the Pencil code [34] and MPI (Message passing interface) on a parallel cluster.

## 1.5 Reynolds-Averaged Navier-Stoke (RANS) Models

Time-averaging any linear term in NS equations gives the identical term for the averaged quantity. But, one gets 2 terms from the quadratic nonlinear term, the product of the average and a covariance:

$$\overline{\tilde{u}_j \tilde{\varphi}} = \overline{(\overline{u_j} + u_j)(\overline{\varphi} + \varphi)} = \overline{u_j} \overline{\varphi} + \overline{u_j \varphi} \quad (1.17)$$

where  $\varphi$  could be the velocity, temperature, enthalpy...etc. The last term is zero

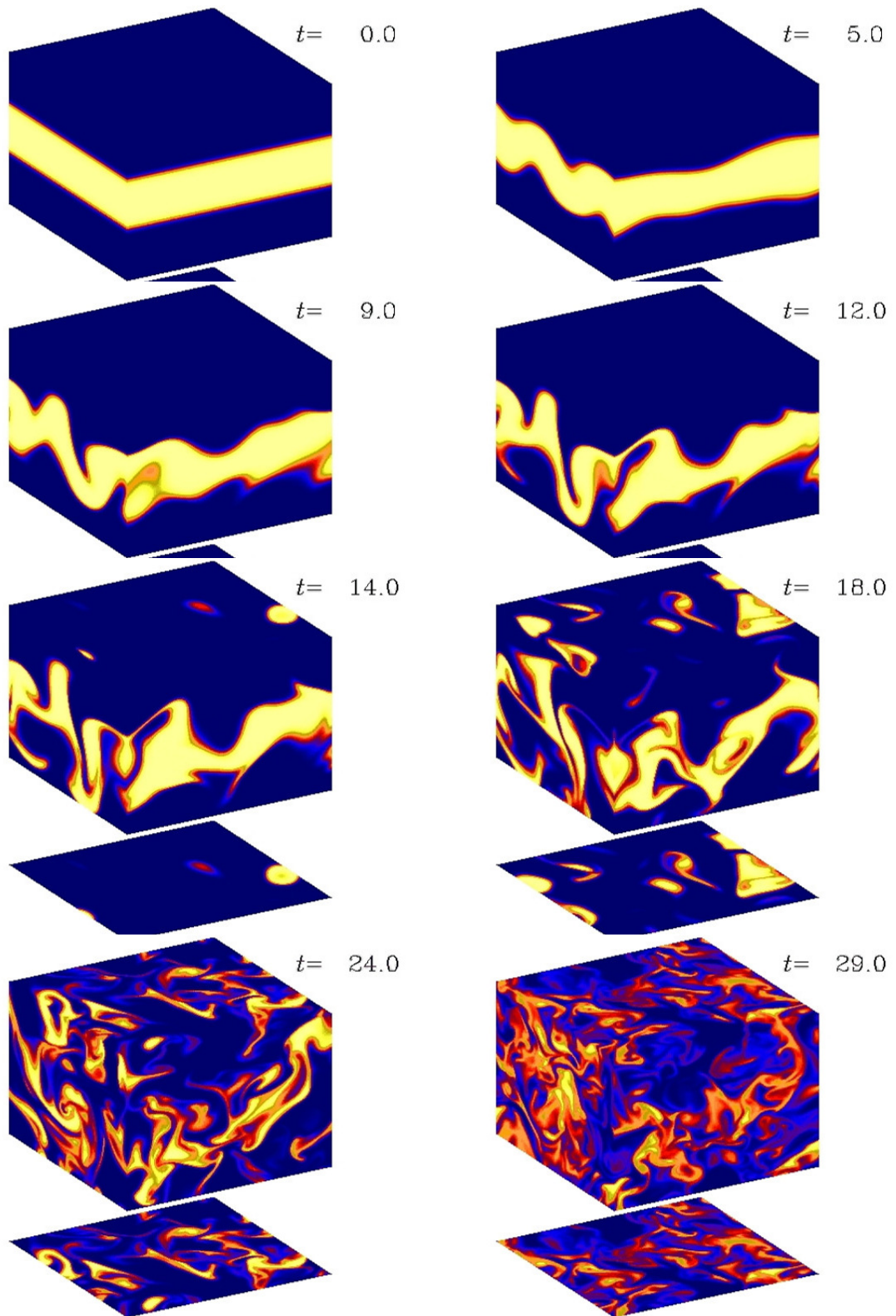


Figure 1.1: A DNS simulation of the NS eq.(1.1) in addition to a diffusion equation of a passive scalar. The size of the grid is  $256^3$  and the initial condition is a top hat [33]. The yellow color here represents the passive scalar (the top hat) and the blue colour represents the medium where the passive scalar will disperse (see also appendix B).

only if the two quantities are uncorrelated; this is rarely the case, and as a result, the averaged NS equations contain quantities like  $\rho \overline{u_i u_j}$ , called the *Reynolds stresses*,  $\rho \overline{u_i \varphi}$ , (the turbulent fluctuation forces).

So we have had one continuity (1.2) equation and three momentum equations (1.1) or four equations in all.

However, after averaging we get for each point in the flow field the following unknown flow variables:

- One mean pressure,  $p$ ;
- Three mean velocity components,  $u_i$ ;
- Six Reynolds stress components

as we see in eqs.(1.5) (1.6) where the Reynolds stress tensor =  $-\rho \overline{u_i u_j}$ , explicitly written in 3 dimensions as

$$-\rho \begin{bmatrix} \overline{u_1^2} & \overline{u_1 u_2} & \overline{u_1 u_3} \\ \overline{u_1 u_2} & \overline{u_2^2} & \overline{u_2 u_3} \\ \overline{u_1 u_3} & \overline{u_2 u_3} & \overline{u_3^2} \end{bmatrix}$$

And this makes a total of 10 unknowns. The difference between the total number of equations and unknowns is 6 and these all come from the above tensor. Finding additional equations to fill this shortage is called *the closure problem*. So one sees from that, that the closure problem appears upon trying to reduce the number of scales that already exist in the NS equations i.e. when one uses averaging techniques to reduce the number of scales. Otherwise, the system of NS equations (without averaging of any kind) is a closed system (4 variables and 4 equations). But there is no analytical solution to this system (eqs. (1.1) and (1.2)), and solving it numerically exceeds the power of the existing computers, as we will detail in one of the next sections.

Thus models were devised to overcome the closure problem in the RANS method (also in the other methods like LES...) , such as:

Name	Number of turbulence equations	Turbulence quantities
Zero equation models	0	None(Prandtl mixing-length model)
One equation models	1	$k$ , turbulent kinetic energy
Two equation models	2	$k$ and $\epsilon$
Stress/flux models	6	$\overline{u_i u_j}$ components

For a review of these models see [12]. Nevertheless we will review some of the

main ideas encountered in zero and one equation models due to their importance.

## 1.6 Boussinesq's Eddy-Viscosity concept

The oldest proposal for modelling the turbulent or Reynolds Stresses  $-\rho\overline{u_i u_j}$  turned out to take the central part of most turbulence models used today. Boussinesq has assumed that in analogy to the viscous stresses in laminar flows, the turbulent stresses are proportional to the mean velocity gradients. This concept may be expressed as

$$-\overline{u_i u_j} = -\frac{2}{3}\overline{u_i^2}\delta_{ij} + \mu_t \left( \frac{\partial \bar{u}_i}{\partial x_j} + \frac{\partial \bar{u}_j}{\partial x_i} \right) \quad (1.18)$$

where  $\mu_t$  is the turbulent viscosity which, in contrast to the molecular viscosity  $\nu$ , is not a fluid property but rather it depends strongly on the state of turbulence (see [27]). So one could close the equations by substituting instead of the Reynolds tensor, eq.(1.18). But then one should know the first term on the RHS, which is the kinetic energy and then inside the turbulent kinetic energy equation there are other quantities that need to be modeled as we have shown previously. In addition to that one should model the turbulent viscosity  $\mu_t$ .

## 1.7 Prandtl's Mixing Length Model

Since the turbulent viscosity dimensions are  $m^2/s$  (where one could see that from (1.18)), one could express it, based on dimensional analysis, as a product of velocity times length

$$\mu_t = C v^* [L] \quad , \quad (1.19)$$

where  $C$  is a dimensionless constant,  $v^*$  the velocity and  $[L]$  is the length. Most of the kinetic energy of turbulence is contained in the largest eddies and the turbulence length scale is therefore characteristic of these eddies which interact with the mean flow. Also the characteristic velocity is connected to the mean flow. Since that the only significant velocity gradient in a two dimensional flow is  $\partial U/\partial y$ , where  $U$  is the velocity scale, then it is dimensionally correct to state that

$$v^* = c l \left| \frac{\partial U}{\partial y} \right| \quad . \quad (1.20)$$

Combining eq.(1.19) with eq.(1.20) and absorbing the product of the two dimensional constants  $C$  and  $c$  into a new length scale  $l_m$  one gets the equation for the *Prandtl mixing length model* [14]

$$\mu_t = l_m^2 \left| \frac{\partial U}{\partial y} \right| \quad (1.21)$$

## 1.8 One Equation Model

Since the velocity scale in the mixing-length model was

$$v^* = l_m \left| \frac{\partial \langle U \rangle}{\partial y} \right| \quad (1.22)$$

The implication is that the velocity scale is locally determined by the mean velocity gradient; and  $v^*$  equals zero when the gradient is zero. But it was seen that there are several cases in which the velocity gradient is zero and yet the turbulent velocity scale is non-zero. Examples are decaying grid turbulence and in the centerline of the round jet [12]. Independently, Kolmogorov and Prandtl suggested that it is better to base the velocity scale on the turbulent kinetic energy  $k$ , i.e.,

$$v^* = c k^{1/2} , \quad (1.23)$$

where  $c$  is an empirical constant. If the length scale is taken again to be the mixing length, then the turbulent viscosity becomes (by using eq. (1.19)) [16]

$$\mu_t = c k^{1/2} l_m . \quad (1.24)$$

The above formula is called the Kolmogorov -Prandtl law.

## 1.9 Discretization, Numerical Grids and Nodes

*Discretization* means the method of approximating the differential equations by a system of algebraic equations for the variables at some set of discrete locations in space and time. In this way this theme is complementary to the theme of modeling turbulence since one has to calculate all the quantities in the previous equations.

There are many discretization methods; some of them are:

- Finite Difference Methods (FD): One starts here with the conservation equation in differential form to cover the solution domain with a *grid*. At each grid point or *node* the differential conservation equation is approximated by replacing the partial derivatives by its approximations (using Taylor expansion or polynomial fitting). In principle this method can be applied to any simple grid type. Its disadvantage is that one could not use it for complex flows [6]. (However, see what is stated below in adaptive grid methods).
- Finite Volume Methods (FV): Here one uses the integral form of the conservation equations. The solution domain is subdivided into control volumes (CV) and the equations are applied to each. The approximation methods are the volume and surface integrals. One could use this method for complex geometries. Its disadvantage compared to FD methods is that methods of order higher than second are difficult to develop in 3D [14].
- Finite Element Methods (FE): The domain is divided into discrete volumes or finite elements that are unstructured. The advantage is that one could use it for arbitrary geometries.
- Spectral Method: The unknowns are approximated by a truncated Fourier series or series of Chebyshev polynomials. Unlike the FD, FE, or FV methods, the approximations here are not local but valid throughout the entire domain (see [23]).
- Other methods: Like boundary element methods, and cellular automata which are used for special classes of problems.

*The numerical grid* is a discrete representation of the geometric domain on which the problem is to be solved. Some of the used grids are:

- Structured (regular) grids: It consists of families of grid lines (these lines need not be orthogonal they could be nonorthogonal) with the property that the lines of a certain family (the  $i$  family for example) do not cross each other but they cross the lines of the other families only once (just like the Cartesian coordinates). These lines do not have to be straight lines just but they could be curves too. This allows the nodes to be numbered consecutively and each position to have a uniquely identified coordinates  $(i, j, k)$
- Block-structured grid: In complex geometries (see ch.8 in [6]) like for example computing the flow around a circular cylinder in a narrow channel one such solution is the block-structured grid. The solution domain is subdivided into several subdomains in such a way that each subdomain can be fitted with a grid.

- Unstructured grids: If one uses the FV or FE method one doesn't need a structured grid. There are coordinate lines that correspond to a constant  $x, y, z$ . This allows maximum flexibility in matching mesh cells with the boundary surfaces and for putting cells where one wants them [21]. Finally we should mention that these grids are generated by specialized programs.
- Adaptive grid: In the unstructured grids method the refinement is done on the subdomains. The purpose from adaptive grid method is to accumulate as much as needed from grid points in those regions of the flow where large gradients in the flow-field properties exist [21].

## 1.10 Estimation of the Needed Number of Nodes

The needed computational power to solve a flow problem could be estimated from the Reynolds number and the needed nodes to cover the solution domain. If one takes  $t_l$  as the *eddy turnover time* or *eddy circulation time* associated with the length scale  $l$  as:

$$t_l \sim \frac{l}{v_l} \quad (1.25)$$

then we could estimate the energy flux by using the above eq. (1.25) as in [101] :

$$Flux = \frac{\text{kinetic energy}}{\text{time}} \sim \frac{v_l^2}{t_l} \sim \frac{v_l^3}{l} . \quad (1.26)$$

Which means that the rate of energy supply to the small-scale eddies is of the order of  $\frac{v_l^3}{l}$ . This energy is dissipated at a rate  $\epsilon$ , which should be equal to the supply rate [1]. Hence

$$\epsilon \sim \frac{v_l^3}{l} . \quad (1.27)$$

Upon taking the eddy turnover time  $t_l \sim \frac{l}{v_l}$  we get upon using eq. (1.27)

$$t_l \sim \epsilon^{-1/3} l^{2/3} . \quad (1.28)$$

For a steady flow of an incompressible fluid with constant velocity, the Navier-

Stokes equations are :

$$\tilde{u}_j \frac{\partial \tilde{u}_i}{\partial x_j} = -\frac{1}{\rho} \frac{\partial \tilde{p}}{\partial x_j} + \nu \frac{\partial^2 \tilde{u}_j}{\partial x_j \partial x_j}. \quad (1.29)$$

From dimensionality considerations one could take the inertia terms as  $U^2/L$  (the left-hand-side of eq. (1.29)), where  $U$  being the characteristic velocity and  $L$  a characteristic length, and estimate in the same way the viscous terms as  $\nu U/L^2$  (the second term on the right-hand-side of eq. (1.29)). At high Reynold numbers the viscous terms survive by choosing a new length scale  $l$  such that the viscous terms are of the same order of magnitude as the inertia terms. Or

$$U^2/L \sim \nu U/l^2 \quad (1.30)$$

which could be reduced to  $U/L \sim \nu/l^2$  and the left-hand-side of eq. (1.30) is equal to  $t_{diff}^{-1}$ , which is the diffusion time. It follows that we get the *Kolmogorov dissipation scale*  $\eta$  upon equating the turnover time (1.28) and the diffusion time, and also exchanging  $l$  with  $\eta$  ( $\epsilon^{-1/3} l^{2/3} = \eta^2/\nu$ ), we obtain

$$\eta \sim \left(\frac{\nu^3}{\epsilon}\right)^{1/4}. \quad (1.31)$$

Substituting (1.27) into (1.31), we obtain [2]

$$l/\eta \sim (\nu_l l/\nu)^{3/4} = Re^{3/4} \quad (1.32)$$

where  $Re$  is the Reynolds number. This means that the number of *nodes* needed to resolve all turbulence scales is  $Re^{3/4}$  which is equal to the ratio of the largest-to-smallest eddy-length scales in one dimension. In 3-dimensions this will rise to  $(Re^{3/4})^3$ . This grid is called *Kolmogorov grid* because  $\Delta = \eta$ . Since a minimum 5-6 points is required to resolve a wavelength  $\lambda$  [11], with the computational time step which accompanies the grid distance, computer-resources requirements rise in proportion to  $(Re^{3/4})^4 = Re^3$ . An estimate of computer requirements arising from this dependence is given in the following table:

Re=	6600	20,000	100,000	$10^6$
N=	$2 * 10^6$	$40 * 10^6$	$3 * 10^8$	$15 * 10^{12}$
T at 150MFlops=	37h	740h	6.5y	3000y
T at 1 TFlops=	20s	400s	8.3h	4000h

where  $N$  is the number of nodes and  $T$  is the time needed for the simulation. To see the meaning of these figures, one could consider an airplane with a 50-meter-long

fuselage and cruising at a speed of 250 meters per second at an altitude of 10,000 meters. One would need  $(10^{16})$  grid points to simulate the turbulence near the surface with reasonable detail. A rough estimate based on current algorithms and software, indicates that even with a supercomputer capable of performing  $(10^{12})$  floating-point operations per second, it would take several thousand years to compute the flow for one second flight time [13].

## 1.11 Space-averaging and Filtering

We have previously looked closely at the averaging in time, it remains to take a look at the other possibility which is averaging in space. One could consider a vicinal space smoothing or filtering process by considering the convolution of  $f(x_i)$  with a space weighting or filtering function (kernel),  $G(x_i)$ . So if we take a 3-dimensional vector, we could write as in equation (1.12) [5]:

$$\bar{f}(\vec{x}, t) = \int_{-\infty}^{+\infty} \int_{-\infty}^{+\infty} \int_{-\infty}^{+\infty} G(\vec{x} - \vec{x}') f(\vec{x}', t) d\vec{x}' . \quad (1.33)$$

The overbar now refers to the spatial, volume-averaged value of  $f(\vec{x})$ , which will be called later the resolved part. The requirements for the space filter  $G(\vec{x})$  are (see also [15]):

- $\int_{-\infty}^{+\infty} \int_{-\infty}^{+\infty} \int_{-\infty}^{+\infty} G(\vec{x}) d\vec{x} \equiv 1$ .
- All moments of  $G(\vec{x})$  exist.
- The width of the filter function  $G(\vec{x})$  is comparable to the shortest resolvable wavelength in the grid on the point  $x_i$ , i.e. the filter width in  $x_i$  is of the order of  $\Delta x_i$ , where the subscript  $i$  indicates that the grid steps does not have to be equidistant in all directions.

As examples for the volume filter functions are:

- The *top hat* or *box* filter : it is defined as (compare with equation 1.11):

$$G(x_i - x'_i) = \begin{cases} \frac{1}{\Delta x_i} & |x_i - x'_i| \leq \Delta x_i/2 \\ 0 & |x_i - x'_i| > \Delta x_i/2 \end{cases} \quad (1.34)$$

for  $i = 1, 2, 3$ .

- The *Gaussian Filter*: Its definition in the x-direction is:

$$G(x_i - x'_i) = \sqrt{\frac{\gamma}{\pi}} \frac{1}{2\Delta x_i} \exp[-\gamma(x_i - x'_i)^2 / (2\Delta x_i)^2]. \quad (1.35)$$

for  $i = 1, 2, 3$  and  $\gamma$  is taken to be equal to 6 [15].

- Spectral or sharp cutoff filter: see [15].

## 1.12 Large Eddy Simulation (LES)

We start with eqs. (1.5) and (1.6) which are in this case space averaged (the bar means in LES space-filtered with one of the above mentioned filters, or averaged quantity). These equations were achieved by decomposing the original velocity exactly as before  $\tilde{u}_i \equiv \bar{u}_i + u_i$  where:

- $\bar{u}_i$  is the filtered, resolvable-scale velocity field, and
- $u_i$  is the subgrid-scale components which should be modelled.

The nonlinear term is expanded:

$$\overline{\tilde{u}_i \tilde{u}_j} = \overline{(\bar{u}_i + u_i)(\bar{u}_j + u_j)} = \overline{\bar{u}_i \bar{u}_j} + \overline{\bar{u}_i u_j} + \overline{u_i \bar{u}_j} + \overline{u_i u_j} \quad (1.36)$$

In contrast to the results obtained in the case of time-averaging (see eq. (1.17) for instance), all the above four terms must be considered and in general:

$$\overline{\bar{u}_k u_l} \neq 0 \quad (1.37)$$

The second, third and fourth terms contain small-scale, non-resolvable components  $u_l$ , and so must be modelled.

Defining the subgrid-scale stresses (SGS) as:

$$\tau_{ij} \equiv \overline{\bar{u}_i u_j} + \overline{u_i \bar{u}_j} + \overline{u_i u_j}. \quad (1.38)$$

The second and the third terms in (1.36) are denoted as  $C_{ij}$  and called the *cross-stress tensor* because they represent the interactions between large (grid) and small (subgrid) scales. The term  $\overline{\bar{u}_i \bar{u}_j} = R_{ij}$  is the Reynolds stress that we have seen in the RANS formulation and reflects the interactions between the subgrid scales [15]. Equation (1.38) is also written as:

$$\tau_{ij} \equiv \overline{\tilde{u}_i \tilde{u}_j} - \overline{\bar{u}_i \bar{u}_j} \quad (1.39)$$

The second term in (1.39) poses a difficulty in simulation since it means that one should apply the filter two times. The above is called *double decomposition* in contrast to the *triple decomposition* which follows. A number of solutions have been found to remedy this difficulty, two of them are:

- Deardorf-Schumann: They take  $\bar{u}_i$  as constant within each control volume. This means that  $\overline{\bar{u}_i \bar{u}_j} = \bar{u}_i \bar{u}_j$  and  $\bar{u}_i \equiv 0$ . Thus  $\tau_{ij} = \overline{u_i u_j}$  and the LES equations are again identical to the RANS equations [15].
- Leonard stress tensor  $L_{ij}$ : It represents the interaction between the large scales. The decomposition that Leonard, also called the *triple decomposition* as indicated above, has proposed is:

$$\begin{aligned} \overline{u_i u_j} &= (\overline{\tilde{u}_i \tilde{u}_j} - \bar{u}_i \bar{u}_j) + \bar{u}_i \bar{u}_j \\ &= L_{ij} + \bar{u}_i \bar{u}_j \end{aligned} \quad (1.40)$$

In this case the subgrid stress is obtained by joining eqs. (1.36), (1.38) and (1.40):

$$\begin{aligned} \tilde{\tau}_{ij} &= \overline{\tilde{u}_i \tilde{u}_j} - \bar{u}_i \bar{u}_j \\ &= L_{ij} + C_{ij} + R_{ij} \ , \end{aligned} \quad (1.41)$$

where the Reynolds tensor is now  $R_{ij} = \overline{\tilde{u}_i \tilde{u}_j}$  and it is just like before, i.e. the correlation between the fluctuations of two quantities, and which could be seen as the last term in eq.(1.5). But, the symbol  $\tilde{\tau}_{ij}$  is now used for a different quantity than  $\tau_{ij}$  which has been defined in (1.38).

An approximation method to estimate  $L_{ij}$  using the Taylor series expansion and a Gaussian filter gives, for the isotropic Gaussian filter with effective filter width  $\Delta x_k$  (see [5], [7] and [8]):

$$L_{ij} = \frac{(\Delta x_k)^2}{6} \frac{\partial^2 (\bar{u}_i \bar{u}_j)}{\partial x_k \partial x_k} + H.O.T. \quad (1.42)$$

It was calculated that for high Reynolds number flows, the Leonard stress accounts for about 14 percent of the total computed energy transfer from the large eddies to the SGS [17].

The cross term could be written as [22]

$$C_{ij} = \frac{(\Delta x_k)^2 \bar{u}_i}{24} \frac{\partial^2 \bar{u}_j}{\partial x_k \partial x_k} - \frac{(\Delta x_k)^2 \bar{u}_j}{24} \frac{\partial^2 \bar{u}_i}{\partial x_k \partial x_k} \quad (1.43)$$

Accordingly one substitutes instead of the advection terms the term:

$$\frac{\partial}{\partial x_j} (\bar{u}_i \bar{u}_j + L_{ij}) \quad (1.44)$$

with (1.42) used to calculate  $L_{ij}$ .

- Germano decomposition: which is a generalization of the Leonard decomposition (see [15]).

### 1.13 The LES equations

The space-filtered NS momentum conservation equations with the double decomposition equation (1.39) will be

$$\frac{\partial \bar{u}_i}{\partial t} + \frac{\partial(\bar{u}_i \bar{u}_j)}{\partial x_j} = -\frac{1}{\rho} \frac{\partial \bar{p}}{\partial x_i} + \nu \frac{\partial^2 \bar{u}_i}{\partial x_j \partial x_i} - \frac{\partial \tau_{ij}}{\partial x_j}. \quad (1.45)$$

where  $\tau_{ij}$  is as in equation (1.38) and the bar means in this case space averaging and not time or ensemble averaging. Where the cross-terms are calculated using the approximation (1.43) or these terms are dropped away using the Schumann-Deardorf previous approximation and we have again  $\tau_{ij} = R_{ij}$ . In addition to that we have on the LHS the first term from eq. (1.36).

Considering the Leonard tensor we obtain the other LES equation by using (1.36), (1.38), and (1.40) (or simply eq. (1.41)) we get [18]:

$$\frac{\partial \bar{u}_i}{\partial t} + \frac{\partial(\bar{u}_i \bar{u}_j)}{\partial x_j} = -\frac{1}{\rho} \frac{\partial \bar{p}}{\partial x_i} + \nu \frac{\partial^2 \bar{u}_i}{\partial x_j \partial x_i} - \frac{\partial \tilde{\tau}_{ij}}{\partial x_j}. \quad (1.46)$$

where  $\tilde{\tau}_{ij}$  is as in (1.41).

By modelling  $\tilde{\tau}_{ij}$  the trace terms are removed from the SGS tensor and added to the pressure because they are normal stresses, so that  $\tilde{\tau}_{ij}$  and  $\bar{p}$  are replaced by [19]:

$$T_{ij} = \tilde{\tau}_{ij} - \frac{1}{3} \sum_{\ell=1}^n \tau_{\ell\ell} \delta_{ij} \quad \text{and} \quad \bar{P} = \bar{p} + \frac{1}{3} \sum_{\ell=1}^n \tau_{\ell\ell}. \quad (1.47)$$

And the above equation (1.46) after considering (1.47) could be written in dimensionless form as

$$\frac{\partial \bar{u}_i}{\partial t} + \frac{\partial(\bar{u}_i \bar{u}_j)}{\partial x_j} = -\frac{\partial \bar{P}}{\partial x_i} - \frac{\partial L_{ij}}{\partial x_j} - \frac{\partial C_{ij}}{\partial x_j} - \frac{\partial R_{ij}}{\partial x_j} + \frac{1}{Re} \frac{\partial^2 \bar{u}_i}{\partial x_j \partial x_i} \quad (1.48)$$

But using the Deardorf-Schumann criterion we get a third LES equation which looks like the previous RANS equation (1.5) with the exception that the averaging is space and not time averaging. This criterion was indeed implemented in the program FLOWSI which was developed by Dr. Claus Wagner in DLR (Deutsches Zentrum für Luft- und Raumfahrt).

## 1.14 Subgrid Scales (SGS) Models

Now that we know how to model the Leonard stress (see equation (1.42)) we need to model the cross stress tensor  $C_{ij} = \overline{u_i \bar{u}_j} + \bar{u}_i \bar{u}_j$  and the Reynolds stress tensor  $R_{ij} = \overline{u_i u_j}$ . Some of the used models are:

- Smagorinsky model: It is the first approach (1963) to model these quantities. This model is an adaptation of Prandtl's mixing-length theory. He assumed that the eddy viscosity is proportional to a scale characteristic of turbulence (mixing length) times a characteristic turbulent velocity. In the same way, Smagorinsky assumed that the eddy viscosity is proportional to the subgrid-scale characteristic length scale  $\Delta$ , and to a characteristic subgrid-scale velocity [25]:

$$v_\Delta = \Delta |\bar{S}| \quad (1.49)$$

where  $|\bar{S}| = \sqrt{2S_{ij}S_{ij}}$  and  $S_{ij} = \frac{1}{2} \left( \frac{\partial \bar{u}_i}{\partial x_j} + \frac{\partial \bar{u}_j}{\partial x_i} \right)$ . Equivalently one could write [19]

$$C_{ij} + R_{ij} \simeq -2\nu_t \bar{S}_{ij} \quad (1.50)$$

where

$$\nu_t = (C_s \Delta)^2 |\bar{S}| \quad (1.51)$$

If one assumes that the cut-off wavenumber  $k_c = \pi/\Delta$  lies within a  $k^{-5/3}$  Kolmogorov cascade  $E_k = C_K \epsilon^{2/3} k^{-5/3}$ , then the constant  $C_s$  is

$$C_s = \frac{1}{\pi} \left( \frac{3C_K}{2} \right)^{-3/4} \quad (1.52)$$

It yields  $C_s \approx 0.18$  for  $C_K = 1.4$ . The researchers prefer to use  $C_s = 0.1$ . And equation (1.46) will look like:

$$\frac{\partial \bar{u}_i}{\partial t} + \frac{\partial}{\partial x_j} (\bar{u}_i \bar{u}_j + L_{ij}) = -\frac{1}{\rho} \frac{\partial \bar{P}}{\partial x_i} + \frac{\partial}{\partial x_j} \left[ (\nu + \nu_t) \left( \frac{\partial \bar{u}_i}{\partial x_j} + \frac{\partial \bar{u}_j}{\partial x_i} \right) \right]. \quad (1.53)$$

It will look like the following in dimensionless form

$$\frac{\partial \bar{u}_i}{\partial t} + \frac{\partial}{\partial x_j} (\bar{u}_i \bar{u}_j + L_{ij}) = -\frac{\partial \bar{P}}{\partial x_i} + \frac{\partial}{\partial x_j} \left[ \left( \frac{1}{Re} + \nu_t \right) \left( \frac{\partial \bar{u}_i}{\partial x_j} + \frac{\partial \bar{u}_j}{\partial x_i} \right) \right]. \quad (1.54)$$

- Structure function models: see [25]

## 1.15 Detached-Eddy Simulation (DES)

Due to the discrepancy that the LES exhibits near the walls, a hybrid technique has been first proposed by Spalart et al in 1997 [24]. DES reduces to a RANS treatment with a modified one equation model (Spalart-Almaras model 1992 [12]) near boundaries (in the so to say the attached eddies or region) and LES away from the wall (in the detached region or eddies) with a seamless transition between the two regions. DES combines the strengths of RANS and LES in a non-zonal manner to treat separated flows (for example flows over airfoils) at high Reynolds numbers.

## Chapter 2

# Diffusion and the Master Equation

When large ensembles of particles, molecules, bacteria, defects, dislocations, fractures, ...etc move from one place to another or interact with each other in a way dependent on their initial concentrations, their velocity fields and potentials, e.g. electrical, magnetic, chemical, ...etc, that exist in their environment, it is often possible to describe the spatio-temporal patterns that these movements produce with linear and nonlinear diffusion processes. The final result of describing the turbulent mixing with the NS Eq., and with the diffusive mixing with the equations of this chapter is the same, but the physical mechanisms are very different. In turbulence the transport of materials through the physical domain is the more dominant part than the molecular diffusion represented by the second term on the RHS of eq. (1.1). Indeed if the factor of this term, which is the viscosity  $\nu$  is small enough then we get a turbulent flow but if it is large then we get diffusion and molecular diffusion and the flow will be called laminar.

The development of the equations of diffusion in this chapter has the intention of highlighting the importance of not only using the actual physical conditions in a problem to model it but also to use more abstract constructions like the master equations.

### 2.1 Diffusion

Watching a drop of passive tracer (ink or even heat as long as buoyancy have minor effects) diffusing in another solution, one notices that the distribution of the concentration of the passive scalar changes depending on the distance from the center of the drop. The case described here is called Brownian motion or molecular diffusion since the diffusion happens due to the molecules movement themselves because of

their thermal energy and not due to the advection of the fluid. From this simple observation one could write immediately the following equation [26])

$$\tilde{c}(x+a) - \tilde{c}(x) = l_m \frac{\partial \tilde{c}}{\partial x} , \quad (2.1)$$

where  $\tilde{c}$  is the concentration of the tracer, and  $l_m$  is the distance traveled by the molecules (the mean free path) and  $x$  is in the direction of the gradient of the tracer. This reasoning was used by Prandtl as we have seen before in his mixing length hypotheses. At this stage we need to define another quantity: the flux which is the mass of the substance  $\Delta M$  passing an area element  $A$  during a time interval  $\Delta t$ , or

$$F = \frac{\Delta M}{A \Delta t} .$$

The net flux could be written as  $F = u_1 \tilde{c}_1 - u_2 \tilde{c}_2$  which describes the movement with two different velocities  $u_1$  and  $u_2$  between two zones of different concentrations  $\tilde{c}_1$  and  $\tilde{c}_2$ . One could check easily that both definitions of the flux and the net flux are by dimensional analysis the same and there unit is  $Kg.s^{-1}.m^{-2}$ . The velocities  $u_1$  and  $u_2$  are taken as equal (hereafter will be written as  $\tilde{u}$ ) since the motion is Brownian and the movement is isotropic . From the above discussion and eq.(2.1) we get

$$\tilde{F} = \tilde{u} (\tilde{c}(x+l_m) - \tilde{c}(x)) = -\tilde{u} l_m \frac{\partial \tilde{c}}{\partial x} . \quad (2.2)$$

## 2.2 Fick's law

Equation (2.2) could be written in 3-dimensions as

$$F = -D \nabla \tilde{c} , \quad (2.3)$$

where  $D = \tilde{u} l_m$  is called the *diffusion constant* and has the units of  $[L^2/T]$  where  $L$  denotes the length and  $T$  the time scales. Equation (2.3) is called *Fick's law* . This equation is also called the *heat equation* or *Fourier's equation* depending on the nature of the dependent variable.

Using the principle of conservation of mass [27] one could derive another useful equation from transport considerations. Since the current (or the total flux) leaving a control volume is equal to

$$I(t) = \int_A F.n.dA = \int_V F.dV ,$$

where  $I(t)$  is the current,  $F$  the flux,  $n$  a vector perpendicular to the control volume and in the direction of the flux,  $A$  the area of the control volume, and  $V$  is the volume. The second step in the above equation has been obtained upon using the divergence theorem. In addition to the above definition of the current, it is also defined as  $\partial\tilde{c}/\partial t$  (in electricity it is  $\partial Q/\partial t$  where  $Q$  is the electrical charge). From both definitions we get

$$\int_A \left( \frac{\partial\tilde{c}}{\partial t} + \nabla F \right) dV = 0 \quad ,$$

which yields

$$\frac{\partial\tilde{c}}{\partial t} = -\nabla F \quad , \quad (2.4)$$

which is the previous continuity equation (see eq. (1.2)). Substituting (2.3) in (2.4) we get the diffusion equation (*Fickian diffusion*)

$$\frac{\partial\tilde{c}}{\partial t} = D \Delta\tilde{c} \quad . \quad (2.5)$$

When there is a laminar convection in the flow, then Fick's law is written as

$$F = \tilde{u}\tilde{c} - D \nabla\tilde{c}$$

and (2.4) will be

$$\frac{\partial\tilde{c}}{\partial t} = -\nabla(\tilde{u}\tilde{c} - D\Delta\tilde{c})$$

and in this shape it is called the *diffusion advection equation*. Alternatively, it can be written with the substantive operator  $D = \frac{\partial}{\partial t} + \tilde{u}\cdot\nabla$  as (where the previously mentioned diffusion constant  $D$  has been changed to  $\kappa$  just to avoid confusion)

$$\frac{D\tilde{c}}{Dt} = \kappa \Delta\tilde{c} \quad . \quad (2.6)$$

A (1+1) dimensional simulation for the Fickian diffusion, as in Eq.(2.5) is shown in Fig. 2.1. The figure shows clearly the contours of the diffused zones.

A spectral discretization method with 2048 nodes and periodical boundary conditions, was used. The spectral method was chosen due to its high accuracy instead of the finite difference methods (see [30] and [37]). This spectral method will be used for all the simulations in this chapter unless otherwise is mentioned. In addition to the above, it should also be mentioned that the dispersion relation,

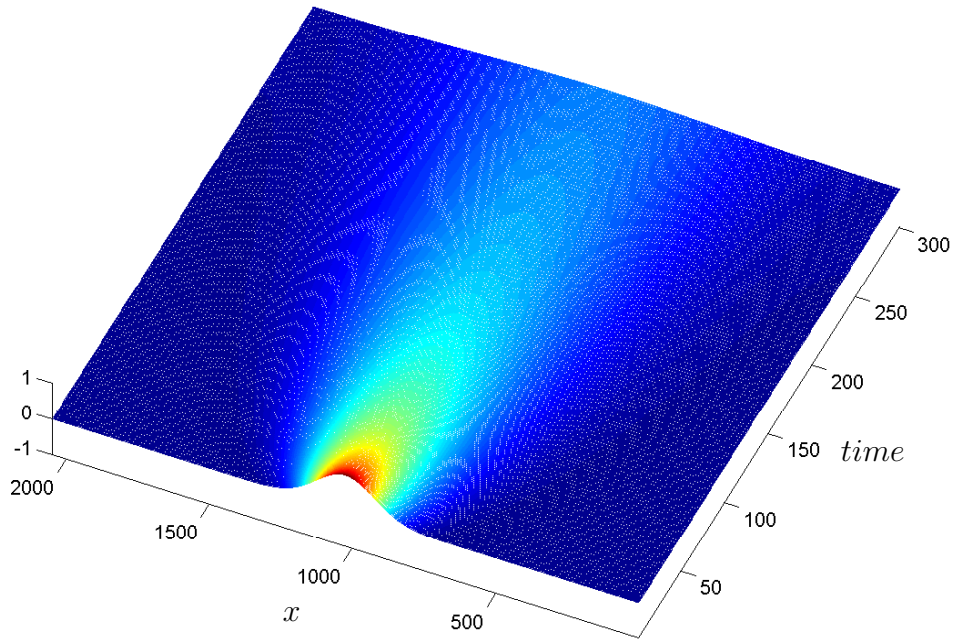


Figure 2.1:  $1+1$  dimensional Fickian diffusion simulation with a Gaussian initial condition according to eq.(2.5) (or equivalently according to eq.(2.15) with the parameter values taken as  $a = 1$  and  $\tau = 6$ ). The interpretation of the colours starting from this figure until the end of the thesis is explained in appendix B. It should also be mentioned that the dependent variable called  $x$  in all the figures of this chapter could be a concentration, probability density function, height... etc., as it is defined in the context of the simulated equation.

which is gained through the von Neumann Ansatz  $u = u_0 e^{i(kx - \omega t)}$ , has been used in the simulations instead of the actual differential equation. This choice was made because of the fact that showing the development of the wave numbers  $k$  in time is analogous to showing the development of the dimensions in physical space. In any case the solution is just substituting the dispersion relation in the above mentioned Ansatz.

## 2.3 Non-Fickian diffusion and the $\tau$ approximation

Now, using the Reynold's decomposition (1.4) in (2.4)

$$\partial_t \tilde{c} = -u \nabla \bar{c} - u \nabla c , \quad (2.7)$$

where  $\tilde{c} = \bar{c} + c$ ,  $\bar{c}$  is the mean concentration and  $c$  is the fluctuation. Upon averaging (2.7) we get

$$\partial_t \bar{\tilde{c}} = -\overline{u \nabla \bar{c}} - \overline{u \nabla c} \quad (2.8)$$

and here we are again with the tensor  $\overline{u \nabla c}$  which is as problematic as the Reynolds tensor  $\partial_{x_j} \overline{u_i u_j}$  which we met in (1.5) and we will have to search for a closing solution .

One way to find a closing solution is by using the same procedure in section (1.3) another alternative is to use an improved Eulerian approach [29]. By subtracting (2.8) from (2.7) we will have terms that represent the departure of the concentration from its average i.e. the fluctuations

$$\partial_t c = \partial_t \tilde{c} - \partial_t \bar{\tilde{c}} = -u \nabla \bar{c} - u \nabla c + \overline{u \nabla \bar{c}} + \overline{u \nabla c} . \quad (2.9)$$

Taking the time derivative of (2.8) we obtain

$$\partial_{tt} \bar{\tilde{c}} = -\partial_t (\overline{u \nabla c}) = -\overline{(\partial_t u) \nabla c} - \overline{u \nabla (\partial_t c)} . \quad (2.10)$$

Taking the last term from the above equation (2.10) and substituting (2.9) in it we then have

$$-\overline{u \nabla \partial_t c} = \overline{u_i u_j \partial_i \partial_j \bar{c}} + \overline{u_i \partial_i v_j \partial_j c} + \overline{u \nabla (u \nabla) c} . \quad (2.11)$$

Using homogeneity and isotropy simplifications with the equation of motion  $\partial_t u = -u \cdot \nabla u - \nabla p$ , the terms either vanish or they are turned to triple correlations . Combining the triple correlations together and using the double correlation divided by a relaxation time  $\tau$  to represent them in the equation is what is called a  $\tau$  approximation (for more details see [29] and [33]). The final result will be

$$\partial_{tt} \bar{\tilde{c}} + \partial_t \bar{\tilde{c}} / \tau - \frac{1}{3} \overline{u^2} \Delta \bar{\tilde{c}} = 0 . \quad (2.12)$$

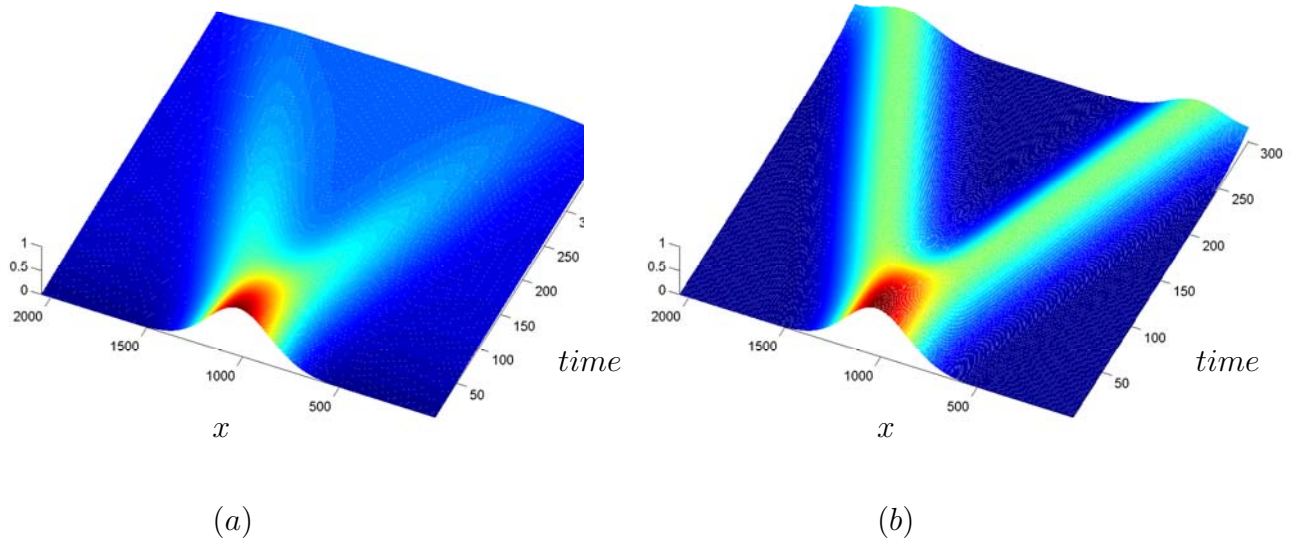


Figure 2.2: (a) The non-Fickian diffusion according to eq.(2.12), taking  $\tau = 10$  and  $u = 1$ . (b) The wave equation according to eq.(2.13) with  $c = 1$ .

The above equation (2.12) is called the *non-Fickian diffusion equation* (see [28], [33] and [29]).

One notices its similarity with the wave equation

$$\partial_{tt}\varphi - c^2 \partial_{xx}\varphi = 0 \quad , \quad (2.13)$$

where  $\varphi$  is the wave amplitude and  $c$  is the wave velocity in this case. The difference between the non-Fickian diffusion equation and the wave equation is only the term  $\partial_t \bar{c}/\tau$  which is clearly a damping term of the type  $kv$  found in harmonic oscillators. Indeed eq.(2.12), as a PDE (partial differential equation), is similar to the *damped harmonic oscillator* equation. That is why one could call the non-Fickian diffusion a damped wave. Indeed examining Fig.2.2(b) closely will show, first the two solutions of the wave Eq. simulation clearly and second that they don't lose their intensity. While in Fig.2.2(a) they are blurred and damped and because of that they lose their intensity after a while until they vanish (dissipate). Moreover, increasing the order of the expansion to 8th. order in space will cause the complete disappearance of the wave-like effect of the two branches and we retain again the classical diffusion shape of Fig.2.1. The same parameters have been used in both simulations including the Gaussian initial condition.

## 2.4 The very basic master equation

One of the simplest master equations which describe the movement of a particle to the left and the right could be written as [39]

$$P(x, t + \tau) = p * P(x + a, t) + q * P(x - a, t) , \quad (2.14)$$

where  $P(x, t + \tau)$  is the probability of finding the particle in position  $x$  and at time  $t + \tau$ ,  $p * P(x + a, t)$  is the probability that the particle was in position  $x + a$  at time  $t$  multiplied by the transition matrix  $p$ , and at last the term  $q * P(x - a, t)$  says that the particle comes from the opposite direction with  $q$  as its transition matrix. If  $p = q = 1/2$  then we say that the flow is isotropic .

### 2.4.1 The isotropic case

The master equation in this case is as we have stated before

$$P(x, t + \tau) = 1/2 * P(x + a, t) + 1/2 * P(x - a, t) . \quad (2.15)$$

Taylor expanding both sides in 1st order in time and 2nd order in space and using the convention  $P_t$  to mean  $\partial P / \partial t$ , we obtain

$$\begin{aligned} P(x, t) + \tau P_t(x, t) &= \left[ \frac{1}{2} P(x, t) + \frac{1}{2} a P_x(x, t) + \frac{1}{4} a^2 P_{xx}(x, t) \right] \\ &+ \left[ \frac{1}{2} P(x, t) - \frac{1}{2} a P_x(x, t) + \frac{1}{4} a^2 P_{xx}(x, t) \right] . \end{aligned} \quad (2.16)$$

Canceling similar terms and simplifying we get

$$P_t(x, t) = \frac{a^2}{2\tau} P_{xx}(x, t) . \quad (2.17)$$

We notice that this Eq. (2.17) is the same as Eq. (2.5) and more than that the term  $a^2/2\tau$  has the units of  $L^2/T$  and thus it resembles the diffusion constant  $D$  in Eqs. (2.3) and (2.5). One concludes that, indeed an isotropic diffusion, according to this basic master eq., is a Fickian diffusion .

Now, we expand both sides of Eq. (2.15) in 2st order in time and 2nd order in space and get

$$\begin{aligned}
P(x, t) + \tau P_t(x, t) + \frac{\tau^2}{2} P_{tt}(x, t) &= \left[ \frac{1}{2} P(x, t) + \frac{1}{2} a P_x(x, t) + \frac{1}{4} a^2 P_{xx}(x, t) \right] \\
&+ \left[ \frac{1}{2} P(x, t) - \frac{1}{2} a P_x(x, t) + \frac{1}{4} a^2 P_{xx}(x, t) \right] . \quad (2.18)
\end{aligned}$$

Upon canceling similar terms and simplifying we get (see also [35] and [36])

$$P_{tt}(x, t) + \frac{2}{\tau} P_t(x, t) - \frac{a^2}{2\tau^2} P_{xx}(x, t) = 0 . \quad (2.19)$$

Comparing the above Eq. (2.19) with Eq. (2.12) repeated here for convenience

$$\partial_{tt}\bar{c} + \partial_t\bar{c}/\tau - \frac{1}{3}u^2\Delta\bar{c} = 0 \quad (2.12)$$

We notice the similarity between them, to the extent that even the factor  $u^2$  corresponds to the factor  $a^2/\tau^2$  where both have the same units  $[L^2/T^2]$ .

## 2.4.2 The nonisotropic case

Keeping the shape of the original master eq. as is, namely

$$P(x, t + \tau) = p * P(x + a, t) + q * P(x - a, t) \quad (2.14)$$

expand it in 1st. order in time and 2nd. order space, cancel similar terms, make  $p + q = 1$  to normalize the transition probability and at last divide by  $\tau$ , we obtain

$$P_t(x, t) = \frac{a}{\tau}(-p + q) P_x(x, t) + \frac{1}{2\tau} a^2 P_{xx}(x, t) . \quad (2.20)$$

We see that if  $p = q = 1/2$  as in the isotropic case we retrieve the diffusion eq.(2.5). The above equation (2.20) is the linear *Fokker-Planck eq.* also called a forward and backward Kolmogorov Eq. (see [40], [41] or [42]) depending on the sign of the factor  $(-p + q)$ , whether it is positive or negative. Indeed one notices that the coefficient of the first term on the right hand side of the eq.  $a/\tau$  has the units of  $[L/T]$  which makes it with the term  $(-p + q)$  a drift coefficient and the units of the coefficient of the second term is  $[L^2/T]$  and these are the units that we have seen before for a diffusion coefficient.

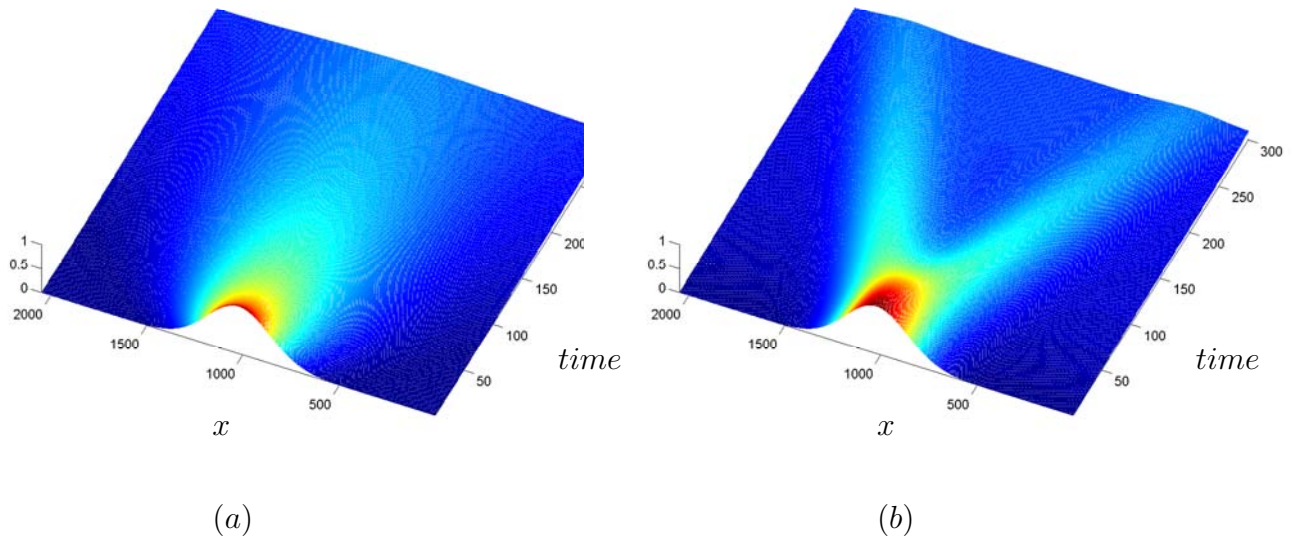


Figure 2.3: (a) The nonisotropic Fickian diffusion or simply Fokker-Planck diffusion according to eq.(2.20) with  $a = 10$  and  $\tau = 10$ . (b) The nonisotropic non-Fickian diffusion or a 2nd order in time Fokker-Planck according to eq.(2.21) with  $a = 10$  and  $\tau = 10$ .

Now expanding Eq.(2.14) in 2nd. order in time and as before 2nd. order in space we obtain the non-Fickian Fokker-Planck eq. written as

$$P_{tt}(x, t) + \frac{2}{\tau}P_t(x, t) - \frac{2a}{\tau^2}(-p + q) P_x(x, t) - \frac{a^2}{\tau^2}P_{xx}(x, t) = 0 \quad . \quad (2.21)$$

Fig. 2.3 shows a simulation of the two linear Fokker-Planck equations. Fig. 2.3(a) is for Eq.(2.20), and (b) is for Eq.(2.21). In 2.3(a) we notice the typical diffusion pattern while in 2.3(b) we see that the two typical solutions for the wave (see Eq.(2.13)) appear again but they are again blurred because of the existence of the damping term  $\frac{2}{\tau}P_t(x, t)$  as was the case with fig. 2.2(a). Here also the wave-like effect of the two branches disappears completely upon expanding to the 4th. order in space which means that the newly gained terms simply attenuate the effect of the 1st. term in Eq. (2.21).

## 2.5 The Kramers equation

The Kramers equation is a motion equation for the phase-space distribution function  $P(x, v; t)$  describing the Brownian motion of particles in an external driving field (see [40], [43], [28], and [44]),

$$\frac{\partial P(x, v; t)}{\partial t} = \left[ -\frac{\partial}{\partial x} v + \frac{\partial}{\partial v} \left( \gamma v - \frac{F(x)}{m} \right) + \frac{\gamma k T}{m} \frac{\partial^2}{\partial v^2} \right] P(x, v; t) , \quad (2.22)$$

where  $P(x, v; t)$  is a *bivariate joint distribution* for the particles position  $x$  and its velocity  $v$ ,  $\gamma$  is the friction (damping) constant,  $m$  is the particle mass,  $T$  is the temperature of the fluid,  $k$  Boltzmann's constant, and  $F(x) = -mx$  is the external driving force. The method of integration that was used here is the method of lines of fourth order [45]. This equation is also called the bivariate quasilinear Fokker-

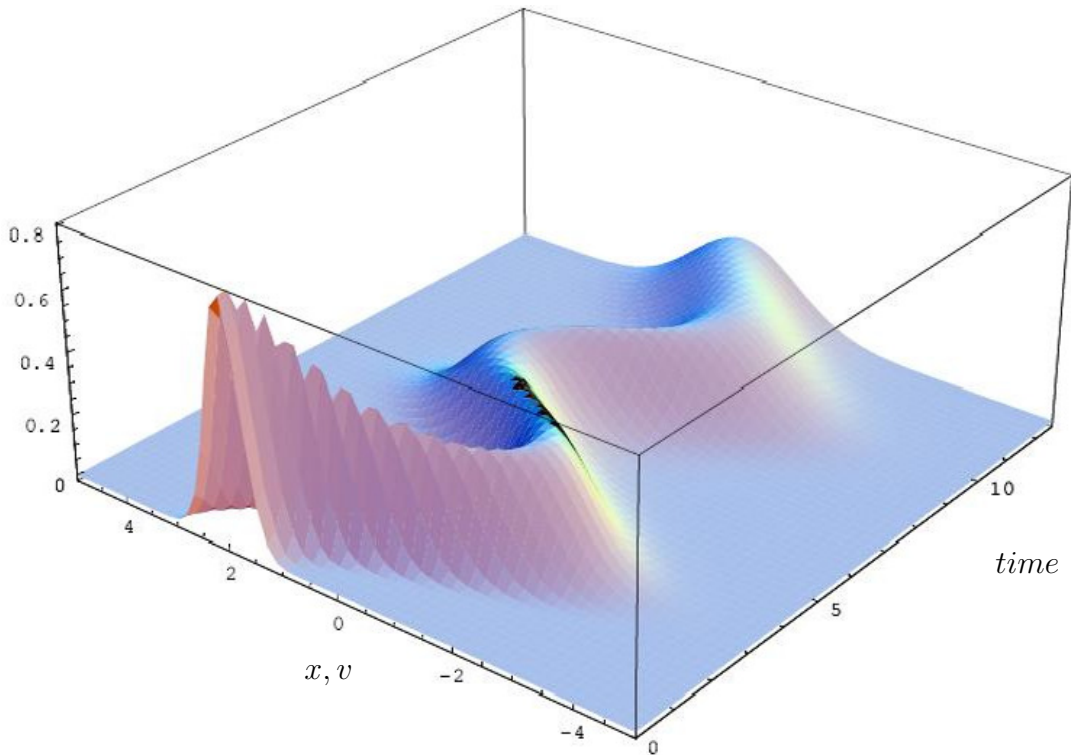


Figure 2.4: *The Kramers eq.(2.22) with a Gaussian initial condition. The parameters are taken as  $\gamma = 0.2$  and  $\frac{\gamma k T}{m} = 0.2$ . The vertical axis represents the magnitude of either  $x$  or  $v$ .*

Planck equation (see [41]). The quasi-linearity comes from the nonlinearity of the term  $\frac{\partial F(X)}{\partial v}$ .

## 2.6 Nonlinear Diffusion Equations

All the equations that were investigated in this chapter were linear (except the quasi-linear Fokker-Planck namely the Kramers eq.). To model turbulence we must have other nonlinear terms (like dispersion, reaction, ... terms) as well as the diffusion term as we have seen in the NSE in the first chapter.

### 2.6.1 Burgers' equation

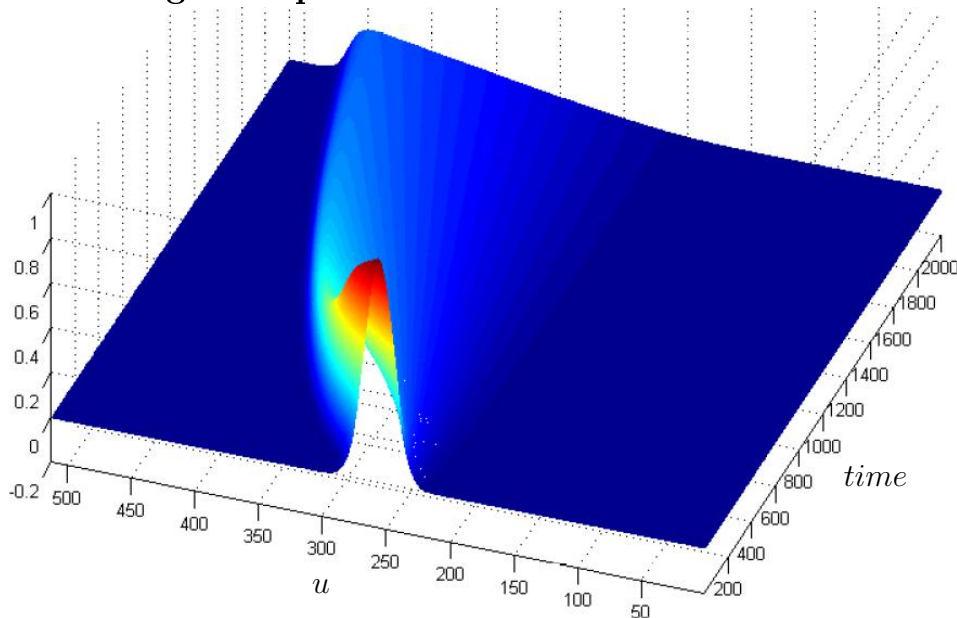


Figure 2.5:  $(1+1)$ dimensional Burgers equation (2.23) with a Gaussian initial condition and  $c = 0.1$ .

A simple equation that combines nonlinearity and diffusion without having to go into the details of the body forces and pressure term, as in the case of NSE, is the *Burgers equation*.

$$u_t + uu_x = cu_{xx} . \quad (2.23)$$

It looks like a *nonlinear Fokker-Planck equation* [43]. But it is actually the same as the previous diffusion equation with drift (2.6). In Fig.2.5 one notes the expected nonlinear development of a Gaussian initial condition, but nevertheless it is still a

diffusion process. The Burgers equation has been integrated using the ETD4RK method (exponential time differencing with fourth order Runge-Kutta)(see [37] and [38]). It is worth mentioning that eq. (2.23) is integrable (by using the Hopf-Cole transformation) and so it does not show any chaos or even any significant deviation from the known diffusive pattern, even if a random forcing is added to it [74].

### 2.6.2 Kardar-Parisi-Zhang equation (KPZ)

Another variation on the theme of nonlinear diffusion equations and particularly on Burgers equation is the *Kardar-Parisi-Zhang equation (KPZ)* which is written as

$$h_t(x, t) = \nu h_{xx}(x, t) + \frac{\lambda}{2}(h_x(x, t))^2 + \eta(x, t) , \quad (2.24)$$

where it describes the fluctuation of the height  $h(x, t)$  of an interface from its mean value. One gets the KPZ equation by linearizing Burgers eq. (2.23) with the Hopf-Cole transformation to get the diffusion equation (eq.2.5), by substituting  $u = -\nabla h$  in the resulting diffusion equation, integrating for  $x$ , and at last adding the forcing random term. In the KPZ, the first term on the RHS describes interfacial smoothing by a surface tension  $\nu$  in a direction lateral to the main growth, the second term is for growth in a direction normal to the interface, where  $\lambda$  is the growth velocity, and at last the third term is Gaussian noise. This third term makes the equation a Langevin-like equation . The KPZ eq. has been used to describe a variety of physical processes, like ballistic deposition, the formation of cell colonies in bacteria or tissue cultures (*Eden model*) just to name few (see [64] and the references therein). A flame propagation version of the equation [65] is written as

$$h_t(x, t) + v.h_{xx}(x, t) = \lambda(1 + (h_x(x, t))^2)^{1/2} + u , \quad (2.25)$$

where  $h(x, t)$  is the interface height,  $x$  is transverse to the direction of overall propagation,  $u$  and  $v$  are the longitudinal and transverse components of the flow field, respectively.

The linear stochastic equation that comprise the building block for the KPZ is a noisy diffusion equation called *Edwards-Wilkinson equation (EWE)* [71] (simply the diffusion eq. plus noise)

$$h_t(x, t) - Dh_{xx}(x, t) = \eta(x, t) , \quad (2.26)$$

where its constituents are defined as before. The implications of Edwards equation is that the deposition of surfaces on each other is a stochastic process.

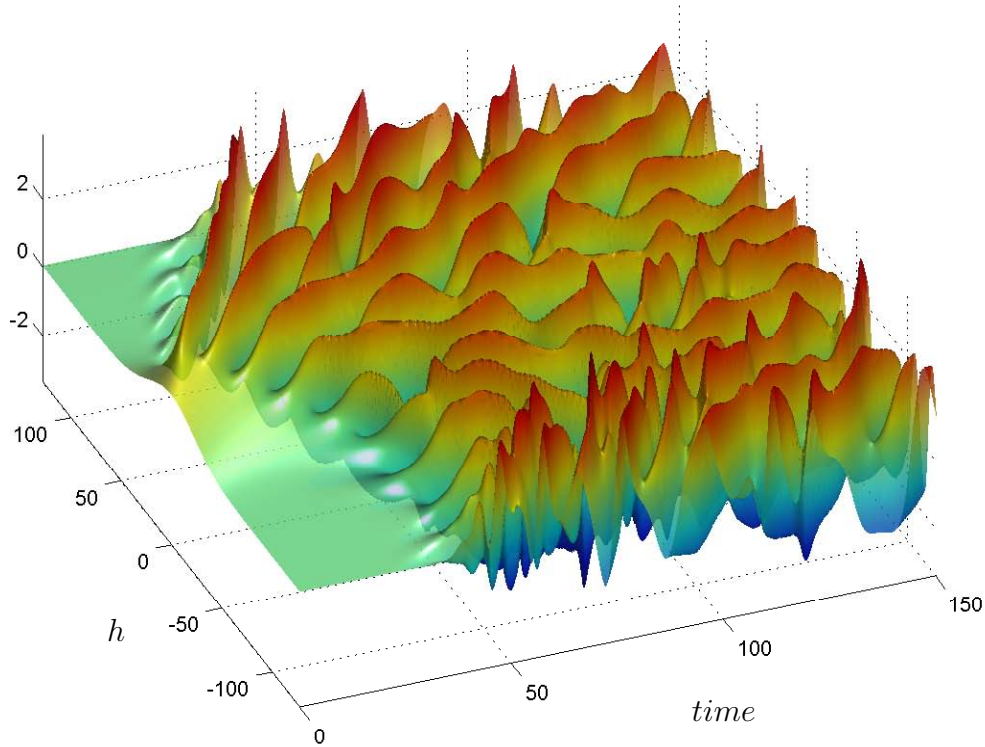


Figure 2.6:  $(1+1)$ dimensional Kuramoto-Sivashinsky equation (2.27) with a Gaussian initial condition and  $\nu = \mu = \lambda = 1$ .

And here we go again, of course, there must be an Edwards-Wilkinson equation with a drift term (see [72] and compare it with eq.(2.6)). Since this section was about describing the stochasticity of surfaces one should also mention the linear Fokker-Planck analysis presented in [73].

At last, the KPZ eq. becomes unstable at an instability called Benjamin-Feir-Newell instability (see [74] and the references therein), when  $\nu$  becomes negative. One has to add a fourth order stabilizing term to KPZ (2.24) and the new equation is written as

$$h_t(x, t) = -|\nu|h_{xx}(x, t) - \mu h_{xxxx} + \lambda(h_x(x, t))^2 . \quad (2.27)$$

The above eq. (2.27) is called the *Kuramoto-Sivashinsky equation (KSE)* [74]. Fig. 2.6 is a simulation of the KSE. One notices here that there are chaotic surface structures even without having to add a random forcing.

### 2.6.3 Gravity Waves equation

Another example that shows the effect of other terms that could make a diffusion process not only nonlinear but also exhibit other natural phenomena like dispersion in addition to branching, as we have seen in the wave equation, is the gravity waves equation (see for example [46] [47] and the references therein)(Fig.2.7). The equation in general looks like:

$$u_{xt} = \frac{3g(1-3\theta)}{2vh}u - \frac{1}{2}u_{xx}u - \frac{1}{4}u_x^2 + \frac{3h^2}{4v}u_{xx}u_x^2, \quad (2.28)$$

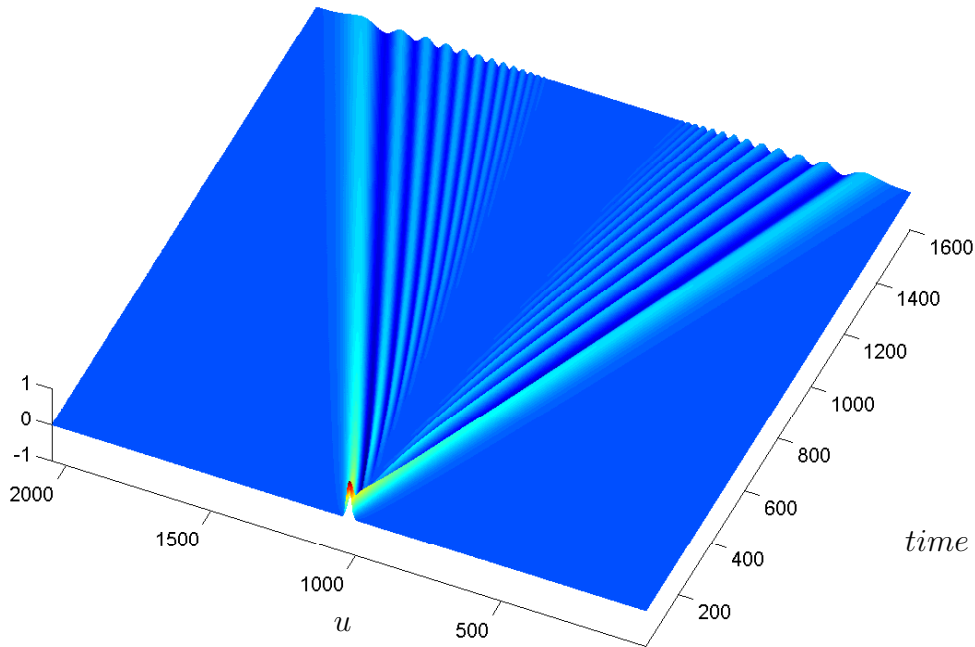


Figure 2.7: *Nonlinear and dispersive propagation of surface waves according to Eq.(2.28) with a Gaussian initial condition. All the parameters were taken equal to one.*

where  $g$  is the gravity,  $h$  the depth,  $\theta$  the Bond number,  $v$  a constant that is determined via the surface tension, and  $u$  is the surface velocity of the waves.

## 2.7 Testing the programs for conservation

We have dealt with different quantities ,i.e. different in nature, in the previous equations, e.g. concentrations, probabilities, velocities, wavefront heights, etc... . To show that they all follow the same conservation laws during there dynamical development within the time range specified in the integration algorithm it is sufficient to test that the subject quantity has not changed from the beginning till the end of the process. Said in another way that there should be no sinks or sources in the equation itself nor due to numerical dissipation or augmentation [108]. In fig. (2.8) the first number represents the area of the initial condition (which in all the cases happens to be Gaussian) and the rest of the numbers represent the areas for the slices at the later times. We notice that there are slight changes in the areas which could be attributed to the nature of the used boundary conditions in the integration algorithm, which were simply periodic.

## 2.8 Physical significance and applications

So far the equations were without a source term that resembles a production of particles (energy or whatever) to replenish the diffused ones (except for KPZ and EWE). The linear diffusion equations become nonlinear with the addition of the production term. For example *Fisher's equation* is simply the linear diffusion equation added to it a nonlinear production term

$$\frac{\partial \tilde{c}}{\partial t} = D \Delta \tilde{c} + a\tilde{c}(1 - \delta\tilde{c}) \quad , \quad (2.29)$$

where  $\tilde{c}$  stands for a population density of a species, and the last term  $a\tilde{c}(1 - \delta\tilde{c})$  is the driving term (also called forcing term, or as above production term) and is in this case the logistic equation which represents a birth-death process. This equation (2.29) was used to model the spread of an advantageous gene in a population [48]. We see in this eq. (2.29) the term which resembles a reaction process  $\tilde{c}^2$  that is why the Fischer equation is one in a family of equations called the reaction-diffusion equations, e.g. the oregonator [49], the brusselator [51], the Gierer-Meinhardt model [50] in chemistry, FitzHugh-Nagumo in a nerve conduction [52] and in semiconductor optical amplifiers models [53].

Since the classical Fick's law (2.3) is a parabolic equation (see [10] and [9]) and these types of equations violate *causality* , a hyperbolic equation was needed to overcome this aspect. This made many researchers go to the hyperbolic non-Fickian diffusion equation ((2.12) or equivalently (2.20))to model their applications. This is

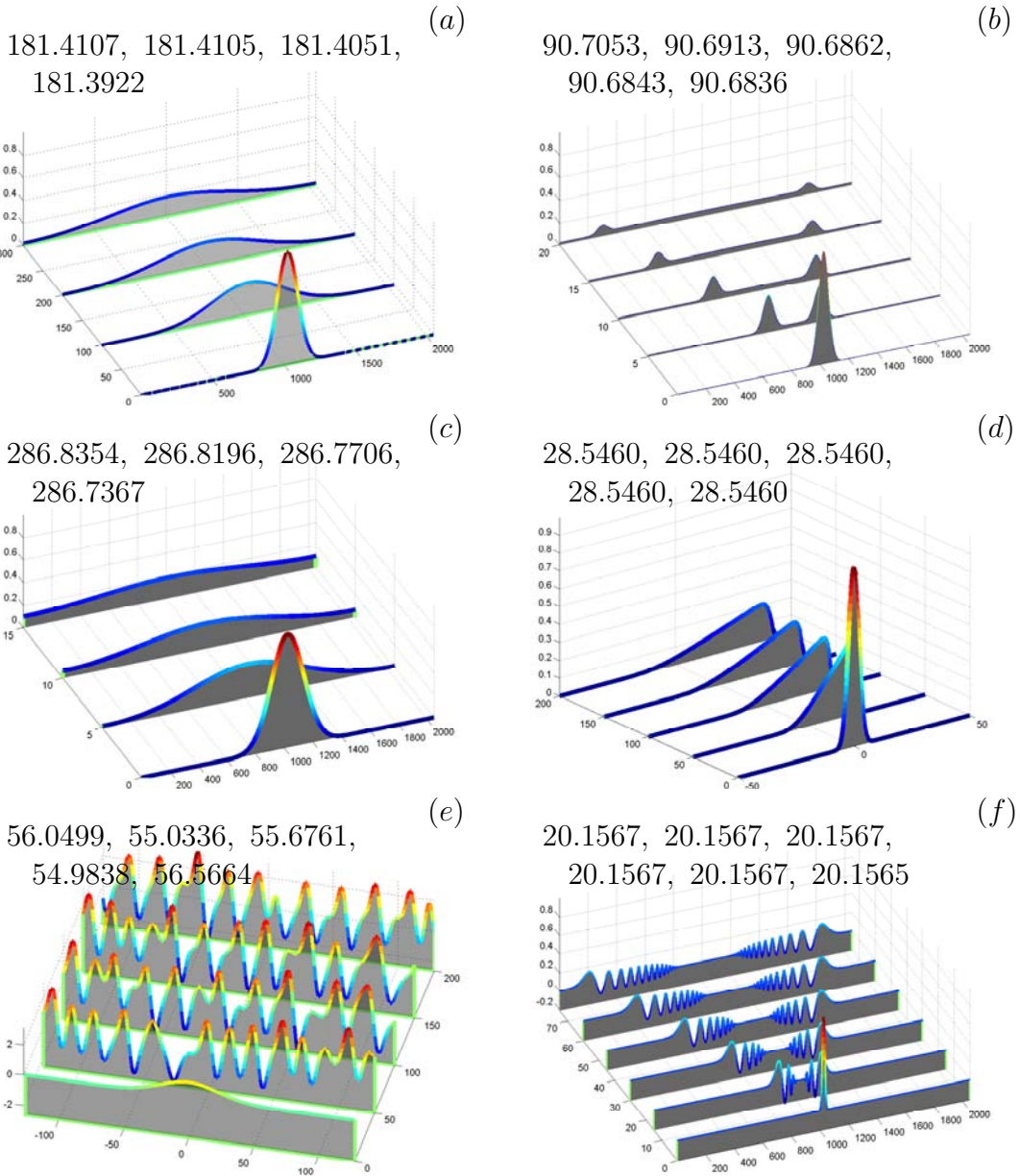


Figure 2.8: Testing the conservation of the different previous diffusion processes, by calculating the area of the different sections shown on the top of each figure: (a) Fickian diffusion (eq.(2.5)). (b) Non-Fickian diffusion (eq.(2.12)). (c) Fokker-Planck (eq.(2.12)). (d) Nonlinear Fokker-Planck or Burger's (eq.(2.23)). (e) Kuramoto-Sivashinsky (eq.(2.27)). (f) Gravity waves (eq.(2.28)).

one of the reasons why this hyperbolic equation (the non-Fickian diffusion eq.) has from time to time surfaced in the scientific literature under other names like Maxwell-Cattaneo's eq. [54] [55] or the telegrapher's eq. [59] [60] [61] [62]. The equation

applications range from solving heat conduction problems in semiconductors [57] to relativistic nuclear problems [58], just to name few of its applications.

An equation, that is used in the analysis of the plasma waves in long Josephson junction in the superconducting physics field, is an oscillator equation called the perturbed sine-Gordon eq. (see [67], [68], [69] and the references therein)

$$\varphi_{xx} - \varphi_{tt} = \sin\varphi + \alpha\varphi_t - \beta\varphi_{xxt} + \gamma \quad , \quad (2.30)$$

where  $\varphi(x, t)$  is the superconducting phase difference between the electrodes of the Josephson junction,  $\alpha$  and  $\beta$  are dissipation coefficient, and  $\gamma$  is a bias current density. We notice on the LHS of (2.30) the wave operator or the relativistic schrödinger operator also called d'Alembert operator  $\square^2 = \frac{1}{c^2} \frac{\partial^2}{\partial t^2} - \nabla^2$ . But then there is also a *sin* term, which adds more structures to the *Klein-Gordon equation*, a perturbing term and a driving term. Here again we see the non-Fickian diffusion equation resembled by the RHS of (2.30) plus the second term on the LHS.

# Chapter 3

## Dynamical Systems

It is worth noting that at the time that Reynolds was experimenting with fluids to investigate the transition from laminar to turbulent flows, Poincaré was finding out that simple nonlinear dynamical systems were capable of showing a chaotic- and random-in-appearance behaviour are in fact deterministic. It was not until the meteorologist Lorenz who has shown that there is a possible link between chaotic dynamics and turbulence [76].

### 3.1 Time series and Intermittency

Measured one dimensional data, whether be it velocity, temperature, stokes and shares,... etc are called time series. These time series could be natural or measured in a laboratory or produced through a model (continuous differential equations or difference equations).

In fig.3.1 we show some of the time series that we will be dealing with or some other similar ones. In (a) a random signal produced from a Pareto distribution . It is a heavy tailed distribution meaning that a random variable following a Pareto distribution can have extreme values. The Pareto distribution is written as

$$f(x) = \frac{a}{x^{a+1}} \quad \text{for } x \geq 1 \quad , \quad (3.1)$$

where  $x$  is a random variable and  $a$  is called a shape parameter. One notices that this series is intermittent or shows *intermittency* . When a motion alternates abruptly between approximately laminar silent phases interrupted by irregular bursts we say that the motion (and hence its time series) is intermittent and that there is intermittency. We see that the other series in the figure are more or less intermittent.

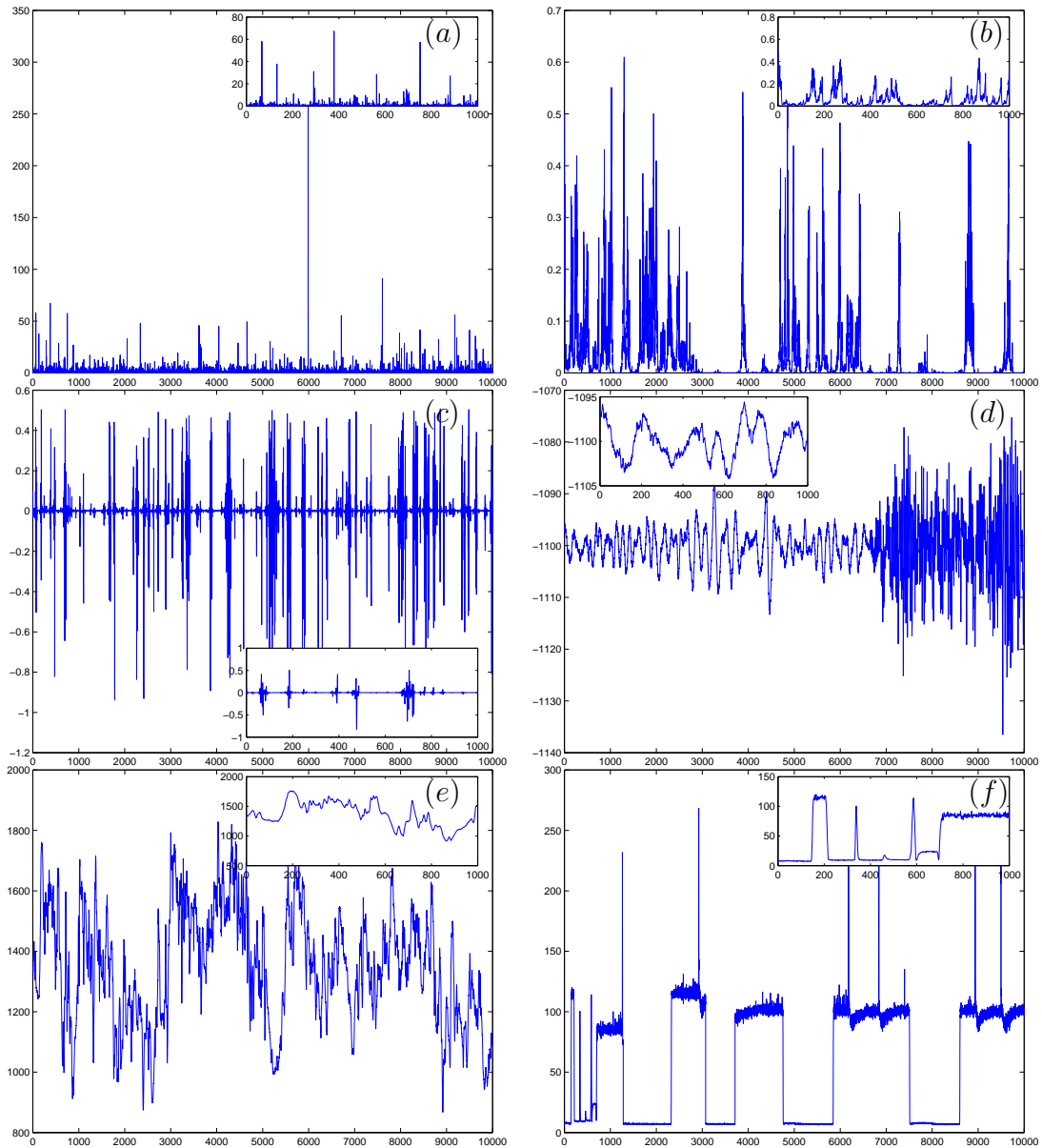


Figure 3.1: *Time series of different signals: (a) Random time series produced from Pareto distribution as in eq. (3.1) ( $a = 4.9$ ). (b) Flare from eq.(3.6) taking  $a = 4$ ,  $b = 1$ ,  $c = .4$  and  $d = 0.6$ . (c) Flare from eq.(3.7) taking  $a = 1.5$ ,  $b = 1.8$ ,  $c = .9$  and  $d = 0.3$ . (d) Iran Earthquake. (e) Oldenburg's air-tank free-jet experiment. (f) The pulsar GRO. In the inset we show a blowup for a shorter range for the same signal as in the main figure.*

In the same figure we notice that the signal in (a) is produced with eq. (3.1), (b) with eq. (3.7), and (c) with eq. (3.6) (more details in [70]) while the signals shown

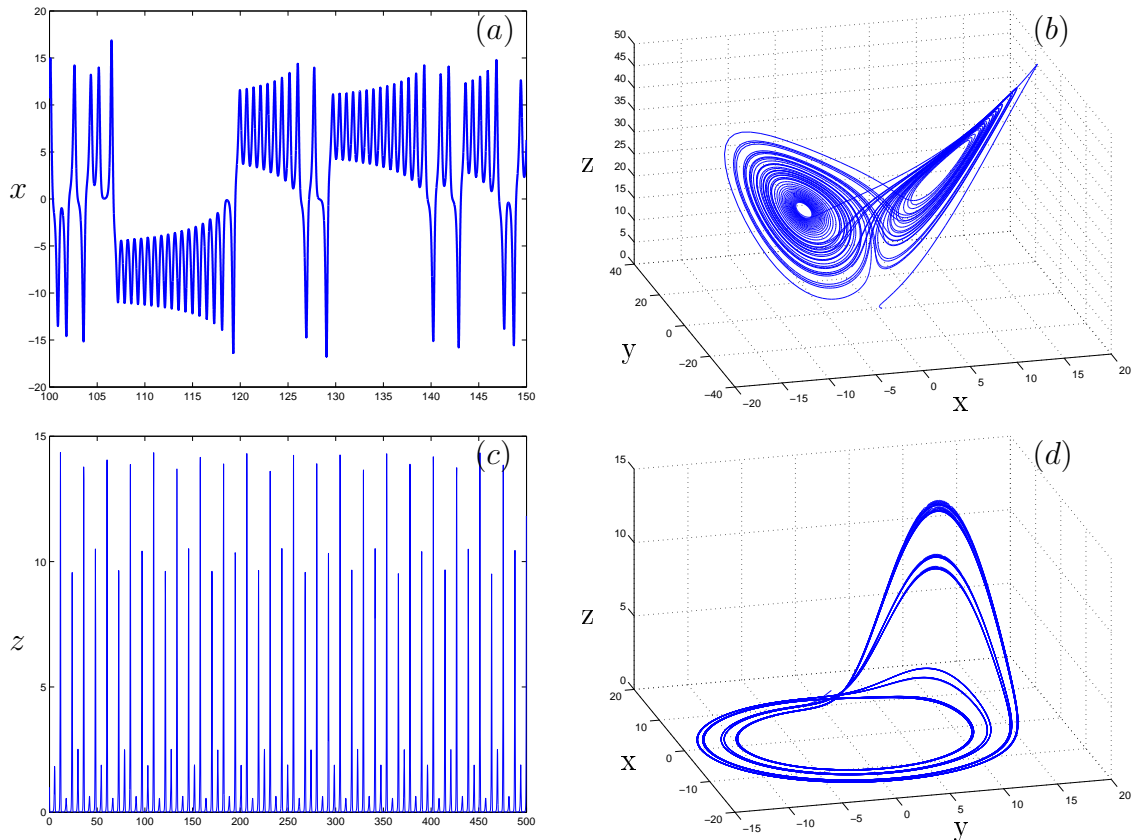


Figure 3.2: *The time series and the phase space for (a) and (b) Lorenz attractor eq.(3.2) taking  $Pr = 10$ ,  $Ra = 28$  and  $b = 8/3$ , and (c) and (d) for Rössler attractor eq.(3.3), taking  $a = 0.2$ ,  $b = 0.2$  and  $c = 10$ , respectively.*

in (d), (e), and (f) are natural signals. (d) shows part of an Earthquake signal that happened in Iran [117], (e) is an experimental signal from Oldenburg's air-tank free-jet experiment and it is totally turbulent [118], and at last (f) is a signal for a pulsar star catalogued as GRO J1744-28 [120].

## 3.2 Lorenz and Rössler Models

The equations of the Lorenz model, which is a simplified weather model derived from the NS equations (1.1) plus an extra equation to account for the buoyancy effects due to the heat (called also the Saltzman convection equations [78]), are

$$\begin{aligned}
 x_t &= Pr(y - x) \\
 y_t &= Ra x - y - xz \\
 z_t &= -bz + xy \quad ,
 \end{aligned}
 \tag{3.2}$$

where  $x(t)$  is amplitude of the convective flow,  $y(t)$  and  $z(t)$  are the horizontal and vertical temperature distribution (variations) respectively,  $Pr$  is the Prandtl number which is the ratio of viscosity to thermal conductivity,  $Ra$  is the Rayleigh number which is the ratio of the temperature difference between the upper and lower surface of the fluid,  $b$  is a geometrical factor and is the ratio of the width to the height of the slab [78]. They represent a situation where a fluid slab is heated from below and a fixed temperature difference is maintained between the top surface which is kept cold and the bottom heated surface.

Yet another simpler set of equations introduced by Ott Rössler and consists of two linear and one nonlinear equations and shows chaotic behaviour, is written as

$$\begin{aligned}x_t &= -y - z \\y_t &= x + a y \\z_t &= b + z(x - c) .\end{aligned}\tag{3.3}$$

A number of things could be inferred from fig.3.2. Most importantly is that the irregular aperiodic transitions from positive to negative values (in the case of the Lorenz model) corresponding to the system orbiting around one or the other fixed point. As for the Rössler system, the movement of the attractor is either in xy-plane or in the z-axis this is why one observes that the time series for the z-axis is only positive.

The main features in dynamical systems (that we want here to emphasize) are

- Sensitivity dependence on the initial conditions, and from this emerges the unpredictability associated with such systems. This sensitivity is clearly evident from fig. 3.3. This property is offset by another property called *shadowing* which insures the boundedness and validity of the numerical simulations [88] or [89].
- The second main feature, is that these systems (whether maps or flows) could produce chaos if they have nonlinear terms and if the sensitivity factors in these equations are adjusted to that purpose [76].
- The third main feature is that the attractors are self-similar (self-affine).

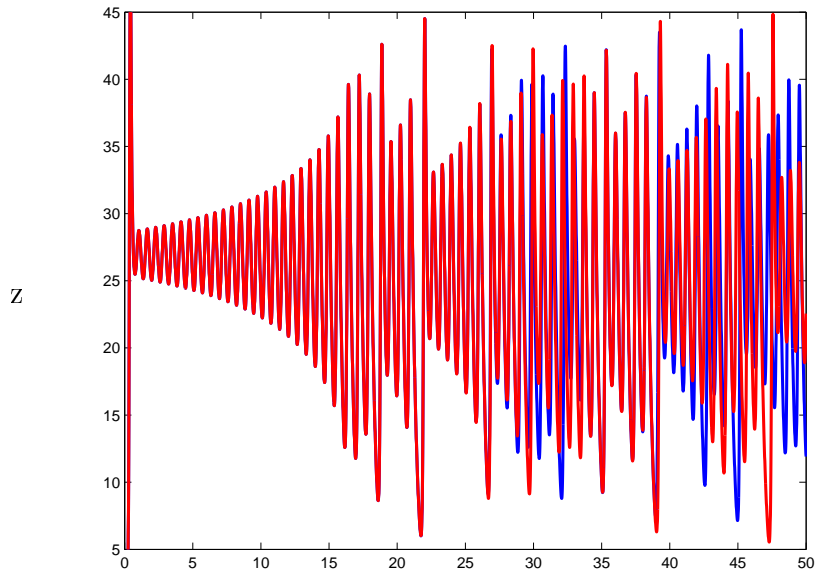


Figure 3.3: *Changing the initial condition from 1 to 1.0001 produces another orbit for the Lorenz attractor. One notices that a change in the initial condition of only 0.0001, makes the second orbit diverge from the first between 25-30. Using the same parameters as in fig.3.2*

### 3.3 Flare maps and Intermittency

The understanding of the route to chaos has been paved by the logistic map (LM) (with or without drift term see [79]) , written as

$$x_{n+1} = r x_n(1 - x_n) , \quad (3.4)$$

where  $r$  is an adjustable parameter (sensitivity parameter). This equation has been the building block for probably most of the flare (burst) equations. The importance of the study of these equations lies in the fact that in addition to the mechanism of *bifurcation* as a route to chaos, i.e. to produce chaos, there is another mechanism for that called *intermittency* (see [82]), also on-off intermittency [83], or the in-out intermittency [85].

Intermittency is essentially defined as events of large amplitude separated by long periods of low amplitude events (laminar or periodic movement). The importance for equations to describe and quantify intermittency lies in the diversity of natural phenomena that needs to be described and eventually predicted by these class of equations. Examples of these natural phenomena and the significance of studying intermittency for each case are: sunspots and there connection to sun flares and the disruptions caused by it in the electrical and communication net-

works, wind bursts (gusts) and the damages to wind electricity mills, explaining the attitude of Pulsars (PULSating stARS), the spatial intermittent patterns of distribution of galaxies in astrophysics, or the distributions of mountains and bacteria, or even the intermittent shape of earthquake signals and trying to forecast them, just to name few.

The three flare equations that will be examined here are

$$\begin{aligned}x_{n+1} &= r_n x_n(1 - x_n) \\r_{n+1} &= a w_n + b \\w_{n+1} &= 4 w_n(1 - w_n) .\end{aligned}\tag{3.5}$$

$$\begin{aligned}x_{n+1} &= a x_n(b - x_n) \\w_{n+1} &= w_n + w_n(x_n - c) - d w_n^2 .\end{aligned}\tag{3.6}$$

$$\begin{aligned}x_{n+1} &= x_n \exp^{a(1-x_n^2)} + w_n \\w_{n+1} &= w_n(1 + b(c - x_n) + d) .\end{aligned}\tag{3.7}$$

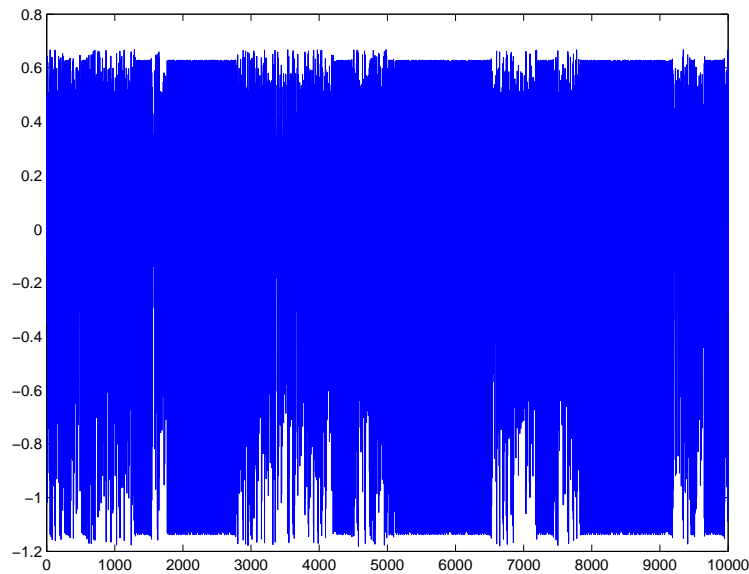


Figure 3.4: *Intermittency route to chaos for eq.(3.7).*

In the first equation (3.5) (see [87]), the sensitivity factor  $r$  in the LM is defined through another LM, which in its turn behaves like a tent map because of the factor (4) which appears in calculating  $w$  [76]. Its time series (fig. 3.6a) shows an intermittent signal in the sense defined above.

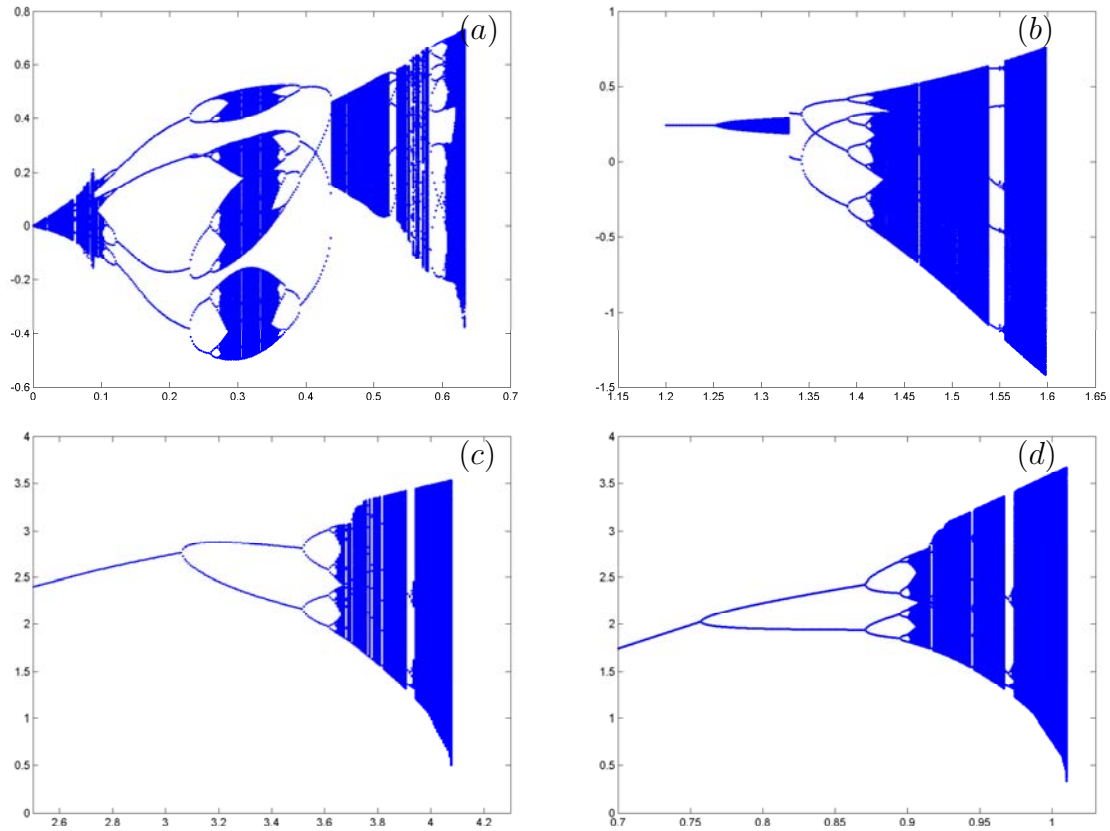


Figure 3.5: Some of the bifurcation diagrams for eq.(3.7) (figures (a) and (b)). Figures (figures (c) and (d)) are for eq. (3.6).

The next two equations (3.6 and 3.7) exhibit also a flare behaviour (or intermittent as is in fig. 3.1a-c and also(f)). Figures 3.5 show the bifurcation diagrams which help in finding the values of the parameters  $a$ ,  $b$ ,  $c$ , and  $d$  which control the behavior of these equations. For instance to see at which ranges of a certain parameter (whether  $a$ , or  $b$ , ...etc.) the bifurcation process starts and goes on until the process exhibits chaos through the *route of bifurcation* , or at these values the process returns back from chaos to periodic oscillations and then jumps again into chaos after showing a third period oscillation (which happens for instance after the x-axis value of 0.95 until  $\sim 0.97$  in fig. 3.5(d)). Choosing values for the parameters at such periods, i.e. where the process relaxes from chaos to periodic and then directly becomes chaotic again, is called *intermittency route to chaos* . Such a behaviour is evident in figure 3.4 which shows the behaviour of the time series in such a region.

In figures 3.6(a) the time series of eq. 3.5 and in (b)its phase space or state space. In (c) and (e) the time series of eq. (3.6) is shown for two different values of the parameter  $a$  (3.96 and 4.0 respectively). While in (d) and (f) the state space for these two different values. The time series for eq.(3.6) with its state space is shown

again to emphasize at this early stage the importance of the shape of the state space and how drastically it sometimes changes with a small change in the equations parameters. The importance of the state space will be met again in connection with the *embedding dimension*.

### 3.4 Fractals, multifractals and dimensions

*Fractals* are geometrical objects that are self-similar or scale-invariant, i.e. subsets of a fractal have essentially the same form as the whole. Another definition from Mandelbrot to fractals is that they are objects with noninteger Hausdorff dimension [84]. The most intuitive definition for dimension comes from trying to cover objects with balls or squares (or cubes). To cover a piece of line with squares one needs  $N(r) \propto 1/r$  where  $N(r)$  is the number of boxes needed to cover a line of length  $r$ . So if  $r = 1$  then  $N$  equals one too but if we choose  $r = 1/2$  then we will need  $N = 2$  to cover the line and so on. For covering a square with an  $r = 1/2$  we need  $N = 4$  which is  $1/(1/2)^2 = r^{-2}$ , here we should be able to notice that the exponent 2 is actually the dimension of the square. If we choose the length  $r = 1/3$  then we need  $N = (1/3)^{-2} = 9$  boxes and so on. The same logic is applied to 3-dimensional objects to find out that we need  $r^{-3}$  to cover a cube. So for Euclidean objects there is no problem with this intuitive definition, namely

$$N(r) \propto r^{-d} \quad , \quad (3.8)$$

where  $d$  is the dimension of the object. So, Euclidean objects have an integer dimension.

With some algebra one could write the power law eq.(3.8) as

$$K = \frac{\log N(r)}{\log 1/r} \quad , \quad (3.9)$$

where  $K$  is the dimension (in (3.8) we called it  $d$ ) which is *Kolmogorov's dimension* in this case. Other names for it are the *box-counting dimension* or the *capacity dimension*. The similarity is evident between eq. (3.8) and an equation from the next chapter (4.23), which actually implies an equivalence between the box-counting technique and the structure function which will be the theme of the next chapter.

Now taking a *Koch curve* (see fig. 3.7(a)) which is constructed by taking a stage one curve (which is on the top LHS) and using it as a motif to replace each line segment of the later stages and calculating the  $K$  dimension according to eq. (3.9) we find that it gives  $\log(4)/\log(3) = 1.2619$ . This process of using an object as a motif to construct a new self-similar one is called an iterated function system (IFS) another name is (i.e. it has fractional dimension).

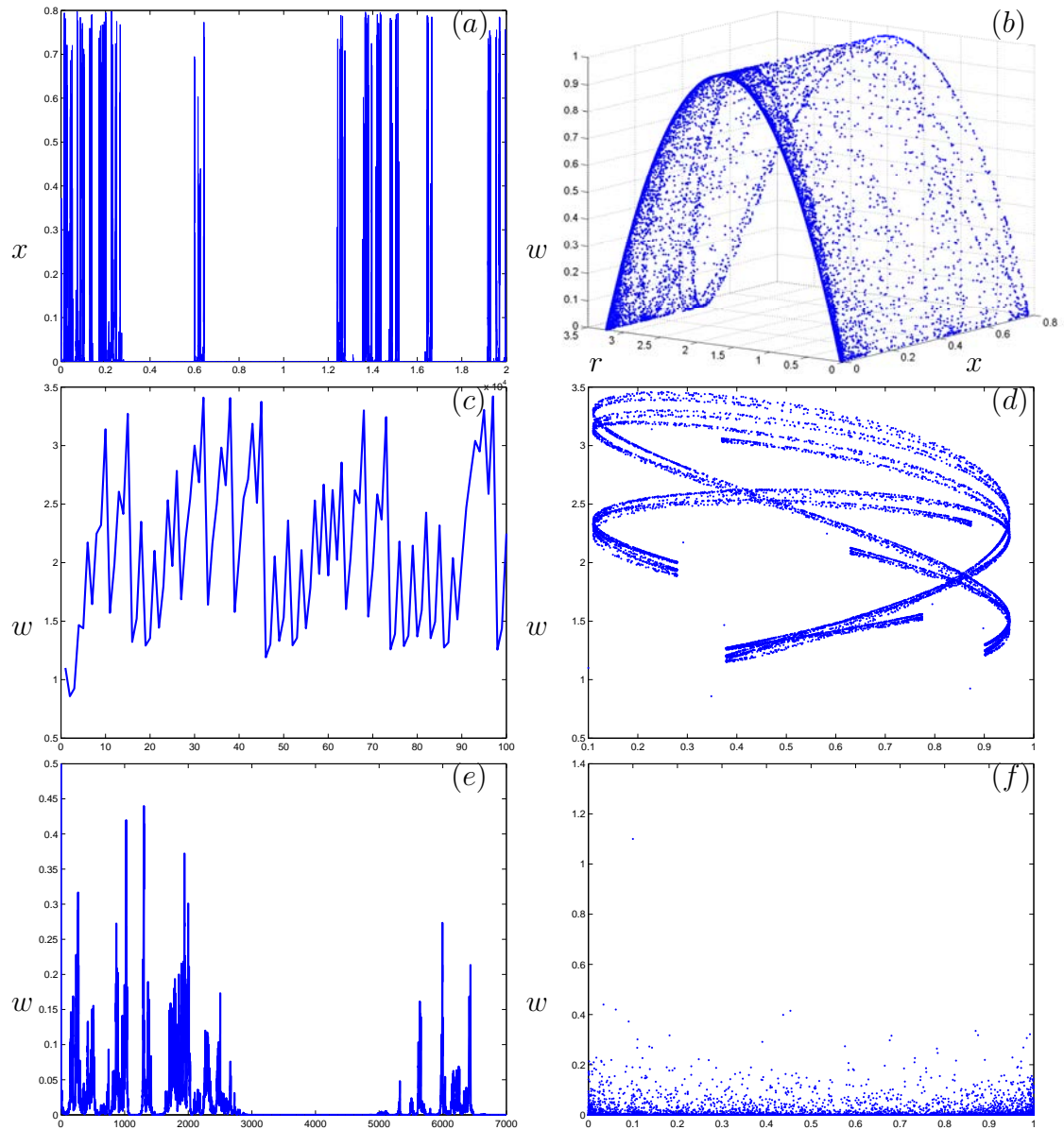


Figure 3.6: The time series and phase space of eq. (3.5) and eq. (3.6). In (a) and (b) the time series and the 3D phase space of eq. (3.5) are shown. As for (c), (d), (e), and (f) the time series and the 2D phase space of eq. (3.6) are shown, where in the first two figures the parameter  $a$  in the equation was chosen as 3.95 and in the last two figures (e and f) the parameter was equal to 4. The other parameters are of  $O(1)$ .

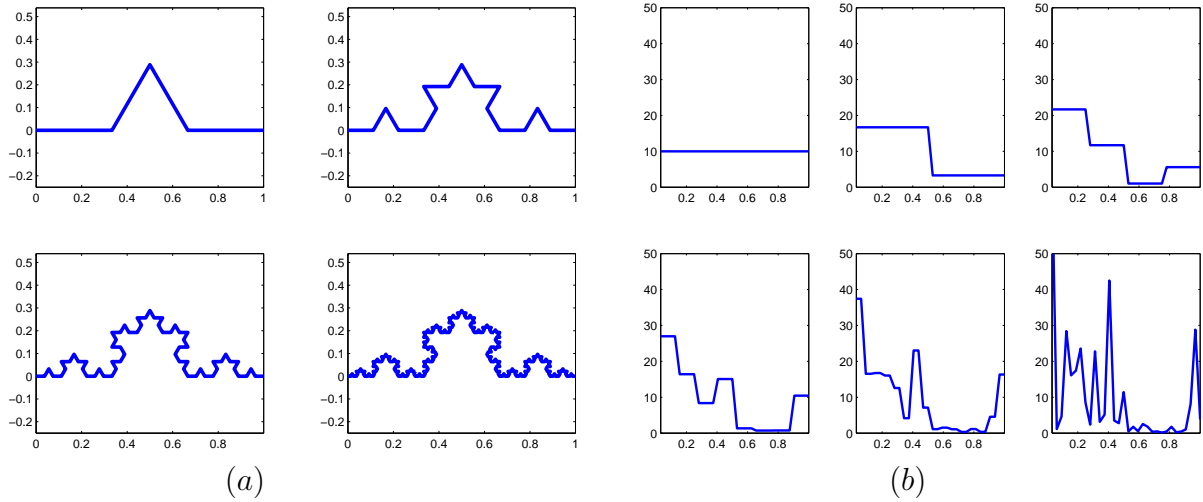


Figure 3.7: (a) Koch curve with four stages. Where the first frame on the top LHS represents stage one and the last one on the bottom RHS represents stage four. (b) The development of a multifractal in a random way. Were we start with a rectangular mass with mass  $10 \times 1$  and redistribute it according to  $n^{stage}$ . On the top LHS we start with stage zero and end on the RHS with stage 8 where  $n=2$ .

Comparing figs. 3.7(a) with figs. 3.7(b) it is evident that there are two different procedures here. In (a) the motif was a geometrical figure used for an ever reduced scale to achieve the self-similarity. In (b) one starts with a square with a certain area and starts in cutting it in a random way and sticking the new pieces beside each other on the condition that the area (mass or the probability density function (PDF)) of the whole is kept constant (the normalization condition) (see [90] and [91]). So in other words one could also build a Koch multifractal by using a PDF or mass for the segments other than the fractal one which is  $1/3$  (the one in fig. 3.7(a)).

Calculating the box-counting or the *fractal dimension* is a process limited by the resolution of the graphics, because at some point the boxes will be too small to include a piece of the object inside it. So one should estimate the object dimension with few points (probably as high as 10) which is mostly not enough.

Another similar dimension to the box-counting is the *correlation dimension* (CD), which is often used to estimate dimensions in experimental physics (see [92] and [95]) and is written as

$$CD = \lim_{r \rightarrow 0} \frac{\log C(r)}{\log r} \quad , \quad (3.10)$$

where  $C(r)$  is the *correlation integral* and is equal to the number of points which have a smaller distance than a given distance  $r$ . That is to say one uses each of the

points as reference and counts how many of the other points are within distance  $r$  from it [94].

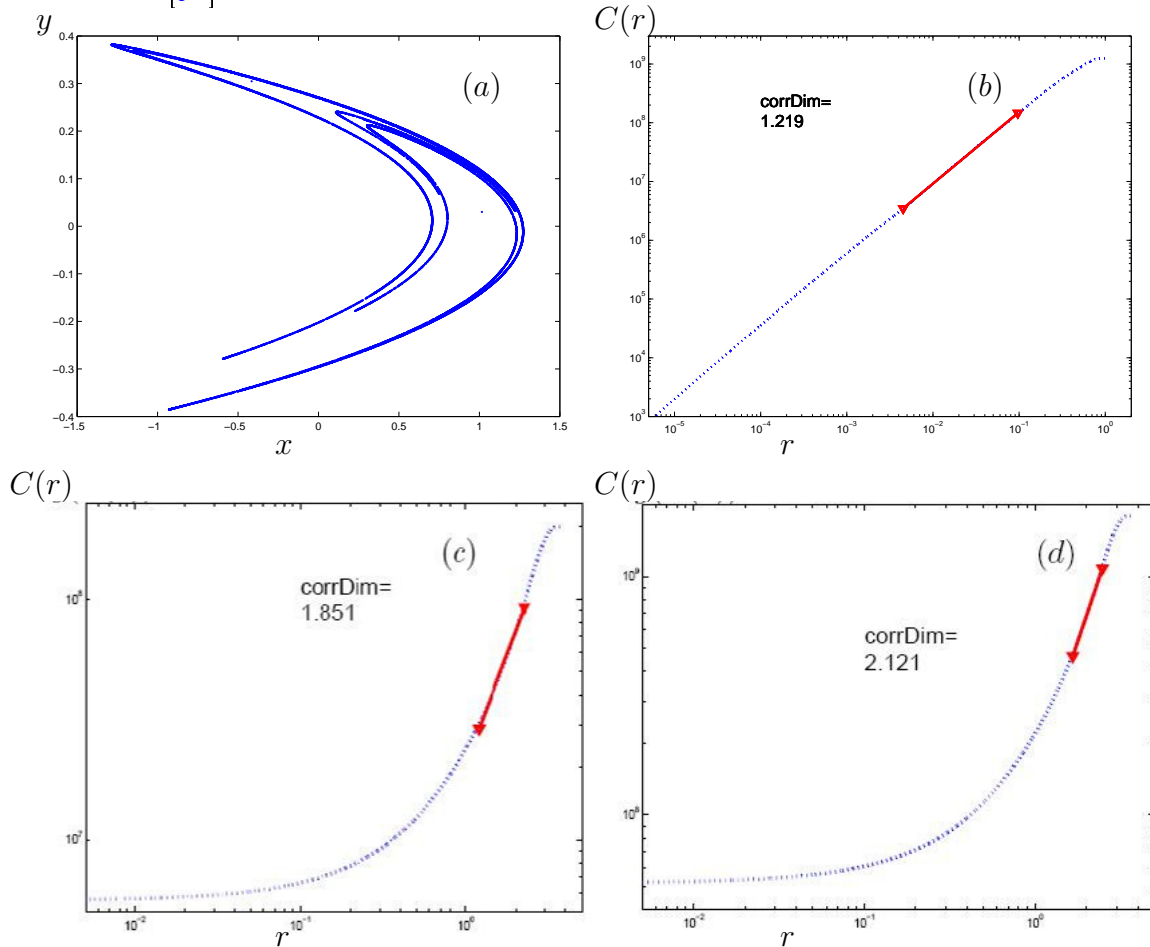


Figure 3.8: (a) Henon attractor and (b) its correlation dimension. (c) and (d) are the correlation dimension for Lorenz attractor (see eq. (3.2) and fig. 3.2b) for 20,000 points and 60,000 points respectively.

As a check for the algorithm, the Henon attractor (which is shown fig. 3.8(a)) the CD was calculated as in fig. 3.8(b). The calculated value is approximately equal to the value found in [92]. In figs. 3.8(c) and 3.8(d) we notice a number of things. First, that upon increasing  $r$  we get three distinct regions, the first one where there are no points and the correlation dimension has a constant value. In the second region the number of points begins to increase and stabilize according to the power law eq. (3.10) and in the third region it stabilizes again as the number of points does not change. The second thing that is noted, is that increasing the number of points used to calculate the CD will increase the accuracy of the results. One could find nearly the same values for the CD of Henon attractor and Lorenz attractor in the literature ([76], [93] and [77]).

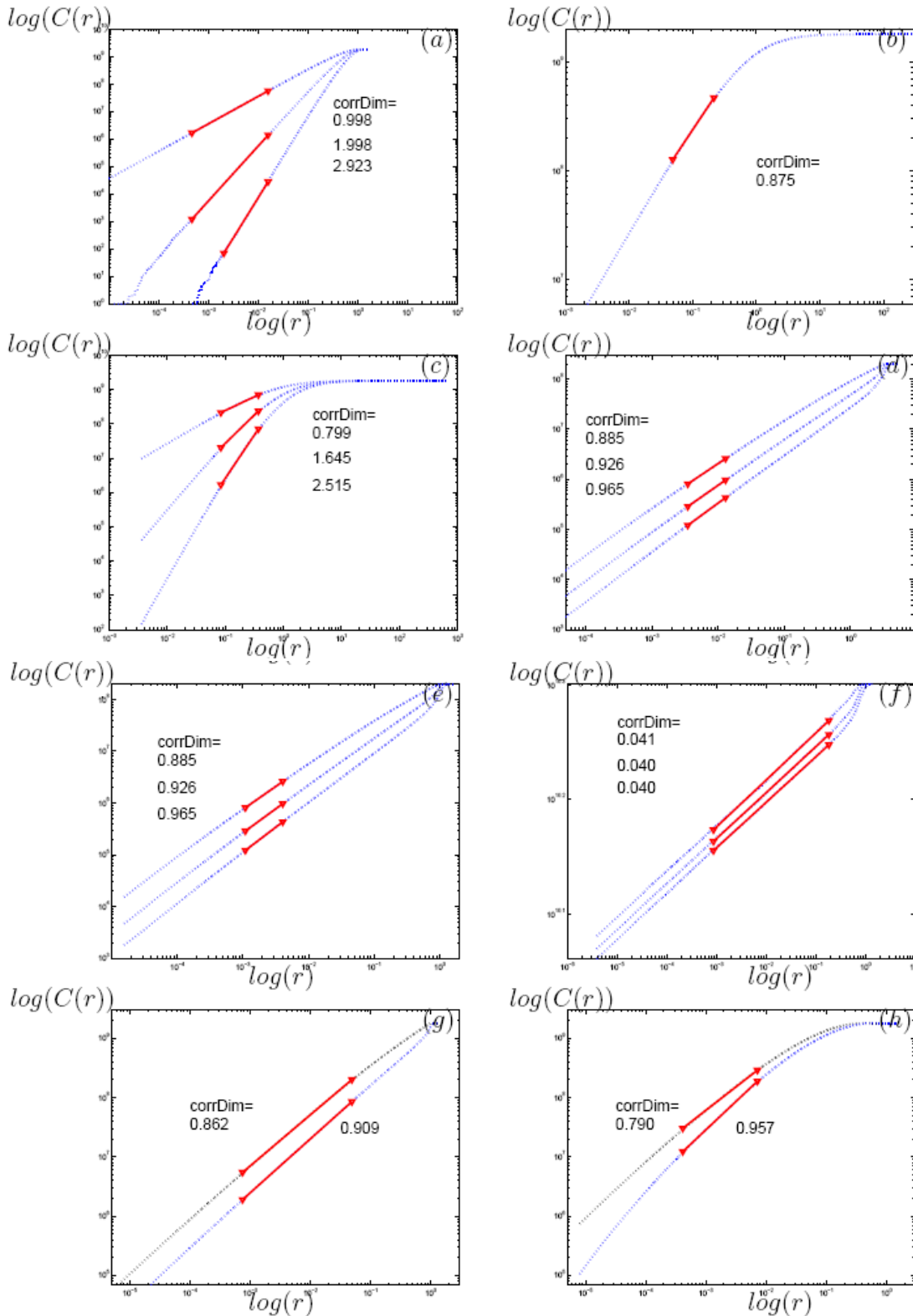


Figure 3.9: The correlation dimension of (a) Gaussian distributed data (60k points), (b) Pareto distributed data 60k points ( $ED=1$ ), (c) Pareto distributed data 60k points ( $ED=3$ ), (d) Blamforth attractor (3.5) 20k points on the  $r$ -axis ( $ED=3$ ), (e) Blamforth attractor 20k points on the  $w$ -axis ( $ED=3$ ), (f) Blamforth attractor 200k points on the  $x$ -axis ( $ED=3$ ), (g) Flare eq. (3.6) 60k points on the  $x$ -axis ( $ED=3$ ), (h) Flare eq.(3.6) 60k points this time on the  $w$ -axis ( $ED=3$ ).

If the time-series is a random process, the CD increases with the embedding dimension (ED) linearly, as is seen in fig. 3.9(a) where the CD is approximately equal to the ED = 1, 2, 3. If the time-series is a deterministic signal, the CD does not increase further when the ED exceeds the CD. Thus a plot of the CD as a function of the ED may show whether a signal is random noise or deterministic chaos [94].

In 3.9(b) and (c) the CD for the intermittent signal of Pareto distribution is calculated for ED = 1 and ED = 3 respectively. It seems that we need more points for such highly intermittent signals to calculate the CD reliably.

In 3.9(d), (e) and (f) one observes the difference of the value of the CD when it is calculated on the different axes, which happens to be the  $r$ ,  $w$  and  $x$  axes (see the Blamforth map (3.5) in fig. 3.6(b)). In fig. 3.9(g) and (h) we see that the CD value calculated on different axes of the flare attractor eq.(3.6) changes with the axes which confirms what we have seen above with the Blamforth map eq.(3.5).

### 3.5 Embedding dimension (ED)

Phase space constructions have an important role in describing the development of a system of equations in time. But usually, in an experiment one registers in his instruments a time series for one variable (whether space variable or temperature ...etc.). By finding the ED one could reconstruct some of the main features of the state space by using this time series of the measured variable. So, if our time series is the vector  $X = x_1, x_2, \dots, x_N$  we could construct a matrix by using time delay construction to get again the 2 or 3 (or more) vectors we need to reconstruct the original state space e.g. if we take for example one variable from the Henon map or the flare map eq.(3.6) then the  $ED = 2$ . So our new vectors will look like  $X_N, X_{N-h}, X_{N-2h}, \dots, X_{N-(m-1)h}$ ...etc., where  $h$  is the time lag used in the embedding, and  $m$  is the embedding dimension. The ED should be larger than the correlation dimension (or the box-counting fractal dimension) to ensure the replication of our original attractor [95]. This geometrical replicating of the dynamics is due to Takens [96].

We show some examples in fig. 3.10 where in (a) a replication of Rössler attractor was made, and in (b) the previous Blamforth attractor (compare these with figs. 3.2(d) and 3.6(b)). In fig. 3.10 (c) and (d) an embedding for Oldenburg's free jet data was tried in two different EDs, 3 and 10. We observe that due to the high degrees of freedom (dimensions) possessed by the particles and the intersection of the trajectories one could not see any structures (one would assume that one could see a Kármán street or even a simple eddy for example), while in (a) and (b) there were some of the original geometrical features because the trajectories do

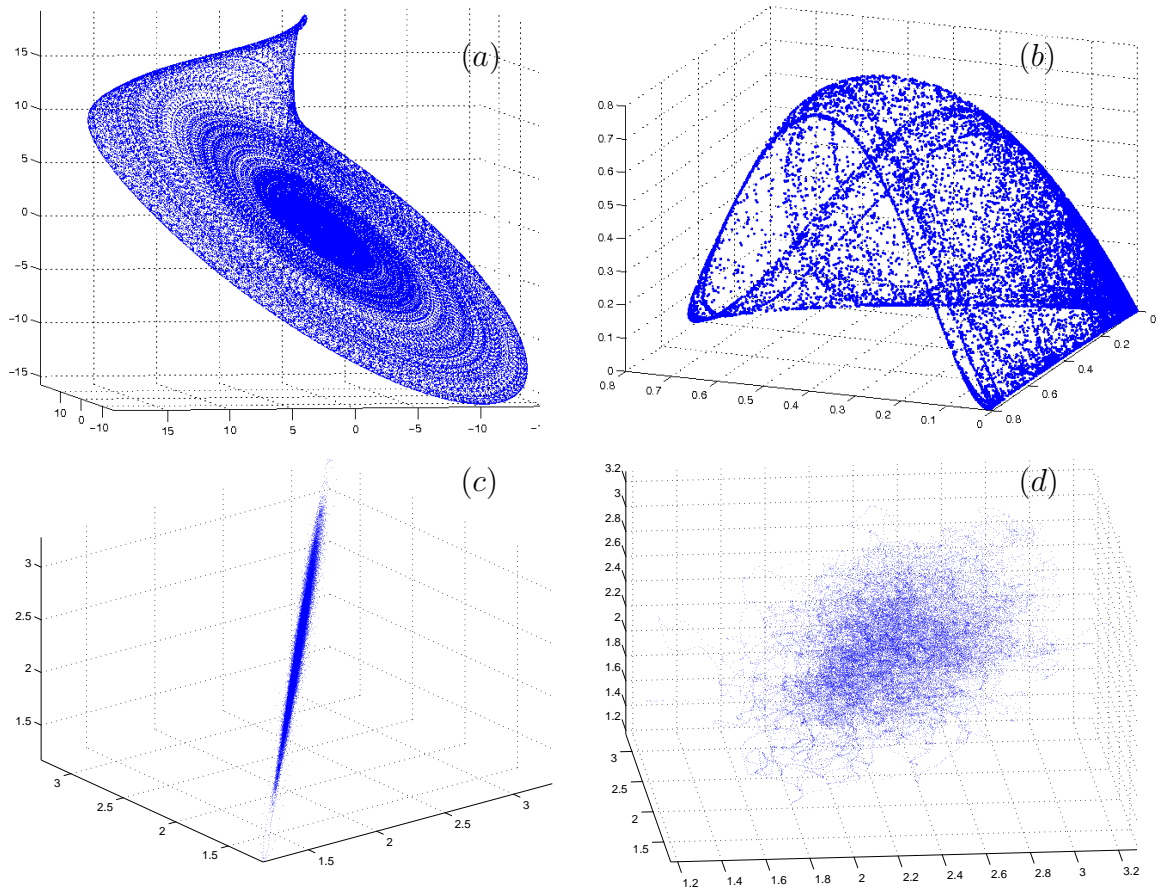


Figure 3.10: The embedding of (a) Rössler system eq.(3.3), (b) Blamforth eq.(3.5), (c) and (d) are for Oldenburg's airtank data [118] with the embedding dimensions equal to 3 and 10 respectively. There are no dramatic changes upon increasing the embedding dimension to more than 10.

not intersect. So one has to use different lags and higher embedding dimensions to disentangle the trajectories.

### 3.6 Dimensions reduction

Following the same line of thought which we started from the beginning and in order to minimize the processed quantities of data, the next method *principal component analysis (PCA)* combined with embedding and lagging could do the purpose. There are various names for the PCA method depending on the context, like for example *Karhunen-Lòve transform* used for second order stochastic processes, *independent component analysis (ICA)* used in multivariate data analysis (see [97], and [98]),

and *singular spectrum analysis* (SSA) in the context of dynamical systems [99]). The technique has to do with working with the time series represented by its main components i.e. the singular values, (gained from a singular value decomposition (SVD) ) in a delay embedding space [95].

First one should calculate the *covariance matrix*

$$C_{ij} = \langle x_i x_j \rangle = \frac{1}{N - m + 1} \sum_{n=1}^{N-m+1} x_{n-m+i} x_{n-m+j} \quad , \quad (3.11)$$

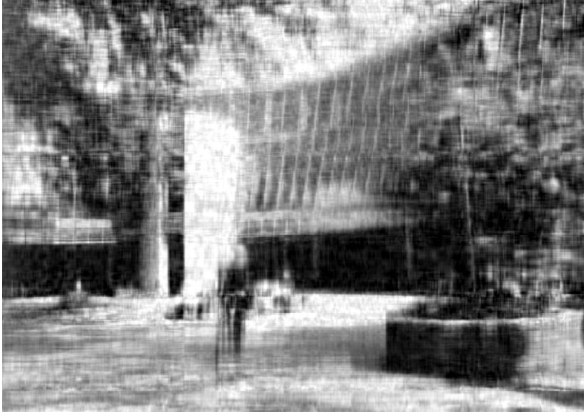
(a) true image rank = 588



(b) rank = 100



(c) rank = 25



(d) rank = 10



Figure 3.11: *PCA for Oldenburg university foto (2-d matrix) showing from (a)-(c) the rank of the matrix used in the approximation.*

where  $C_{ij}$  is the covariance matrix (which is actually the non-normalized Reynolds tensor ),  $x$  the time series,  $m$  the embedding dimension, and  $N$  is the length of the time series.

Second decompose the embedded covariance matrix by using a singular value decomposition (SVD) .

Generally, a matrix  $A_{m \times n}$  could be decomposed to  $A = USV^T$ , where  $U_{m \times m}$  is an orthogonal matrix and its columns are the eigenvectors of  $AA^T$ , while the columns of  $V_{n \times n}$  are the eigenvectors of  $A^T A$ . The matrix  $S$  is diagonal and contains the singular values of matrix  $A$  (see for example [100]). Upon performing the decomposition of the embedded covariance matrix (3.11) one could get the principal components by multiplying the singular values  $S$  by the eigenvectors  $U$ .

In fig. 3.11 the original photo was read as a matrix and then analyzed into its components using SVD and at last we have picked some of the ranks to manifest the usability of SVD as a dimension reduction method.

In fig. 3.12 a time series (one dimensional) was used (the Oldenburg airtank data [118]) in finding the PCA components (in this case it is called SSA). One notices how the other two components follow the original signal in its ups and downs.

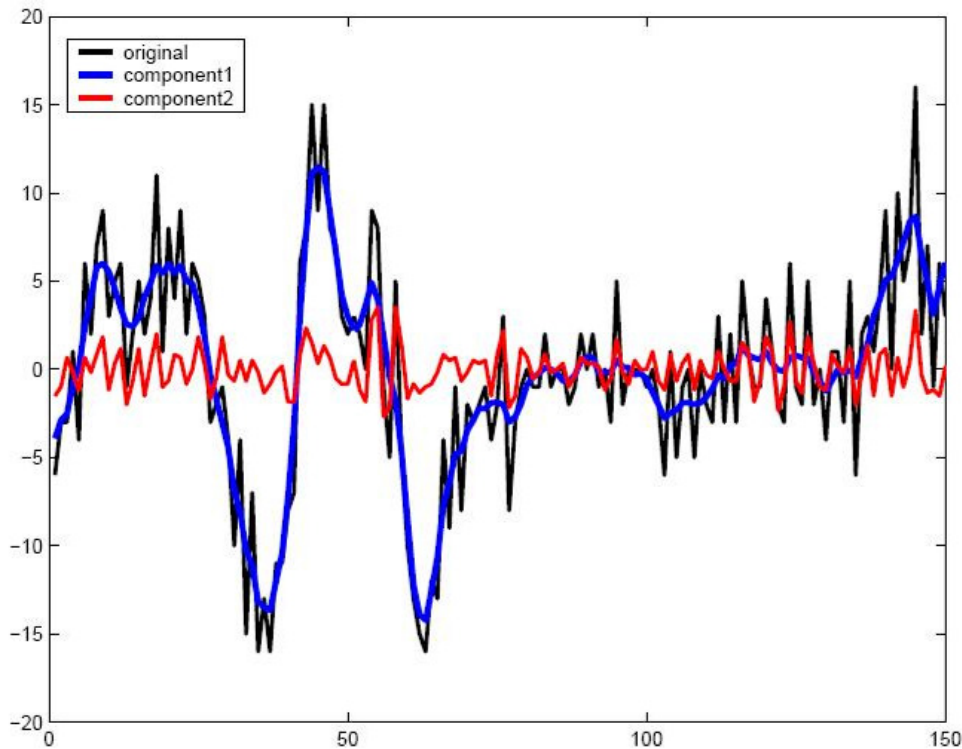


Figure 3.12: *Singular spectrum analysis (SSA) for the incremented turbulence data produced in Oldenburg's university airtank.*

# Chapter 4

## Statistical Turbulence

One of the basic concepts in turbulence has been introduced by Richardson [63] namely the energy cascade in turbulent flows. The idea is that the energy that is fed into a system produces large eddies (swirls) with large Reynolds numbers, and they are unstable. They break up and transfer their energy to smaller eddies. This process of eddy splitting and energy cascading is continued until stable eddies are produced, this is when the effect of the viscosity term in eq. (1.1) becomes larger than the effect of the nonlinear term. After that the kinetic energy is dissipated (thermalised or randomised) by viscosity.

This idea of energy cascading is quantified and measured by the structure functions.

### 4.1 Increments and structure functions

A structure function is the difference between the kinetic energies between two points in a flow. So the main element in the structure function is the velocity. This notion gives us another definition, namely, the increment  $\delta u$ , which is the difference in the velocity between two points. We could view the increment as a first order Taylor expansion for the velocity

$$u(x+r) - u(x) = r \frac{\partial u}{\partial x} , \quad (4.1)$$

where  $u(x)$  is the velocity at point  $x$ ,  $u(x+r)$  is the velocity at a later point in the time series and the distance between both points is  $r$ . From this we deduce that when we use increments and structure functions then we are talking about the velocity fluctuations since the mean of the velocity gets canceled out from the LHS

of (4.1).

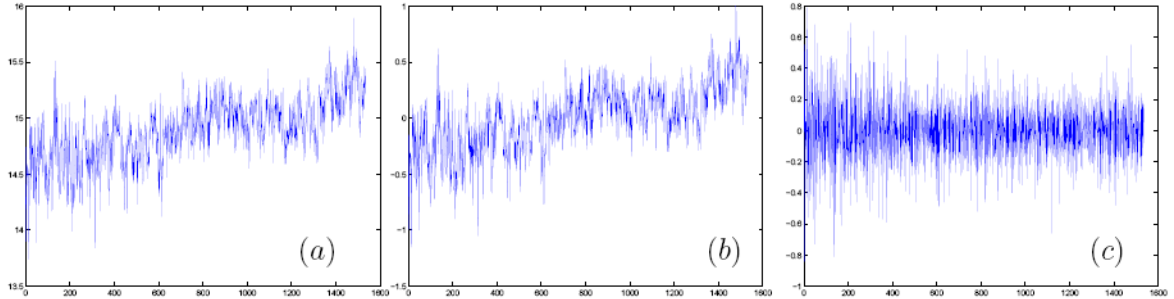


Figure 4.1: A temperature time series showing in (a) a global warming trend. In (b) the time series has been detrended and in (c) the structure function of the same time series in (a) is shown.

In fig. 4.1(a) the temperature time series shows seasonal trends in addition to the global warming trend, so the time series is non-stationary due to the dependence of the mean on time. Trying to get rid of the mean by subtracting it from the time series, it stays non-stationary as in fig. 4.1(b). In fig. 4.1(c) the structure function was used for the same time series and obviously the time series is rendered stationary (or at least weak stationary).

Another important issue is Taylor's Hypothesis of frozen turbulence which simply states that measuring the wind speed in one station at two different times is identical to taking measurements in two stations near each other at the same time, if the flow is stationary and homogeneous in the flow direction. This supplies the simple transformation between space and time which states  $x = \bar{u}t$  [75].

## 4.2 The scaling of the structure functions

From the following considerations one could infer the scaling law for the structure functions:

- We define first the fluctuation between two points which are a distance  $r$  apart from each other (or we say a fluctuation of a scale size  $r$ ) and a time scale  $t = r/\delta u$  by  $S_u(r) =: \delta u = |u(x+r) - u(x)|$ .
- We notice, as stated before, that the energy per mass unit is proportional to  $\propto (S_u(r))^2$ .
- The energy fed to the system and dissipated as heat per mass unit and time is  $\epsilon \propto (S_u(r))^2/t = (S_u(r))^3/r$ .

From the above we see immediately that the structure function scales as

$$S_u^2(r) = C.(\epsilon.r)^{2/3} \quad , \quad (4.2)$$

where  $S_u(r)$  is the increment  $C$  is the proportionality constant and is called Kolmogorov's constant. We could generalize the above by taking not only the 2nd exponent but by taking  $p$ -exponents

$$S_u^p(r) \equiv \langle |u(x+r) - u(x)|^p \rangle \quad , \quad (4.3)$$

where the brackets  $\langle . \rangle$  means averaging. Since we are talking here about stationary processes (the mean or the drift does not depend on the position or time) and it is assumed that these processes are *ergodic* then this averaging could be time averaging or ensemble averaging due to the equivalence between them. A stochastic variable is self-similar if it posses a unique exponent  $p$ , such that

$$u(x + \lambda r) - u(x) = \lambda^p(u(x+r) - u(x)) \quad , \quad (4.4)$$

otherwise (as we shall see later in this chapter) the structure is called a multifractal, which means that we have an exponent (or a dimension if we wanted to use the ideas of the last chapter) for every scale.

### 4.3 The Kolmogorov 1941 paper (K41)

In 1941 Kolmogorov [66] has shown that in a 3-dimensional fully developed turbulence, the spectrum in the *inertial subrange* of energy follows a power law scaling of the form

$$\langle |u(x+r) - u(x)|^p \rangle = C_p(\langle \epsilon \rangle r)^{p/3} \quad . \quad (4.5)$$

It is evident that the above equation is in physical space, but transforming it to Fourier space is as follows. First we write the equation in parameters suitable for the Fourier space with unknown exponents to be found later:

$$E(k) = C\epsilon^\alpha k^\beta \quad ,$$

where  $E(k)$  is the energy spectrum and is the Fourier transformation of the structure function (the second power of the increment) this is because the second order increment  $S_u^2(r)$  is itself the kinetic energy in physical space,  $C$  is a constant. Now, to find the values of  $\alpha$  and  $\beta$  we use dimensional analysis. Since the spectrum indicates the amount of turbulent kinetic energy contained in a specific length scale, then it is energy times length, written as  $\frac{L^2}{T^2}L$ . While on the RHS we have the

dissipation  $\epsilon$  which has the units of energy per time  $\frac{L^2/T^2}{T}$  and the wave number unit is  $\frac{1}{L}$ . Substituting these dimensions in the above equation we obtain

$$\left[ \frac{L^3}{T^2} \right] = \left[ \frac{L^2}{T^3} \right]^\alpha \left[ \frac{1}{L} \right]^\beta .$$

Equating the exponents of both sides to get  $2\alpha - \beta = 3$  and  $3\alpha = 2$  which gives  $\alpha = 2/3$  and  $\beta = -5/3$  and the spectrum is

$$E(k) = C\epsilon^{2/3}k^{-5/3} . \quad (4.6)$$

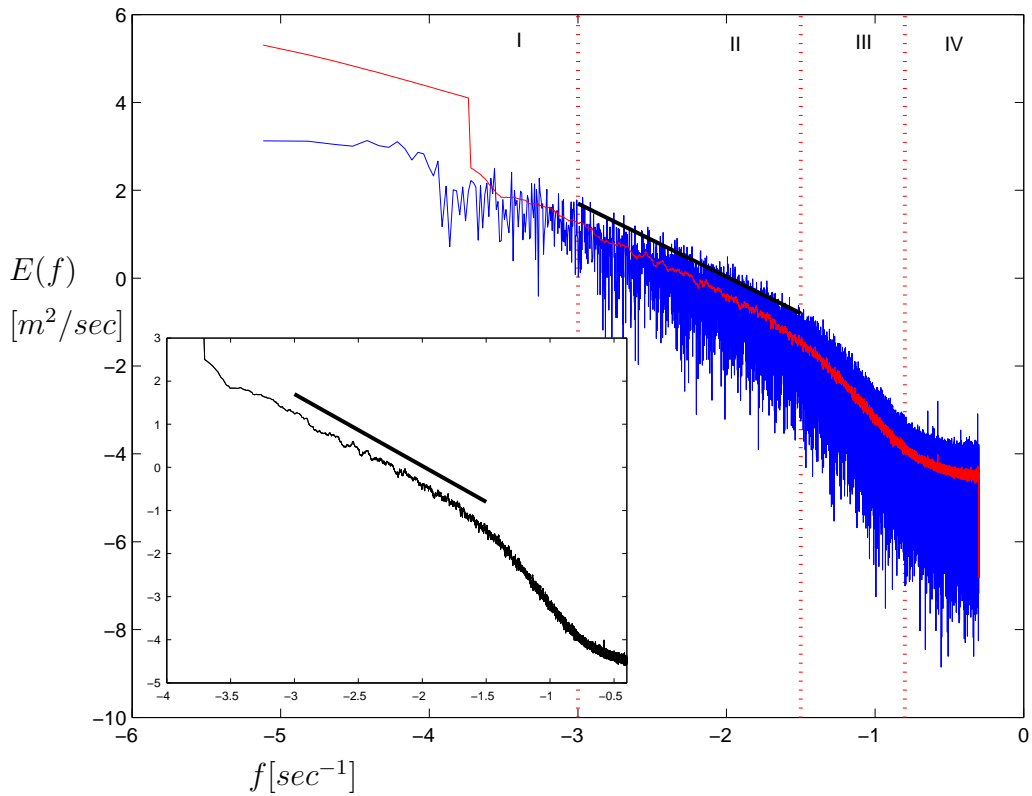


Figure 4.2: The spectrum of experimental data (the Oldenburg airtank). In the main figure a simple averaging filter was used to filter the original signal (in blue). The filtered signal is in red. Whereas in the inset a convolution was used for the same purpose i.e. filtering and also to show that both filtering techniques give the same result in the inertial range. In both figures the parallel line to the spectrum has  $-5/3$  slope. The figure shows also four distinct regions.

In fig. 4.2 the spectrum of a data set, which was produced in a free jet flow experiment in an air-tank in Oldenburg university laboratory, is shown. Two filtering methods were used in the figure. A simple averaging method (moving average) was used in the main figure and in the inset a convolution kernel (see chapter one in this thesis). We notice that the distribution of the energy on the different frequencies follows indeed eq.(4.6). Namely it is a power law of  $(-5/3)$  slope and this means that the process is scale invariant and the structure under study is self-similar [101] (see chapter 3 also).

In fig.(4.3) the spectrum of different signals were shown for comparison with fig. 4.2. In all of these figures one notices a deviation from the scaling of  $-5/3$  in the inertial subrange . In (a) one notices a flat spectrum  $E(k) \sim 1/k^0$  which means that the energy is distributed equally on all wave lengths and this is why it is called white noise. In (c), (d) and (e) we have signals with an energy spectrum of  $E(k) = f^{-2}$ , such an energy distribution is called brown or red noise. Two lines are drawn on the figure to try to figure out which scaling does the energy spectrum has a  $-2$  or a  $-5/3 = -1.667$  which is typical for turbulent signals as we have seen from eq. (4.6).

## 4.4 The autocorrelation and the structure function

An important tool that is used extensively in experimental physics and specifically in signal analysis is the autocorrelation. The autocorrelation is defined as: the expected value of the product of a random variable or signal realization with a time-shifted version of itself. In this way the autocorrelation provides a measure of dependence among the random variables of our signal. Thus a spatial correlation between two signals (measured with two hot wires for instance) is written as

$$R_{ij}(x, r, t) = \overline{u_i(x, t)u_j(x + r, t)} \quad , \quad (4.7)$$

while the temporal correlation with itself for a stationary process, or simply autocorrelation (measured with one hot wire for instance) is

$$R(\tau) = \overline{u(t)u(t + \tau)} \quad , \quad (4.8)$$

where  $R_{ij}$  is the correlation (the correlation coefficient is found by normalizing the correlation) ,  $x$  and  $r$  are the position and the shift (increment) series, and  $u_i$  and  $u_j$  are the two shifted velocities. While  $R(\tau)$  is the autocorrelation and  $\tau$  is the used lag whether it has time or spacial units since the two are equivalent because of the Taylor frozen turbulence hypothesis.

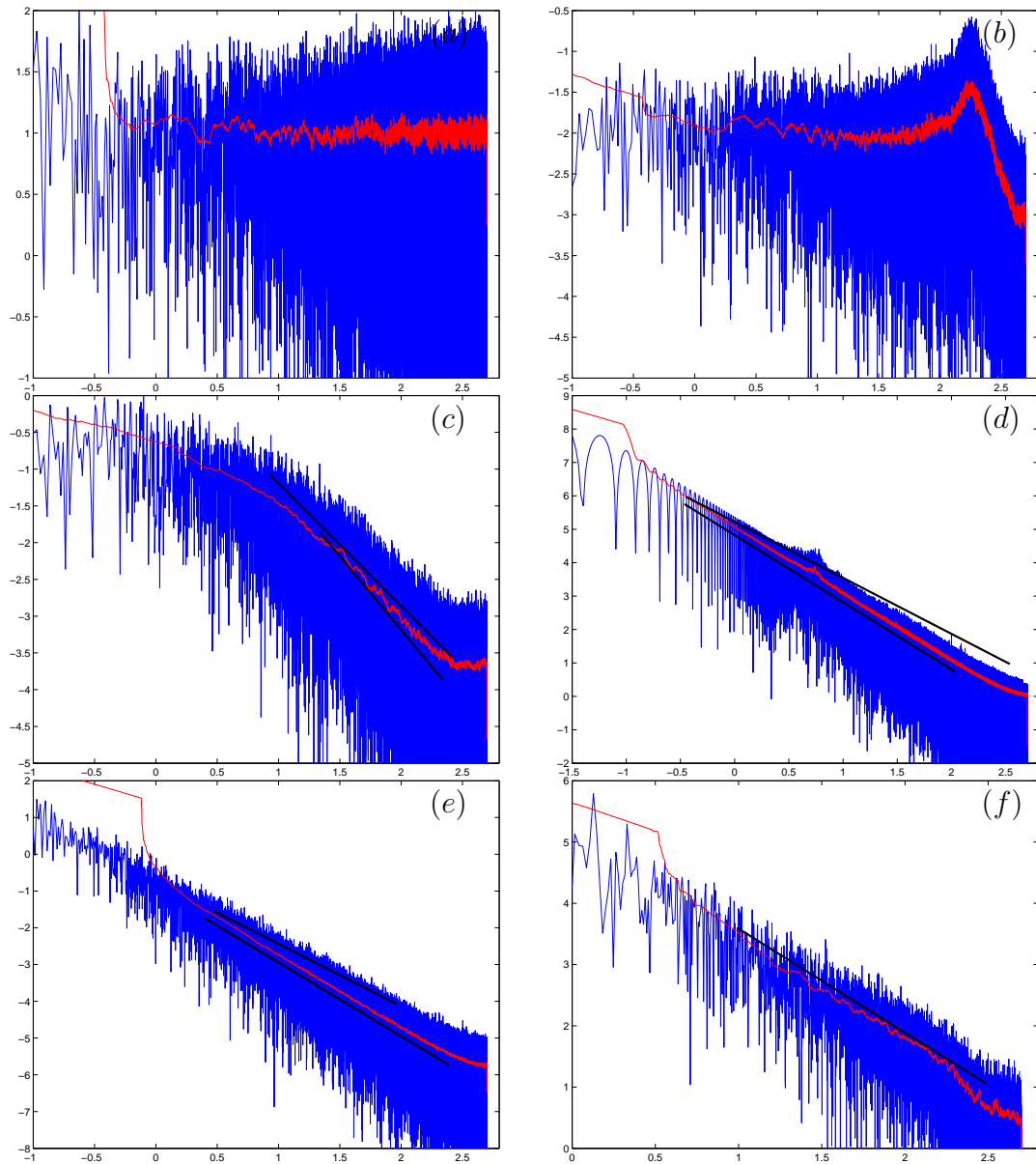


Figure 4.3: Spectra of different signals. The red represents the filtered signal: (a) Random signal from a Pareto distribution as in eq. (3.1). (b) Flare from eq.(3.7). (c) Flare from eq.(3.6). (d) Iran Earthquake. (e) Wiener process signal. (f) The pulsar GRO. In figures (c, d, e) there are two lines to approximate the spectrum. The upper has a  $-5/3$  slope and the one under the spectrum has a slope of  $-2$ . The y-axis in these figures is the energy spectrum  $E(f)$  and the x-axis is the frequency  $f$ .

It is important to mention here that we have already used the convolution to

filter a signal (see Fig. 4.2). The convolution is generally defined as

$$\mathcal{C}(t) \equiv (f * g)(t) = \int_{-\infty}^{+\infty} f(x).g(t - x)dx \quad . \quad (4.9)$$

On the other hand the correlation general definition is

$$\mathcal{R}(t) \equiv (f \circ g)(t) = \int_{-\infty}^{+\infty} f(x).g(t + x)dx \quad (4.10)$$

where  $f$  and  $g$  are any functions,  $C$  the convolution, and  $R$  the correlation. While this may appear to be similar, unlike the convolution where the series is reversed, in the correlation this is not the case. The integral thus no longer represents the output of a filter driven by an input signal as in fig.4.2. Rather it is a tool used to measure the similarity between two signals as it was pointed out earlier. As we will see later, a large correlation value (positive or negative if we are talking about the correlation and not the correlation coefficient) represents a strong similarity between the two signals, while a value near zero represents little similarity.

Another quantity which is mostly used in the literature is the autocorrelation coefficient (also called *autocorrelation function (ACF)* ). It is simply the normalized autocorrelation

$$ACF(\tau) = \frac{\overline{u(t)u(t + \tau)}}{\overline{u^2}} \quad , \quad (4.11)$$

where  $\overline{u^2}$  is the mean square value. In general one could prove the Schwarz inequality [106]

$$\overline{u(t_1)u(t_2)} \leq [\overline{u^2(t_1)}]^{1/2}[\overline{u^2(t_2)}]^{1/2} \quad , \quad (4.12)$$

for a stationary process the mean square value is independent of time, so that the RHS of eq.(4.12) is equal to  $\overline{u^2}$ . From eq.(4.12) and eq.(4.11) we see that

$$ACF(\tau) \leq 1 \quad , \quad (4.13)$$

this result is observed in fig.4.4.

We have mentioned earlier that the ACF does not depend on the absolute time if the flow is stationary. In addition to that it is easy to show that the autocorrelation does not depend on the absolute position in a homogeneous flow (space stationary flow) [27].

Describing a flow with the ACF is equivalent to its description with the structure function, due to the following

$$\begin{aligned}
 S^2(r) &= \langle (u(x+r) - u(x))^2 \rangle \\
 &= \langle (u(x+r))^2 \rangle - 2\langle u(x+r)u(x) \rangle + \langle (u(x))^2 \rangle \\
 &= 2\langle (u(x))^2 \rangle - 2R_{ij}(x, r)
 \end{aligned} \tag{4.14}$$

where we have used again the assumption that the flow is homogeneous and thus the ensemble averaging of the quantities  $\langle u(x+r) \rangle$  and  $\langle u(x) \rangle$  are equal to a constant. At last if we take the Fourier transformation of the ACF

$$\mathcal{E}(\omega) = \int_{-\infty}^{+\infty} e^{-i\omega\tau} \mathcal{R}(\tau) d\tau \quad , \tag{4.15}$$

the other Fourier transform pair is

$$\mathcal{R}(\tau) = \int_{-\infty}^{+\infty} e^{i\omega\tau} \mathcal{E}(\omega) d\omega \quad , \tag{4.16}$$

and the above two relations are general for any function. Now substituting  $\tau = 0$  in eq.(4.16) we get

$$\mathcal{R}(0) = \overline{u(t)u(t+\tau)} = \overline{u^2} = \int_{-\infty}^{+\infty} \mathcal{E}(\omega) d\omega \quad , \tag{4.17}$$

and this shows that the integration of the spectrum  $\mathcal{E}(\omega)d\omega$  in a bandwidth of  $d\omega$  is equal to the energy contained in the integrated frequencies. And in this way the link between the energy, the spectrum, the structure function, and the ACF is firmly established (at least for the second order increment).

## 4.5 The spectrum regions and the length scales

In fig. 4.2 we can distinguish four regions (subranges):

- Region I: This is the region where the system is forced (where the energy is fed into it). The phenomenological picture is, that one finds here the biggest eddies that the system could sustain. They are unstable and break up (cascade) to give smaller more stable eddies. The scales here are usually referred to as being the large scales  $L$ . Supposedly it resembles the physical size of the system where the flow is being forced, because this is the largest size  $L$  that

the eddies could take. Taking a look at the second term on the LHS equation (1.1) (because we are talking here about steady flow, we don't need to consider the first term) and at the viscous term on the RHS, we see that we could form a ratio between the convective forces (which scales as  $U^2/L$ ) and the viscous forces (scales as  $\nu U/L^2$ ). This ratio happens to be the Reynolds number at these scales [2]

$$Re_L = \frac{U^2/L}{\nu U/L^2} = \frac{UL}{\nu} \quad (4.18)$$

Furthermore, comparing the rates at which the turbulent structures are moved around by taking the diffusive time scale  $t_d$  derived from the kinematic viscosity units  $[L^2/T]$  and convective time scales  $t_L = L/U$ , we obtain again the same Reynolds number  $t_d/t_L = \frac{L^2/\nu}{L/U} = Re_L$ . Thus if  $Re$  is large, which means that the diffusive time is very large compared to the convection time, means that the inertial forces are larger than the viscous diffusive forces.

- Region II: This region is called the inertial subrange . In this region the energy is transferred from lower to higher wavenumbers. In this region there is no energy production and the of energy is still negligible as we have seen in the above discussion about Reynolds number. Hence the spectrum at this region is "independent of the viscosity of the fluid". The scaling of  $(-5/3)$  for the wavenumbers holds only in this region .
- Region III: The dissipation range . In this region the viscosity is more effective than it was in the previous range (region II).
- Region IV: The random region . In this region the energy is totally random and the kinetic energy which was fed into the system becomes merely thermal energy at these large wavenumbers, which has no more momentum to move the particles in currents as was the case in the region I.

The above distinction of regions leads to three different length scales which separate these regions.

### 4.5.1 The integral length scale ( $L$ )

Also called the outer scale in the Russian papers [2], is the first one on the LHS when one takes a look at the spectrum 4.2. It separates the large scales where the energy is fed on one side and the region where the energy is merely convected on the other side. It can be calculated by integrating the area under the autocorrelation coefficient curve until the first zero crossing for the x-axis

$$\mathcal{T}(\tau) = \int_0^\infty \mathcal{R}(\tau) d\tau \quad (4.19)$$

where  $\mathcal{T}(\tau)$  is the integral time scale, and the upper limit of infinity is formal because usually the autocorrelation crosses the zero before that (if the process has finite memory). The  $\mathcal{T}(\tau)$  is usually taken as a number with a single unit and not a double unit (area under the integral) and this is done by taking a rectangle with the height one, which is the highest value of the ACF, and the width of this rectangle is the result from eq.(4.19). The integral length scale  $L$  is obtained from the integral time scale  $\mathcal{T}(\tau)$  by multiplying the later with  $\overline{\tilde{u}^2} = \overline{u^2}$ . Thus,  $\mathcal{T}(\tau)$  is a measure of how long the turbulent fluctuations remain correlated and is used to estimate  $L$ . In Fig(4.4) the  $\mathcal{T}(\tau)$  is shown for two datasets: dataset (a) has  $Re = 27,000$  while for dataset (b)  $Re = 750,000$ . We notice that the correlation time is longer when  $Re$  is higher or one would say that the process has longer memory. If one tries to simulate the autocorrelation for a random process produced from an algorithm for a random number generator then one will notice that the process has no memory at all, i.e. the  $\mathcal{T}(\tau)$  has the value one at the beginning (because the random variable is 100 percent correlated with itself) and then falls immediately to zero (see also the Schwarz inequality eq.(4.12)).

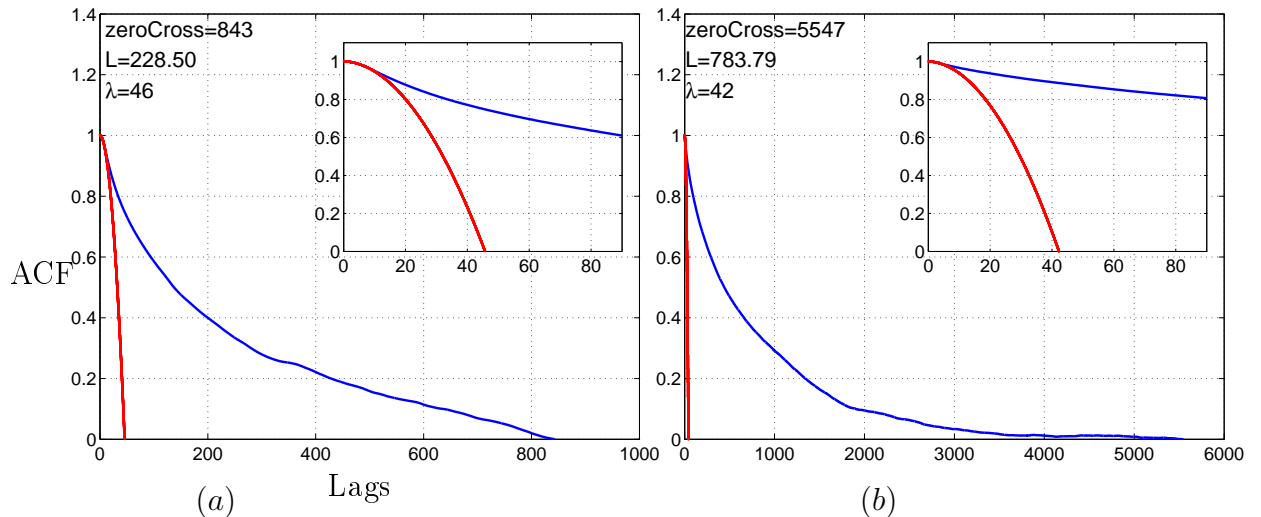


Figure 4.4: The autocorrelation function (ACF) (in blue color) of two data sets are shown: (a) the Oldenburg University wind canal dataset [118], and (b) the Grenoble dataset [105]. The inset shows the parabola intersection (the red line) with the x-axis which defines the Taylor microscale. The units of the lags are the tact of the measurements and the ACF is normalized.

## 4.5.2 The Taylor microscale ( $\lambda$ )

The Taylor microscale [104] which is supposedly the scale at which the viscosity begins to be effective. This microscale is calculated by Taylor expanding the ACF

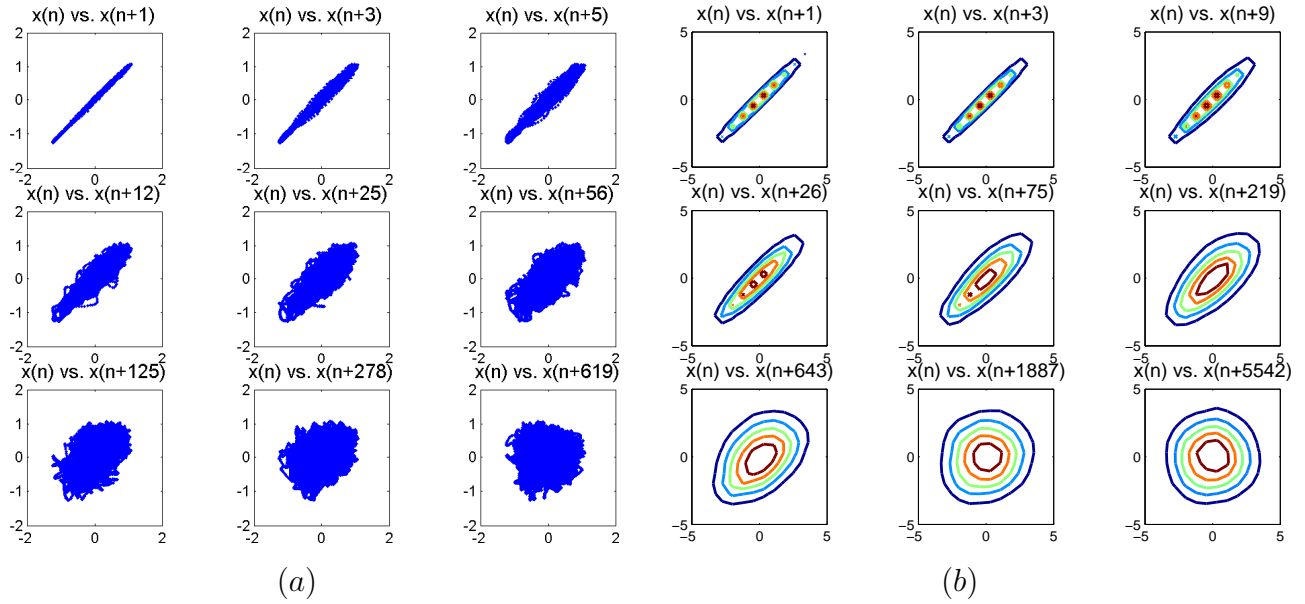


Figure 4.5: Scatter plots showing how the correlation deteriorates until the data becomes zero correlated (random, heat) when the ACF crosses the zero. In fig. (a) the crossing happens at 619 and shows the Oldenburg data [118] and for the RHS fig.(b) the crossing happens at 5542 and it shows Grenoble data [105]. Here the joint PDFs was used instead of the scatter plot and to the same effect.

around the origin

$$R(\tau) = R(0) + \tau R'(0) + \frac{1}{2}\tau^2 R''(0) + \dots \quad , \quad (4.20)$$

We know that  $R(0) = 1$  and  $R'(0) = 0$  (see eq.(11) in [103]). We round off until the term which contains  $\tau^2$ . When the Taylor microscale is defined as  $\lambda^2 = -\frac{2}{R''(0)}$  we have a parabola equation [103] and [102]

$$R(\tau) = 1 - \frac{\tau^2}{\lambda^2} \quad . \quad (4.21)$$

Simply it is at the point where the ACF deviates from its parabolic behaviour one extends a parabola which should meet the x-axis at the point that is called  $\lambda$ . This microscale is the radius of curvature of the spatial correlation at  $y=0$ . Based on the presentation above, it can be said that Taylor's microscale is just an intermediate length scale associated with the energy dissipated by turbulent eddies. In fig. 4.4 we show the ACF crossing the x-axis for two data sets. In fig. 4.4a the data set that was analysed was produced in the wind tunnel of Oldenburg university, while fig. 4.4b shows the same for Grenoble data [105]. In both  $\lambda$  was found by fitting a second order polynomial to the curvature of ACF.

### 4.5.3 The Kolmogorov scale ( $\eta$ )

The Kolmogorov scale (also called the inner scale [2]): where the energy is dissipated as heat.

$$\eta = \left( \frac{\nu^3}{\epsilon} \right)^{1/2}, \quad (4.22)$$

where  $\eta$  represents the smallest length scale the eddies could have.

## 4.6 The K62 and the intermittency

Since in general the structure functions scales to the difference between two measurements  $r$ , as we have seen in eq. (4.3), then one could generalize and write the following

$$S_p(r) \sim r^{\zeta_p}, \quad (4.23)$$

where  $\zeta_p$  is an exponent to be determined.

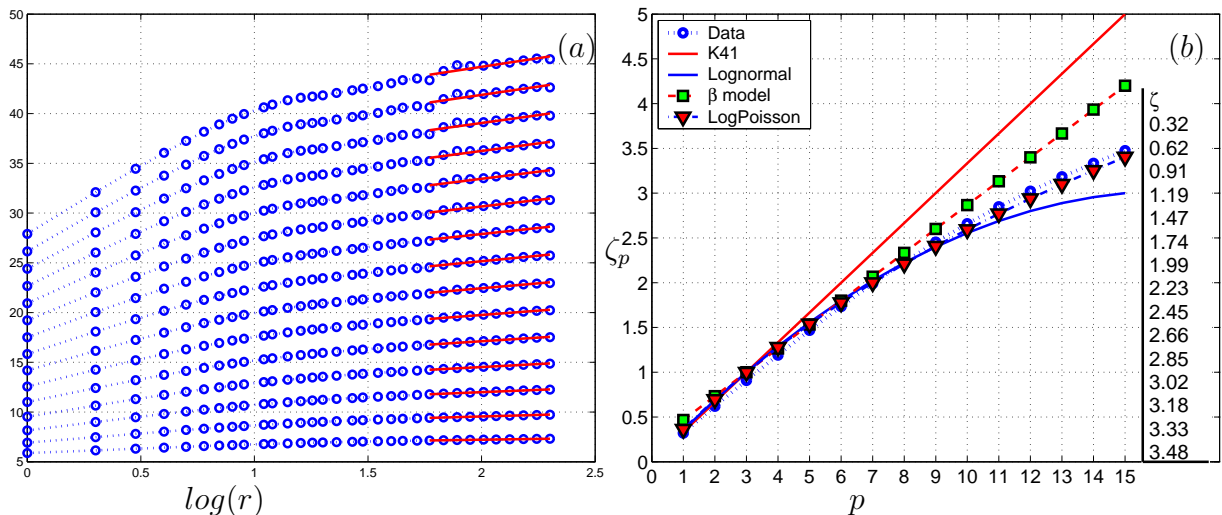


Figure 4.6: The scaling of the structure functions of the Oldenburg data. In (a) the y-axis represents the the structure functions from  $S_1$  until  $S_{15}$  and the x-axis are the increments  $r$  as in eq. (4.3). (b) Shows the exponents  $\zeta_p$  vs. the orders  $p = 15$ .

It is evident from fig.4.6b that the structure functions do not scale according to K41 as in eq.(4.5). Now, rewriting eq.(4.5) in another shape as in eq.(4.23) has the advantage of seeing the exponents as the slopes for the structure functions scaling as in the red slopes in fig.4.6a.

The exponents  $\zeta_p$  were given by the Kolmogorov-Oboukov *lognormal model* as

$$\zeta_p = \frac{1}{3}p - \frac{1}{18}\mu p(p-3) \quad , \quad (4.24)$$

where  $p$  is as before the order of the structure function and  $\mu$  is the intermittency [107].

The lognormal model has the defect that as  $p \rightarrow \infty$ ,  $d\zeta_p/dp < 0$  and this is a decreasing function which gives supersonic speeds and the flow is not incompressible any more [101] which mean that the Navier-stokes equations are not valid anymore which is actually not the case.

Other models for the  $\zeta_p$  are the  $\beta$ -*model* and the *log-Poisson model* which gives for the exponent

$$\zeta_p = \frac{1}{3}p - \frac{1}{3}\mu(p-3) \quad , \quad (4.25)$$

and in the case of the log-Poisson model [101]

$$\zeta_p = \frac{p}{9} + 2 - 2 \left( \frac{2}{3} \right)^{p/3} \quad , \quad (4.26)$$

where  $p$  and  $\mu$  are defined as before.

The generalized equation of the scaling of the exponents of the structure functions i.e. eq. (4.23) is motivated by the fact that the scaling diverges from the K41 (as it is clear from figure 4.6 and this deviation from K41 is explained by noticing that the self-similarity of the structures are broken [101] but also by the suggestion the the dissipation  $\epsilon$  scales as  $r$  (see 4.5 and one of the next sections on dissipation ) and that the two could be joined together as in eq.(4.23).

We notice from eqs.(4.24) and (4.25) that when  $p = 3$  then they both give  $\zeta_3 = 1$  which is the same value of the exponent as in K41. Moreover, when  $p = 6$  both eqs.(4.24) and (4.25) give us again the same exponent namely  $\zeta_6 = 2 - \mu$  which is lower than the K41 by the amount  $\mu$ . As for the log-Poisson model eq. (4.26) the story is different: we still get  $\zeta_3 = 1$  but  $\zeta_6 = 16/9$  and there is no mention of the adjustable parameter  $\mu$  which is the intermittency .

## 4.7 Extended self-similarity (ESS)

Kolmogorov's four-fifth law (see [113]) is written as

$$S_3(r) = -\frac{4}{5}\epsilon r + 6\nu \frac{d}{dr} S_2(r) \quad , \quad (4.27)$$

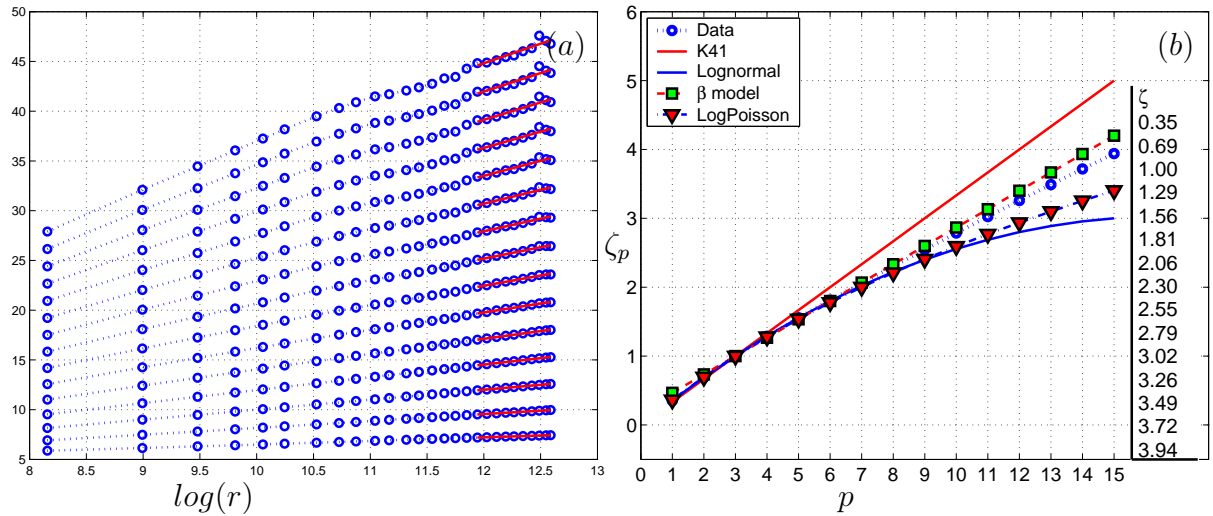


Figure 4.7: (a) Shows the ESS for 15 structure functions exponents (for Oldenburg data 125,000 points) with a least square fitted slope (in red color) on a logarithmic scale. (b) The scaling of the structure functions for the ESS case. Shown also the linear K41 (red) and the lognormal (continuous blue).

see [114] ([111] and the references therein). For small  $r$  values we can neglect the second term on the RHS. This means that the 3rd order structure function is of the order of  $r$ . This was the reason behind writing eq. (4.23) as

$$S_p(r) \sim S_3(r)^{\zeta_p} \quad , \quad (4.28)$$

which means that instead of taking the scaling of the structure functions as  $\log(r)$  one takes  $\log(S_3)$ . This was called *extended self-similarity* (ESS) because in this way the self-similar structures which exist in the inertial subrange of the spectrum is extended deep into the dissipative region, this is the reason behind noticing longer straight structure functions in fig.4.7a than the ones in fig.4.6a. In fig.4.8 the order of exponents was taken till 20 following [116]. Due to the limited number of data used in these analysis (8 million points) the exponents that make sense are until the  $p = 6 - 8$  (see for example [112]).

## 4.8 Dissipation

Kolmogorov's universal equilibrium theory assumes that the rate of energy supply to a system equals the *dissipation rate*. Hence, an estimation to the dissipation rate could be immediately established by multiplying the kinetic energy of the large scales  $u^2$  by the rate at which this energy is delivered to the small scales  $u/L$ . So

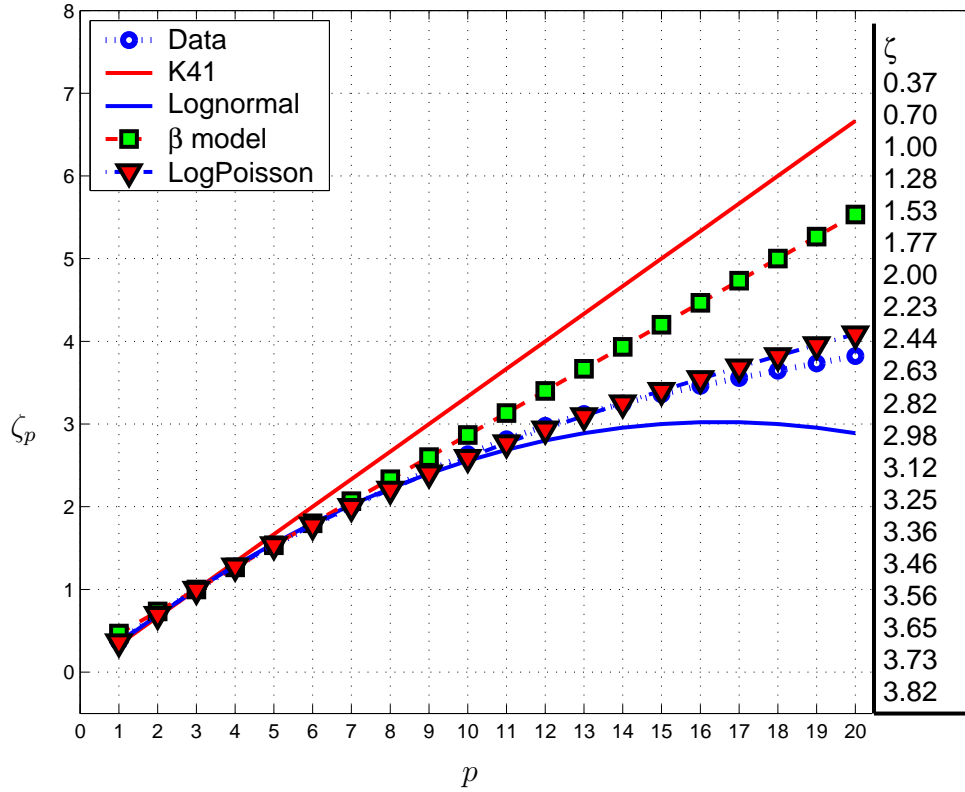


Figure 4.8: *The ESS scaling until the 20 exponent for 8 million points from Grenoble data showing all scaling models just like before.*

the energy that is dissipated is proportional to [102]

$$\epsilon \sim u^2 \cdot \frac{u}{L} = \frac{u^3}{L} , \quad (4.29)$$

where  $L$  is the integral scale. The above equation means that one could estimate the dissipation rate without involving the viscosity. Written in another way, as (see [115])

$$\langle |u(x+r) - u(x)|^3 \rangle \sim \langle \epsilon \rangle r , \quad (4.30)$$

which is the four-fifth law eq.(4.27)

Upon transforming the dynamic equation of homogeneous turbulence [106] (which is actually eq.(1.16)) into Fourier space

$$\frac{\partial R_{jl}(r, t)}{\partial t} - T_{jl}(0, r, t) = 2\nu \nabla^2 R_{jl}(r, t) + P_{jl} , \quad (4.31)$$

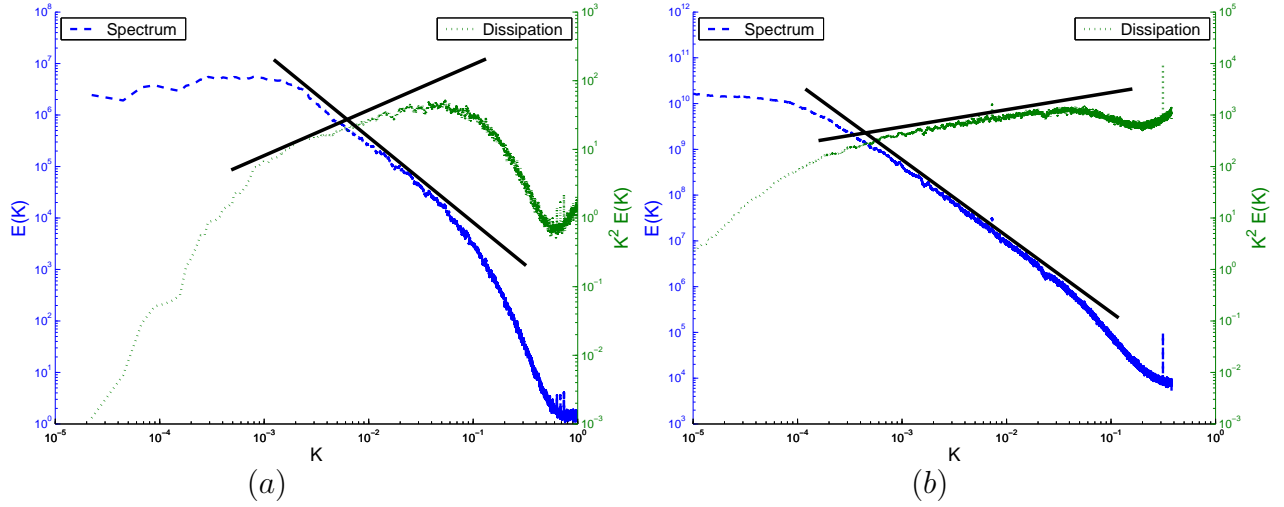


Figure 4.9: The spectrum of (a) the Oldenburg data [118] and (b) Grenoble data [105]. On both one could see the energy spectrum (compare with fig. 4.2) in blue dashed line, which scales as  $-5/3$ , and the dissipation spectrum gained from the energy spectrum multiplied by  $k^2$  in dark green dotted line and its scaling is  $1/3$ . For each figure there are two y-axis the left one belongs to the energy spectrum and the right one to the dissipation spectrum. The x-axis in both figures is the wave number.

we get

$$\frac{\partial E}{\partial t} = T(k, t) - 2\nu k^2 E(k, t) \quad , \quad (4.32)$$

where  $R_{ji}$  is the ACF,  $P$  are the pressure terms multiplied by the velocity and this correlation is zero,  $E$  is the energy,  $T$  is a triple tensor which integrates to zero  $\int_{-\infty}^{\infty} T(k, t) dk = 0$  (because in the inertial subrange this term only transfer the eddies so it is a conservative term),  $\nu$  is the viscosity, and  $k$  is the wave number. Integrating eq. (4.32)

$$\frac{\partial}{\partial t} \int_{-\infty}^{\infty} E = -2\nu \int_{-\infty}^{\infty} k^2 E(k, t) \quad , \quad (4.33)$$

and the RHS of eq. (4.33) integrates to  $dK/dt$  which is the kinetic energy during the process (as could be seen from the RHS), and this equals

$$D(k) = 2\nu k^2 E(k) \quad , \quad (4.34)$$

the dissipation spectrum  $D(k) = -dK/dt$  according to the theory of universal equi-

librium . Now this dissipation spectrum could be simplified to

$$D(k) \sim 2\nu k^2 k^{-5/3} \sim k^{1/3} , \quad (4.35)$$

upon using eq.(4.6). The fact that the dissipation spectrum scales as  $1/3$  is evident from fig.4.9(a) and (b), where in (a) it seems that the number of used points were not enough (125,000 points).

Now, the scaling of the dissipated energy could be looked at through eq. (4.23). We start with by writing the structure function scaling of the energy by using the log-normal model eq.(4.24)

$$S_p(r) \sim r^{\frac{1}{3}p - \frac{1}{18}\mu p(p-3)} , \quad (4.36)$$

which transforms to

$$\frac{S_p(r)}{r^{\frac{1}{3}p}} \sim r^{-\frac{1}{18}\mu p(p-3)} , \quad (4.37)$$

which means that the scaling of the structure functions in the dissipative field should behave like the RHS of the proportionality (4.37) (which should be written on the light of the last statement as  $\langle |\delta\epsilon_r|^p \rangle$ ). If  $p = 3$  then (4.37) is the same as eqs. (4.29) and (4.30) or the four-fifths law (see [101]).

In fig. 4.10 the scaling of the dissipation is shown and according to eq.(4.37) but also by using the extended self-similarity (ESS) . In (a) the lognormal model eq. (4.24) coincides exactly on the dissipation structure function when taking  $\mu$  equal to 0.24 (compare this value with the value mentioned in [121] which is 0.25 for high Reynolds numbers). In (b) it is evident how difficult it is with the  $\beta$  model eq. (4.25) to achieve the same success as the lognormal model.

Now, taking K62 into consideration the spectrum should be corrected accordingly (see eq.(4.37) for instance), were it should be written as

$$E(k) \sim k^{-\frac{5}{3} - \frac{\mu}{9}} , \quad (4.38)$$

were we have used the lognormal model (eq. (4.24)) with  $p = 2$  (see for instance [119]). Accordingly eq. (4.35) could now be written as

$$D(k) \sim 2\nu k^2 k^{-\frac{5}{3} - \frac{\mu}{9}} \sim k^{\frac{1}{3} - \frac{\mu}{9}} , \quad (4.39)$$

which is a value too small to be seen or measured from a curve like fig.4.9. Especially, when one considers that using a moving average or a convolution to smooth the

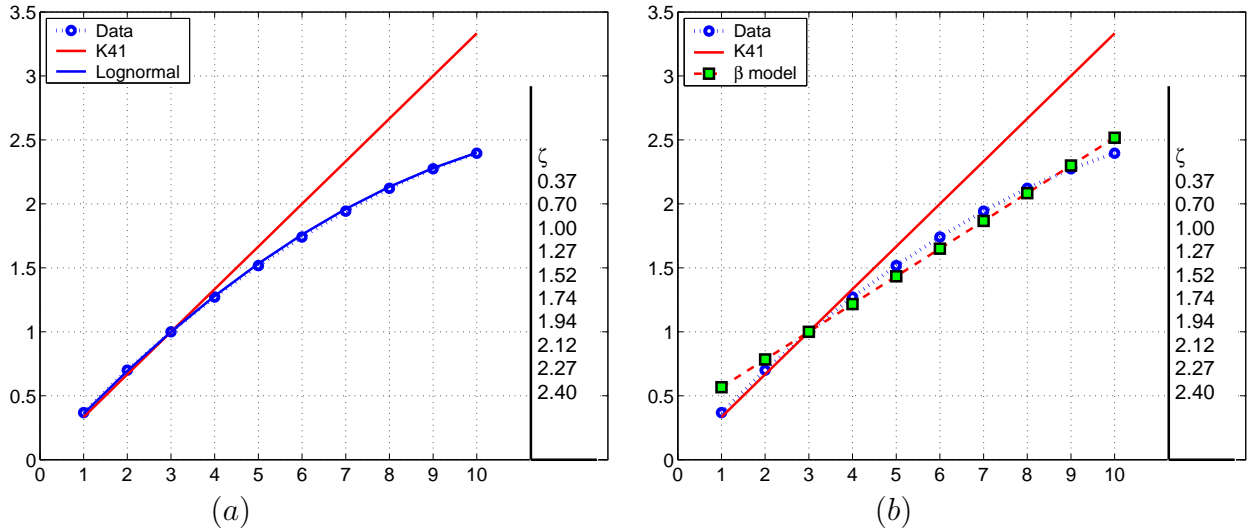


Figure 4.10: The scaling of the dissipative structure functions of the Grenoble data (8 million points) [105]. In (a) the scaling was compared with the lognormal model eq. (4.24) and taking  $\mu = 0.24$ . In (b) the dissipation was compared with the  $\beta$  model eq. (4.25) and taking  $\mu = 0.35$ .

spectrum curves has a big impact on defining the large scale ( $L$ ) if one tries to use a least square estimation to fit a slope to the curve between Taylor's scale  $\lambda$  and  $L$ .

## 4.9 Probability density functions (PDF's)

Yet another tool for describing turbulence is the probability density function . A turbulent variable like the velocity  $\tilde{u}(x, t)$  is given by the PDF and its moments defined as [2]

$$\langle \tilde{u}^n \rangle = \int_{-\infty}^{+\infty} \tilde{u}^n P(\tilde{u}) d\tilde{u} , \quad (4.40)$$

where the brackets  $\langle . \rangle$  means ensemble averaging, and  $P(\tilde{u})$  is the PDF or the histogram of  $\tilde{u}$  and it is usually normalised

$$\int_{-\infty}^{+\infty} P(\tilde{u}) d\tilde{u} = 1 . \quad (4.41)$$

In the above equations (4.40) and (4.41) we have used the whole velocity  $\tilde{u}$  but we could instead write these equations by using only the fluctuations  $u$  because we are still dealing with statistically steady (i.e. stationary) flows.

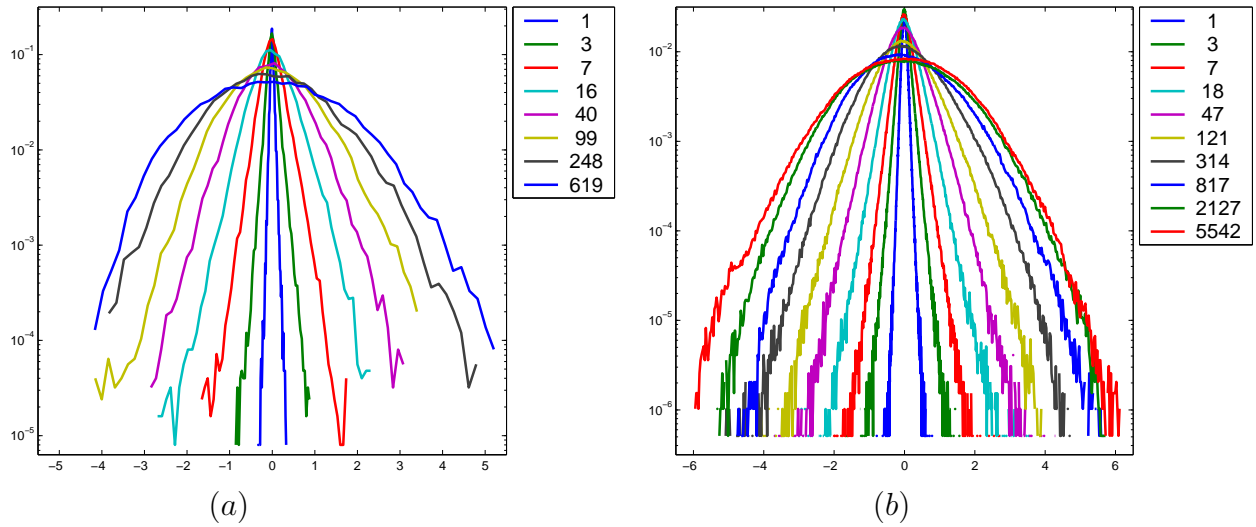


Figure 4.11: The PDF's of (a) the Oldenburg data [118] and (b) Grenoble data [105].

There is also the joint PDF ( $P_j$ ) which tells whether a processes described by many variables show dependency between these variables. For two variables it is usually written as (see fig.4.5b) [2] [101]

$$\int_0^{+\infty} \int_{-\infty}^{+\infty} P_j(u, v) du dv = 1 \quad . \quad (4.42)$$

The various exponents of our measured variable are called the moments . The first moment is the mean as in eq. (1.4) or alternatively

$$\langle u \rangle = \int_{-\infty}^{+\infty} u P(u) du \quad , \quad (4.43)$$

and this quantity is usually made equal to zero, i.e. that is to say the time series is detrended. One should note here that detrending has to be done with carefulness. If for example we are analyzing temperatures one should deal with the different trends (daily trend, seasonal trend and there is also the *global warming trend*) separately.

The departure from the mean value is called the variance

$$\langle u^2 \rangle = \int_{-\infty}^{+\infty} u^2 P(u) du \quad , \quad (4.44)$$

and as we have seen before this happens to be the turbulent kinetic energy (see for instance eq.(1.14)).

Other important moments are the skewness and kurtosis (flatness) . Which describe the symmetry around the y-axis and how far the tails of the PDF go parallel to x-axis (i.e. how long the memory of the process is), respectively. And this is how Gaussian (random) processes differ from turbulent processes, the last have long-tailed (also called thick- or enhanced- tail) PDF's. This divergence from Gaussianity (which have the characteristic values of skewness = 0 and kurtosis = 3) is due to intermittency.

$$F(r) = \frac{S_4(r)}{S_2(r)^2} = \frac{\langle |u(x+r) - u(x)|^4 \rangle}{\langle |u(x+r) - u(x)|^2 \rangle^2} . \quad (4.45)$$

In fig. 4.11 two data sets were taken and they were incremented. We notice that only upon reaching the increment where the ACF crosses the x-axis (see also fig. 4.5) the PDFs of the incremented data becomes Gaussian. In addition to that we see in fig. 4.12 that upon reaching the Gaussian distribution of the data it will stay Gaussian and increasing the number of the used increments will not change anything.

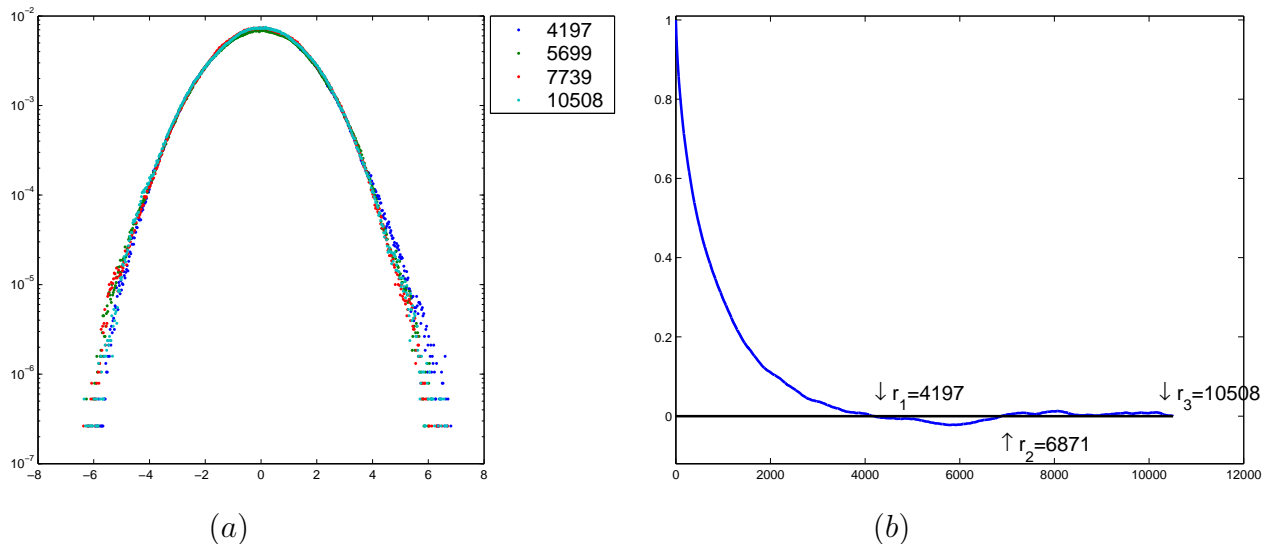


Figure 4.12: PDF's of the Grenoble data [105] and its correlation. The first PDF was taken at the first zero crossing i.e.  $r_1 = 4197$ , and the other PDF's are taken at each further crossing. This shows that the PDF's keep its Gaussian distribution (the fact that they fall on each other) as long as the first zero-crossing has been passed.

Not all PDFs tend to end in a Gaussian distribution after incrementing till the zero crossing of the autocorrelation. In fig.4.13(a) the PDF of Blamforth attractor eq. (3.5) seems to tend towards a uniform distribution otherwise one notices skewness in the data. One notices skewness too in the PDF of the data of the flare attractor eq. (3.6) which is not Gaussian either.

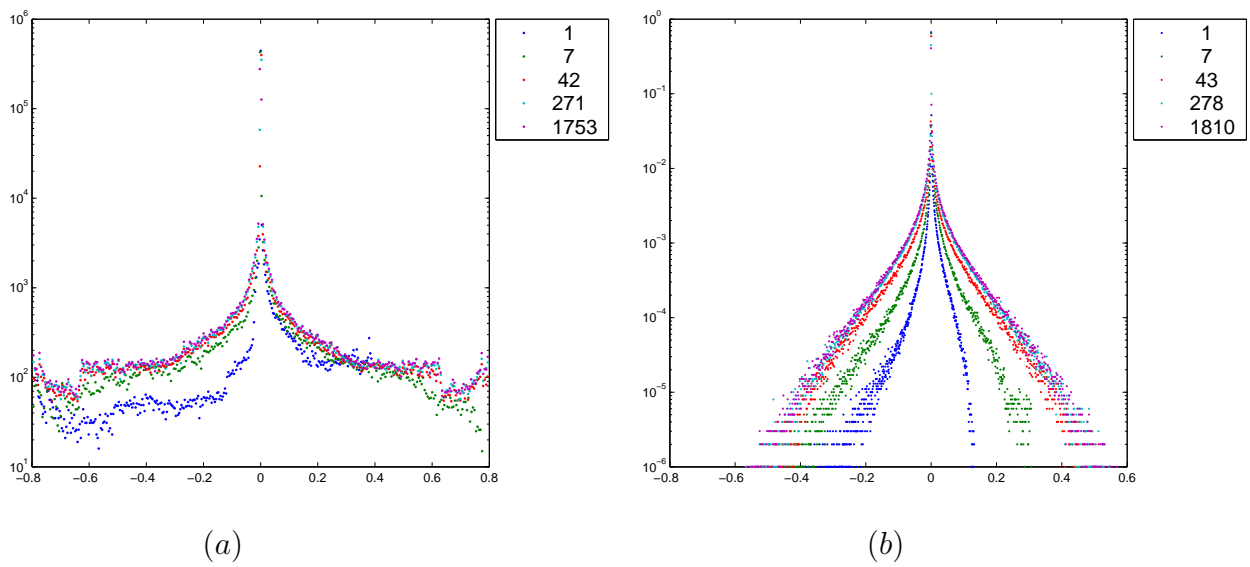


Figure 4.13: The PDF's of (a) Blamforth's attractor eq.(3.5) which seems that it has a uniform distribution after incrementing. (b) is the PDF of eq. (3.6).

# Chapter 5

## Financial Diffusion

The main objective of analyzing financial time series is to understand how prices and other financial instruments behave. The variance (volatility) of these series is the most important parameter. So foreseeing the prices of stocks of tomorrow could be described theoretically with a statistical model. But then also, and actually as an immediate goal, one needs these predictions about the prices to reduce risk and have successful insurance policies and regulations.

Since in the financial context one does not speak of a movement of a price either to the left or to the right as we have seen with the basic master equation (2.14), but rather the prices go either up or down, one could depict here again a  $(1 + 1)$  dimensional lattice with the prices following a random walk path on it. This is why the term financial diffusion is convenient to use, of course, in addition to other considerations that will be elaborated later.

### 5.1 The DAX index data analysis

The main purpose of the previous analysis tools is to take the order of the observations (the measured points of the time series) into account and try to learn something about the data set such as periodicities, trends, repeating patterns, and use such characteristics to infer something about the process being observed (calculate the volatility for instance). One such tool is the autocorrelation as previously defined in eqs. (4.7 or 4.11). If the time-series is non-stationary (the trend and volatility change with time), then the ACF will not come down to zero except for very large values of the lag. When the variance of the random process is constant (as is with the previous turbulence data), we speak of *homoscedastic process*. One could see that by simply taking pieces of different sizes of the turbulent data and check its

PDF. Its opposite is called *heteroscedastic process*, i.e. the variance changes with the amplitude of the signal (often it is simply proportional to it). We will return to the subject of non-stationarity later on.

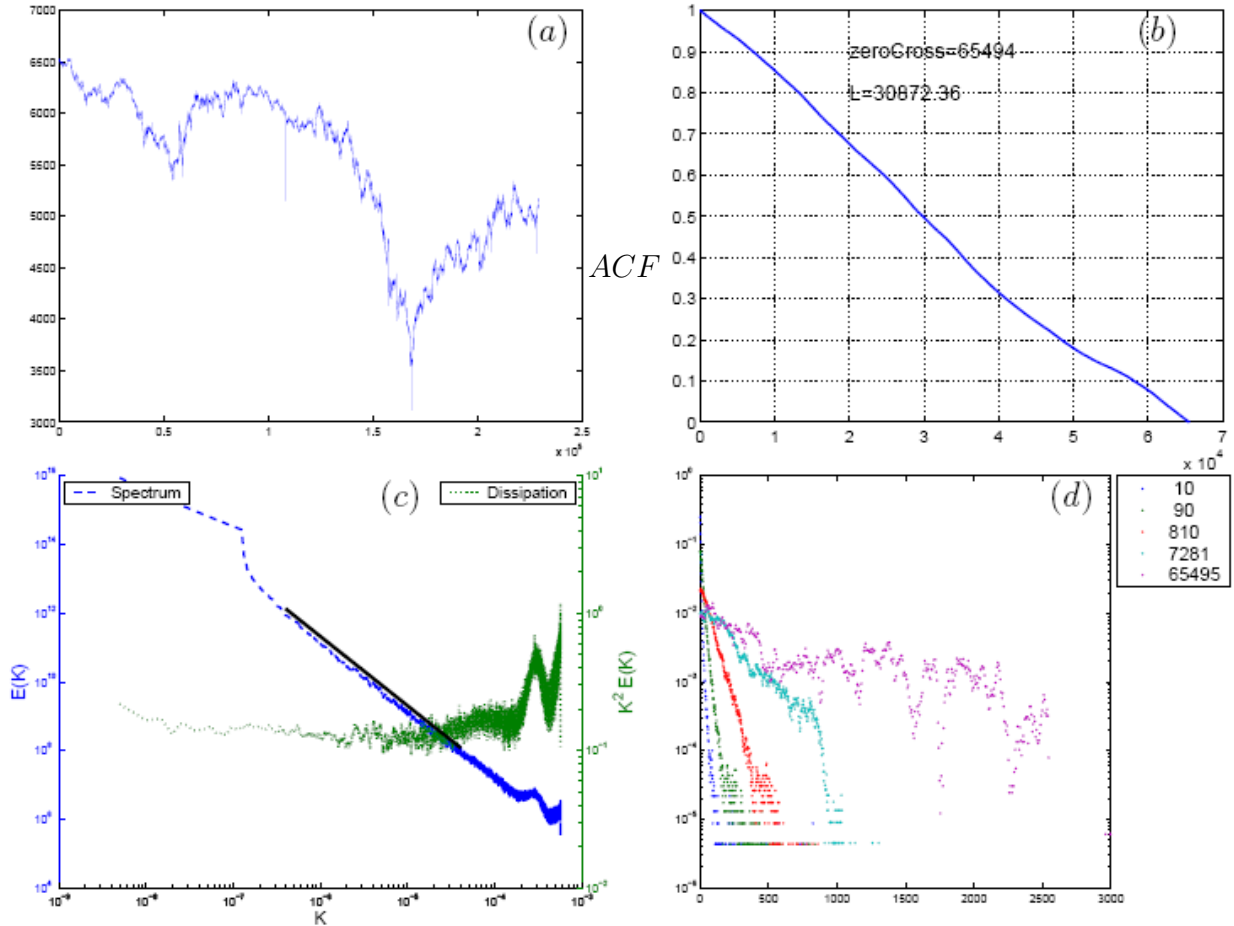


Figure 5.1: (a) Time series of the DAX 16.02-31.12 of the year 2001 [122]. (b) the autocorrelation function (ACF) of the DAX data. (c) Its spectrum and dissipation spectrum. (d) Its PDFs.

The tools of the previous chapters were used to analyze the DAX data (Deutsche Aktien Xchange 30 or the German stock market index) as in fig.5.1. From fig.5.1(a) we notice from the time series that the data are not stationary (at least one could see from the figure that its mean is a function of time). In fig.5.1(b) we see that the ACF is indeed very long due to the above effect (the mean is a function of time). As for the spectrum in fig.5.1(c) it has the usual  $-2$  slope for a Wiener Process (will be discussed later). The spectrum does not show any changes of frequencies in the elapsed time of the process which is indeed a very poor tool in this respect

for the same above reasons (i.e. the dependence of statistics on time). As for the PDFs in fig.5.1(d) it shows the usual non-Gaussian behaviour as a signature for the dependency (correlatedness) of the data.

Solving the problem of non-stationarity by using the structure function (the return in the financial context ) instead of the values of the index themselves, is no solution (like it was before in fig.4.1). Using the return instead of the values of the DAX index makes the autocorrelation drop immediately to zero and the spectrum becomes flat which are the signatures of white noise . The reason for that is, that processes like the DAX index and the models that simulate it are Markovian processes (which will be defined in the following).

## 5.2 The Wiener process as a model for financial Data

A Wiener process is also called standard Brownian motion . A Wiener process  $W_t$ , which is random and time dependent i.e. non-stationary, must satisfy the following conditions [125]:

- Its increments

$$\Delta W_t = \eta \sqrt{\Delta t} \quad , \quad (5.1)$$

where  $\eta$  is a normally distributed random variable with zero mean and unit variance.

- The increments  $\Delta_t$  are independent from each other. So the process is *Markovian* which means that any past information is irrelevant to the future or put more exactly the next realization depends on the present value [124].

Using the above two conditions in addition to taking  $W(0) = 0$ , one could write an algorithm for a Wiener process upon using eq. (5.1) as:

$$W_t = W_{t-1} + \Delta W_t \quad , \quad (5.2)$$

Now, we could generalize this process by giving the white noise  $\eta$  (in eq. (5.1)) any value for its mean (or drift) and variance (or volatility),  $\mu$  and  $\sigma$  respectively. So the new Gaussian noise now becomes  $x = \mu + \sigma * \eta$  and the expectation value of the new stochastic variable  $x$  is  $E[x] = \mu + \sigma * E[\eta] = \mu$ , while its variance is  $V[x] = \sigma^2 * V[\eta] = \sigma^2$ . So, the new generalized Wiener process is now written as:

$$x_t = x_{t-1} + \mu t + \sigma \eta \sqrt{t} \quad , \quad (5.3)$$

A continuous version for the above eq.(5.3) is written as [123]

$$dx_t = \mu dt + \sigma dW_t . \quad (5.4)$$

Fig. 5.2(a) is for a Wiener time series, which is clearly non-stationary, in 5.2(b) its autocorrelation is shown, which again disintegrates after a long time. In fig.5.2(c) the spectrum of the process is shown with two slopes, the one underneath is the  $-2$  slope and the above is  $-5/3$  slope, which is typical for turbulence. While in fig.5.2(d) the PDFs resemble again the same behaviour which we have met in the above section with the DAX analysis.

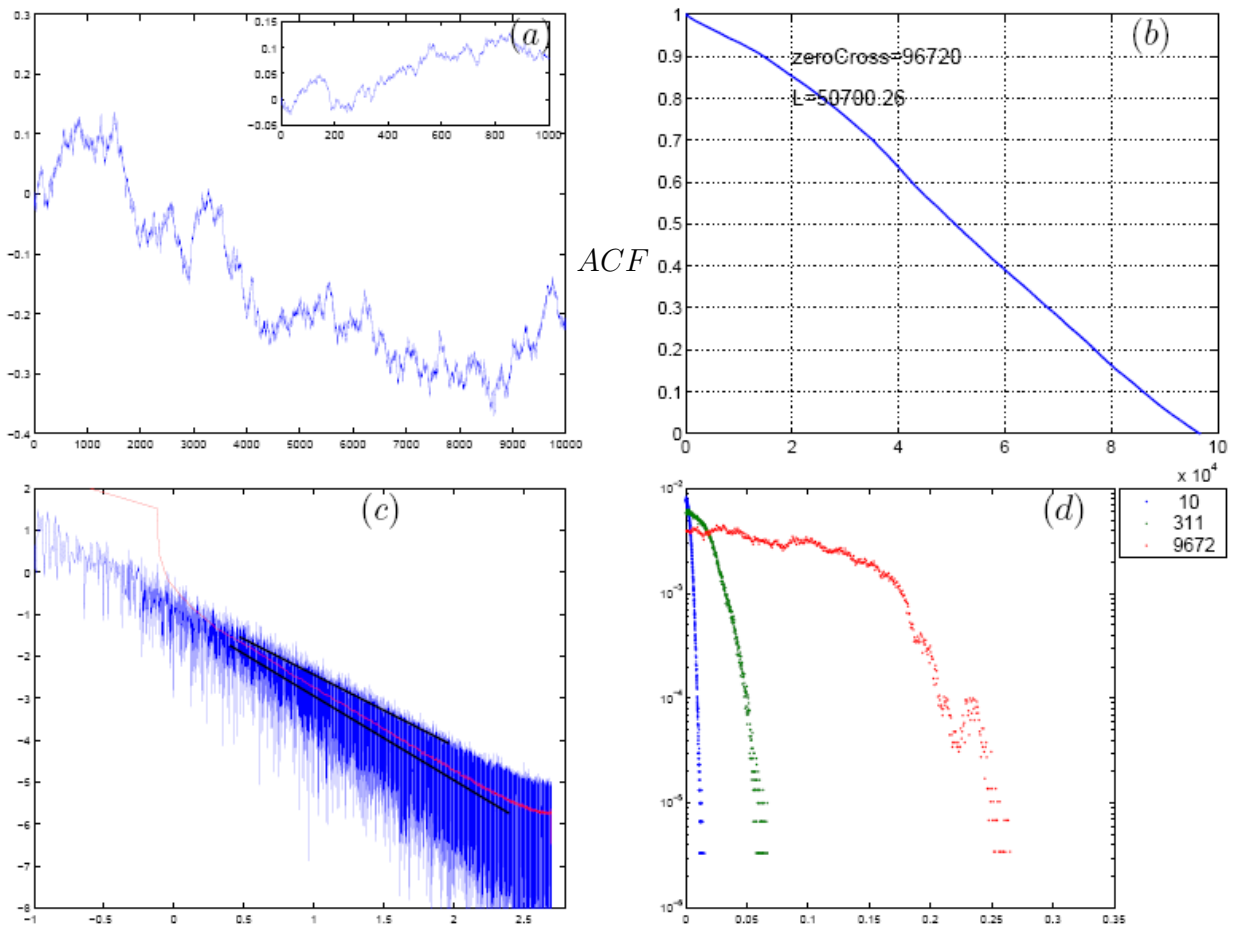


Figure 5.2: (a) Time series of a Wiener process (see eq.(5.2)) (b) the autocorrelation function (ACF) of the Wiener time series. (c) Its spectrum. (d) Its PDFs.

### 5.3 The Karhunen-Lòve decomposition or PCA

In the case of a centered stochastic process  $X_t \in [a, b]$  (where centered means that the expectations  $E(X_t)$  are defined and equal to 0 for all  $t$ , i.e. detrended), admits a decomposition  $X_t = \sum_{k=1}^{\infty} \eta_k e_k(t)$ , where  $\eta_k$  are uncorrelated random variables (white noise) and the functions are continuous real-valued functions on  $[a, b]$  which are orthogonal (this is why in meteorology the term empirical orthogonal functions EOF is used more than PCA). The general case of a process which is not centered can be represented by expanding the expectation function.

Moreover, if the process is Gaussian, then the random variables  $\eta_k$  are Gaussian and stochastically independent. This result generalizes the Karhunen-Lòve transform. An important example of a centered real stochastic process on  $[0, 1]$  is the previous Wiener process and the Karhunen-Lòve theorem can be used to provide a canonical orthogonal representation for it. We have met a manifestation of this theory previously in the context of principal component analysis (see fig. 3.12) [98].

In fig.5.3 an SSA or EOF analysis is shown for part of the return for the DAX index data with only two components.

### 5.4 Itô's process

A more generalized way to write eq. (5.3) is

$$dx_t = \mu(x_t, t) dt + \sigma(x_t, t) dW_t . \quad (5.5)$$

where we have taken into consideration the dependency of the trend or the drift  $\mu$  and the volatility  $\sigma$  on time and the local variables, in the above case  $x_t$ . This generalized equation (5.5) and its solution  $x_t$  is called *Itô's process*. This process is a generalization for the diffusion processes discussed previously in Chapter 2.

Eq.(5.5) is not suitable as an equation for stocks because it permits negative stocks prices (if one interprets  $x_t$  as the stocks price). To avoid that, one takes the stock price as  $S_t = e^{x_t}$  and with this substitution the process is now called a *geometrical Brownian motion (GBM)*. Now, if  $x_t = \ln(S_t)$  have a Gaussian distribution the new variable  $S_t$  has a lognormal distribution, taking this into consideration we could finally write eq.(5.5) as

$$dS_t = \mu(x_t, t) S_t dt + \sigma(x_t, t) S_t dW_t , \quad (5.6)$$

which is the equation of the geometrical Brownian motion (GBM). Using the above equation with *Itô's lemma* one gets the *Black-Scholes equation* [123].

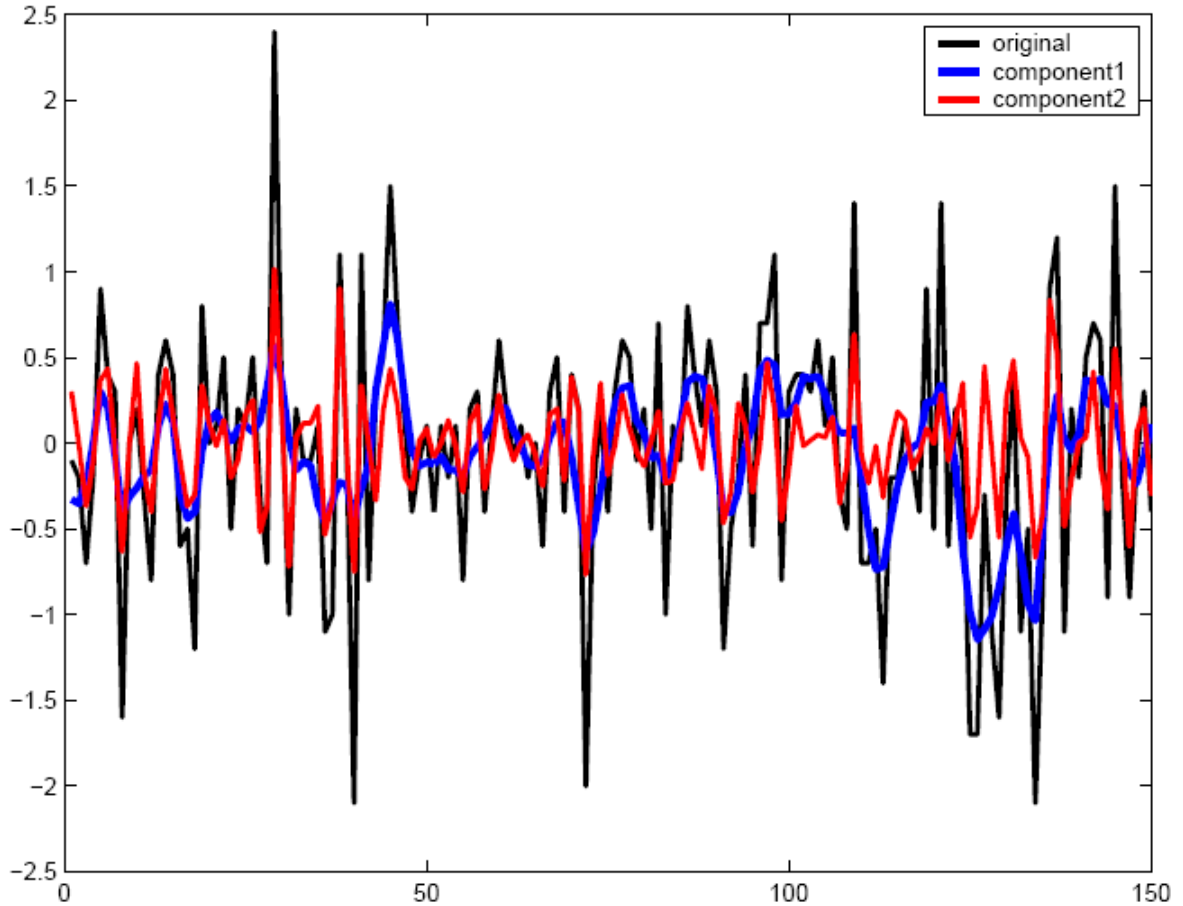


Figure 5.3: *Singular spectrum analysis (SSA) for the DAX returns data showing the return data and two components.*

## 5.5 Stationarity and non-stationarity

A general Gaussian stationary process is called *autoregressive moving average process (ARMA)* , and is written as

$$X_n = aX_{n-1} + \eta_n - b\eta_{n-1} , \quad (5.7)$$

where the constants  $|a| < 1$  and  $b < 1$  give a stationary process, otherwise if  $a = 1$  and  $b = 0$  we get the above non-stationary Wiener process and  $\eta$  is white noise.

Working with structure functions, i.e. the return , whether be it stock return etc... , seems to guarantee the stationarity (or probably just weak stationarity according to the intrinsic hypothesis by Matheron [127]) of the time series under study (see fig.4.1). In some studies, interest rates, foreign exchange rates, or even the price series of a stock or assets are of interest. These series and they tend to be non-stationary. Other important examples for non-stationary signals are earthquakes,

speech signals, Doppler acoustical signals, music, brain storms (EEG), in addition to the financial time series, just to name few.

## 5.6 Tools for non-stationary time series

Looking at a Fourier transform of a non-stationary signal, it is impossible to tell when a particular frequency took place, as we could see clearly from fig. 5.1 were during the attacks on New York the DAX index tumbled down but the spectrum still shows  $-2$  slope. If the signal properties do not change much over time (a stationary signal), then the spectra that we so far calculated (see for instance fig. 4.3) give us what we need. However, the most interesting signals are those which contain numerous non-stationary or transitory characteristics: drift, trends, abrupt changes, and beginnings and ends of events. These characteristics are often the most important part of the signal, and Fourier analysis is not suited to detecting them [129].

## 5.7 Short-Time Fourier Transform (STFT)

In an effort to correct this deficiency in classical Fourier analysis, Gabor adapted the Fourier transform to analyze only a small section of the signal at a time, a technique called windowing the signal. Gabor's adaptation, called the Short-Time Fourier Transform (STFT), maps a signal into a two-dimensional function of time and frequency. The STFT represents a sort of compromise between the time- and frequency-based views of a signal. It provides some information about both when and at what frequencies a signal event occurs. However, one can only obtain this information with limited precision, and that precision is determined by the size of the window. While the STFT compromise between time and frequency information can be useful, the drawback is that once one choose a particular size for the time window, that window is the same for all frequencies. Many signals require a more flexible approach, one where one can vary the window size to determine more accurately either time or frequency [130].

Since one should have a signal and a window (or a kernel see eq. (1.8)) for the STFT, this transform is written as [132]

$$S_t(\omega) = \frac{1}{\sqrt{2\pi}} \int_{-\infty}^{\infty} s(t) W(t - \tau) e^{i\omega t} dt \quad , \quad (5.8)$$

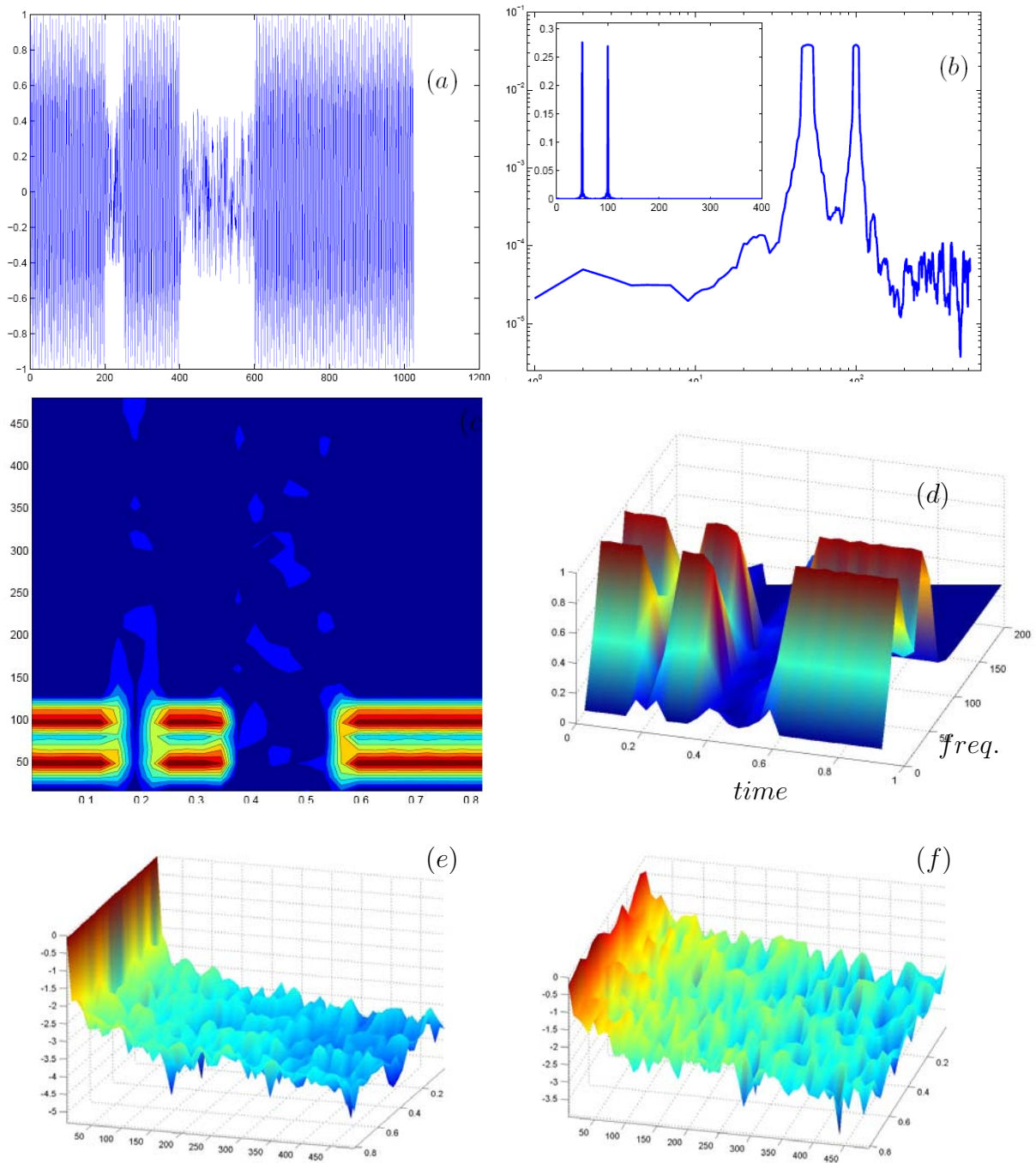


Figure 5.4: (a) This figure shows an intermittent detrended signal showing random activity in the middle of a sinusoid signal of two frequencies 50 and 100 Hz. (b) The logarithmic Fourier spectrum of the signal (just like in figs. 4.3) and in the inset the normal spectrum showing two peaks at 50 and 100 Hz. (c) The contour of the STFT of the signal. The x-axis represents the time and the y-axis the frequency. (d) 3-Dimensional STFT spectrum. Here again the horizontal-axis represents the time and the axis going into the page the frequency, while the vertical axis represents the amplitude. (e) The logarithmic STFT of the DAX (fig.5.1(a)). The axes are just like in figure (d) above. (f) The STFT of the Wiener process (fig.5.2(a)) and the axes are again just like in figs. (d) and (e).

where  $s(t)$  is the signal and  $W(t - \tau)$  is the window. If one chooses the Gaussian function as a window then the transform is called Gabor transform. The above equation is to analyze the frequency at the time  $t$  conversely we could multiply the signal with a frequency window to study the frequency and then it is called short frequency Fourier transform (SFFT).

In fig.5.4(a) a sinusoid with two frequencies 50 and 100 Hz interrupted by periods of random fluctuations is shown, it is a simple intermittent signal. In (b) we have shown its logarithmic spectrum and in the inset without the logarithm. In both one cannot see where the random interruptions has occurred. In (c) and (d) which represents the STFT for this signal, one sees the two frequencies in addition to the interruption positions. In (e) and (f) the logarithmic STFT for the DAX index and the Wiener process are shown respectively.

## 5.8 The Wigner-Ville spectrum

The Wigner-distribution and the Wigner-Ville spectrum (WV) are written respectively as

$$\begin{aligned} WV_t &= \frac{1}{2\pi} \int_{-\infty}^{\infty} s^*(t - \frac{1}{2}\tau) s(t + \frac{1}{2}\tau) e^{-i\omega t} d\tau \ , \\ &= \frac{1}{2\pi} \int_{-\infty}^{\infty} S^*(\omega - \frac{1}{2}\theta) S(\omega + \frac{1}{2}\theta) e^{-i\omega\theta} d\theta \ , \end{aligned} \quad (5.9)$$

where  $s^*(t - \frac{1}{2}\tau)$  is the conjugate of the signal in the past and  $s(t + \frac{1}{2}\tau)$  is the signal in the future,  $\omega$  is the frequency, and multiplying these two signals gives the the Wigner distribution. On the second line of eq.(5.9) we have a multiplication of the spectra  $S$  of the signal. Both expressions give the same result but on the first line one calls it Wigner distribution while on the second it is WV spectrum [126].

In fig.5.5(a) and (b) the distribution is shown in 3 dimensions and as a contour respectively. One notices that in addition to the noisy 300 Hz signal which crosses the figure from left to right (shown at the 600 Hz instead of 300 because of duplicating the signal for computational purposes), one sees the random noise again. In addition to the random noise, which has been added in the same places as in the last signal of fig.5.8, one notices that there are other patches of noise which have to do with what is called the cross terms. These cross terms are a combination of real and complex numbers that arise due to the multiplication in eq.(5.9) [133].

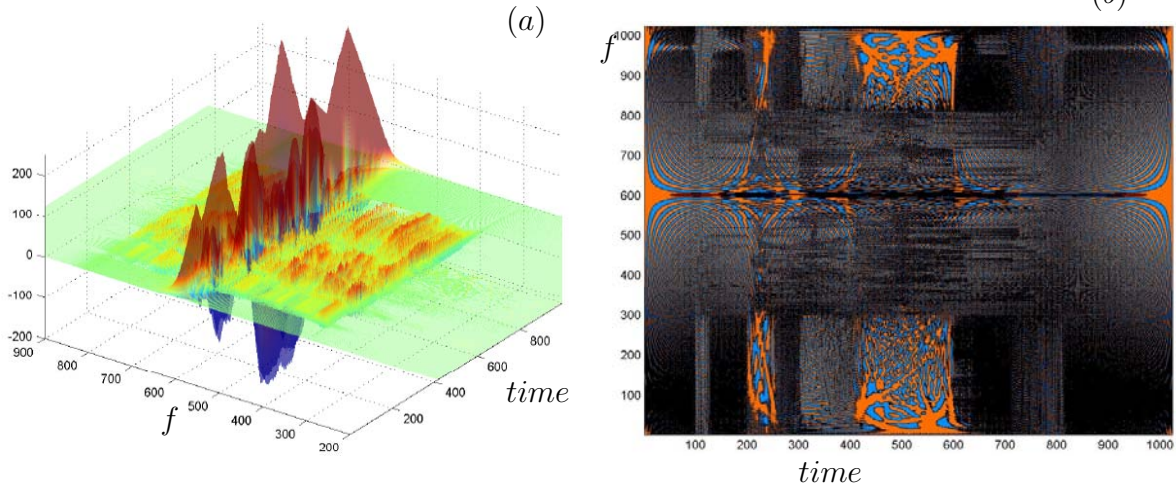


Figure 5.5: (a) The Wigner-Ville spectrum for a noisy sinusoid of 300 Hz frequency. The vertical axis is the amplitude of the signal and  $f$  is the frequency. (b) The contour of the Wigner-Ville spectrum for the same signal. Here too  $f$  is the frequency.

## 5.9 Wavelets

Wavelet analysis represents the next logical step: a windowing technique with variable-sized windows. Wavelet analysis allows the use of long time intervals where we want more precise low-frequency information, and shorter regions where we want high-frequency information [126]. The wavelet transform for a continuous signal is [133]

$$w_x(a, b) = |a|^{-\frac{1}{2}} \int_{-\infty}^{\infty} s(t) W^* \left( \frac{t-b}{a} \right) dt \quad , \quad (5.10)$$

where  $W^* \left( \frac{t-b}{a} \right)$  is the wavelet (compare with eqs.(1.8), (1.10), and (1.33)) which is shifted in time and scaled in frequency domains by the factors  $a$  and  $b$  respectively.

Since the kernel in wavelets is scaled and not modulated by an exponential factor as before in STFT and WV, the produced diagrams are called scalograms instead of spectrograms as in the case of the STFT analysis. The wavelets that has been developed since Morlet has used it to analyze seismic data [131] are numerous, and vary from analytic to real wavelets.

In fig.5.10 we manifest how wavelets could be used to analyze again the frequency content of a signal. In addition to that wavelets are used to denoise noisy signals and reconstruct them again [126].

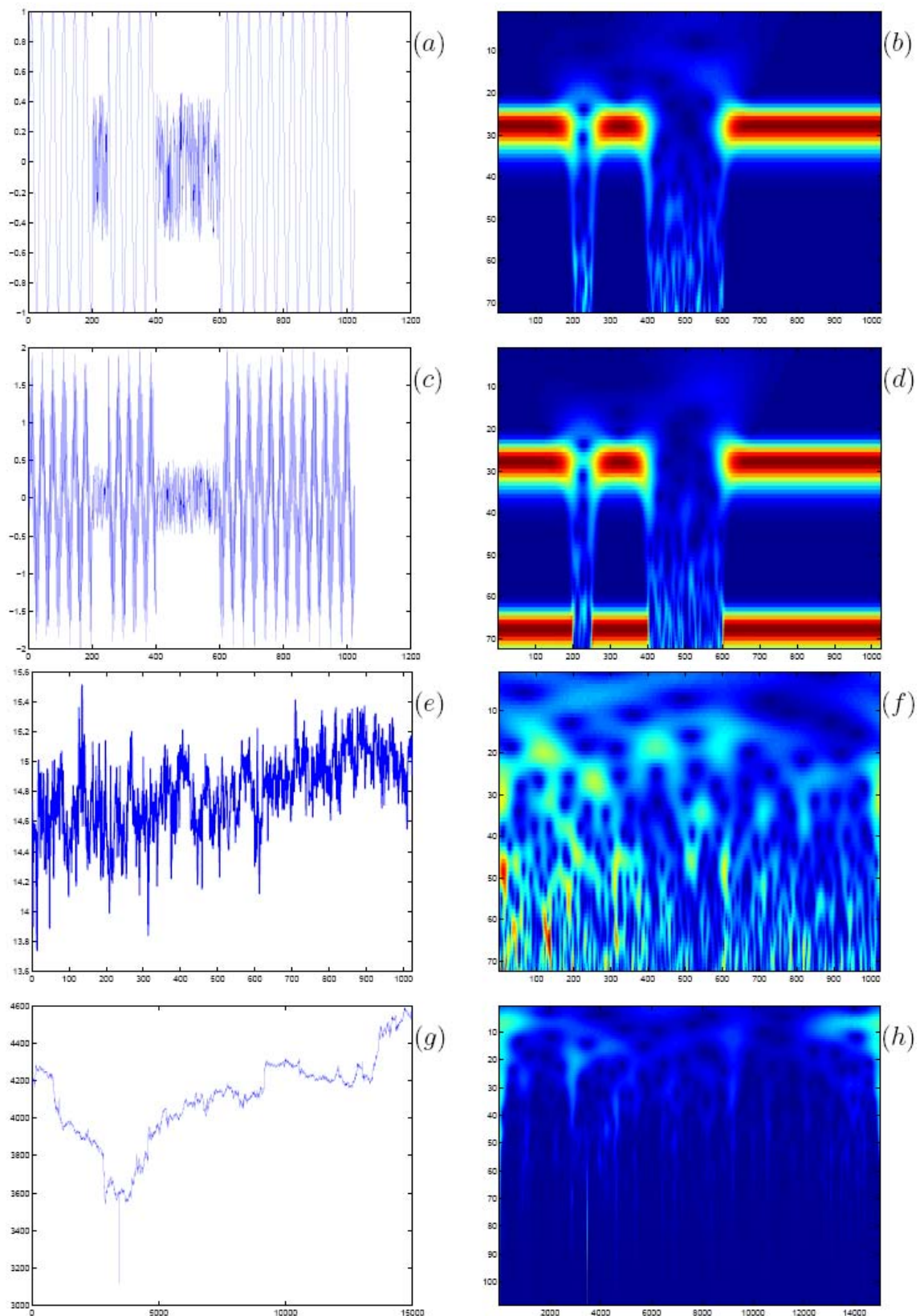


Figure 5.6: (a) and (b) An intermittent signal of 30 Hz frequency and its scalogram. (c) and (d) An intermittent signal with 2 frequencies 30 and 300 and its scalogram. (e) and (f) The previous non-stationary signal of the temperature (fig.4.1) and its scalogram. (g) and (h) The DAX index signal and its scalogram. In all the scalograms the x-axis represents time and the y-axis the scaling of the frequency.

# Chapter 6

## Backlook and Outlook

In Chapter one the basic concepts for modelling turbulence has been reviewed. Complex nonlinear systems which are far away from equilibrium need other methods than the thermodynamic statistics to be analyzed. We have seen that starting with the Navier-Stokes equation (NSE), which are Newton's equations for motion, did not help because of the huge number of degrees of freedom (the DNS simulation of 1.1 with  $256^3$  grid points takes many days on a cluster of computers). Reducing the quantity of data by averaging with tools like RANS and LES enables the industry to use these models in spite of the use of the huge computational capacities that are needed for such computations. Even when we treat the flow as diffusion under certain conditions then one needs big computational resources capacity. We noticed how the time averaging in the RANS differs from the space averaging in the LES, were we have extra terms in the case of LES to be simulated which makes the LES more expensive than the RANS but still less expensive than the DNS.

Choosing only the diffusion and advection terms from the NSE, one gets what is called a diffusion equation as detailed in Chapter two. The (1+1)-dimensional simulations that were conducted for the different equations were done on a laptop. The emphasize was on showing that the Fickian and non-Fickian diffusion regimes could be derived from a basic master equation. There are many variations that could be achieved by using the diffusion equation, in order to describe a variety of phenomena ranging from biology (Edwards-Wilkinson equation (2.26), Fisher's equation (2.29)) to finance (Black-Scholes equation). Some of these achievable variations are, were the following is by noway a conclusive list:

- Using the substantive derivative as in eq. (2.6) to give a non-stationarity feature for the equation.
- Using a drift function (could be a polynomial for example), so that the drift

will be a function of the dependent variable, as in eq. (2.23) to give the equation a nonlinearity feature.

- A volatility function is used with the diffusion term as in Black-Scholes equation, which is used in studying the options markets.
- A driving (forcing) term is added to one or all the above variations to replenish the lost energy and have enduring structures (see the Fisher eq. for example (2.29)), but also to make the equations nonlinear. As we have seen before these driving terms are either a random term or the logistic equation as in the case of the Fisher eq., but it could be anything else, periodical terms for example.
- Using the non-Fickian instead of the Fickian diffusion would add a wave-like branching (polarization) feature to the equation and most important make it hyperbolic (instead of parabolic in the case of the Fickian diffusion) and thus the causality is conserved, i.e. the speed of propagation must be finite, (see section 2.8 and also [134]).
- Adding a dispersion term to the equation gives nondissipative diffusion solitons [135].
- In addition to variations that produce features like the ones seen in Kuramoto-Sivashinsky eq. (2.27) (fig. 2.6) and the gravity waves eq. (2.28) (fig. 2.7).

Going to 3-dimensions in the simulations of the diffusion equations would indeed have its computational costs (if one uses spectral methods as in the case of the simulations of chapter two), but still it would be interesting to see if one gets the  $-5/3$  signature of turbulence (or probably we should say the signature of stationary turbulence).

Reducing the system variables in the way Lorenz [78] did with the NSE would exhibit other qualities of these systems. A dynamical systems analysis has been laid out in Chapter three for some systems. Some of these systems like the flair (intermittent) systems, which use the logistic equation as its main building block, have been analyzed. These bursting systems produce highly intermittent signals, if its parameters are tuned correctly, and could be used to further analyze some properties of the models used to describe chaotic or even assumingly turbulent phenomena e.g. bifurcation, principal components (Lyapunov exponents), ... etc. From the tests that has been carried out it seems that the correlation dimension which was used to determine whether the data are random or stochastic (i.e. chaotic, turbulent, stationary and non-stationary) is not a reliable tool. The assumption that, it becomes reliable if one uses a high number of data points, is questionable and needs more tests because of the computationally intensive algorithms used to calculate it.

A tool used to reconstruct the original phase space by using one dependent variable from the many variables that build an attractor, is the embedding dimension. Upon experimenting with the embedding dimension we have noticed that using the time series of one variable only reproduces some of the features of the original phase space as long as the trajectories do not intersect (see fig. 3.10). With intersecting trajectories one cannot see any features of the original phase space, even with using lagged (incremented) time series. Probably one should experiment with embedding techniques that makes use of more dependent variables than only just one of them (see for example [136]), but then one is back to using more quantities of data contrary to what this work was aiming at, namely, how to average data and still get a picture of the event. One could use the embedding dimension in conjunction with the covariance matrix and decompose the later by using singular value decomposition to arrive at the principal components, as was previously explained. This method needs more testing since one is using a linear method in analyzing, in most cases, nonlinear data. Regardless of that, one sees that the method furnishes a way to reduce the dimensions and probably also to reconstruct the original structure functions of the time series. Working directly on the time series, the method fails to show a gradual decline in the singular values, i.e. the first singular value is widely separated from the rest of the values. That is why we have used the structure functions in figs. 3.12 and 5.3. At last, this method is computationally intensive. It is also worth mentioning here that the photos in fig. 3.11 where originally coloured photos. To reduce their data amount they were rendered into black and white, and then a histogram equalization (a technique used in image processing) was done in order to redistribute the intensity .

Tools like the spectrum and the autocorrelation are very important. In the case of the spectrum, it is important to look at the different regimes of the frequencies that the system exhibits. Here one sees very clearly that the energy is fed at the large scales and cascades down through the inertial range until it dissipates at the small scales and according to a power law. One of the surprises here is the flat spectrum of the Pareto distribution (see eq. (3.1) and fig. 4.3(a)) and at the same time its correlation dimension shows a non-random behaviour as in fig. 3.9(b) and (c). The autocorrelation, as we have also seen, confirms the picture that one sees in the spectrum. In addition to that, the probability density functions (PDF) also give the same message as we have seen. We have seen also that the structure function is an important tool to describe turbulence. These results, i.e. when do the data become random, are again visualized by the scatter plots, which are actually phase plots, of fig. 4.5. If one assumes that the structures of turbulence are fractal then one should get a  $1/3$  power law (as in K41) but in a multifractal analysis procedure the exponents of the structure functions deviate from this power law by an intermittency factor shown to be  $\mu = 0.24$  as in fig. 4.10 which is nearly equal to the reported

value in the literature for incompressible steady homogeneous turbulence.

But, here too one should ask some basic questions about the relation between the spectrum and the autocorrelation. We have noticed that the x-axis of the energy spectrum is the wavenumbers or frequency but the x-axis of the autocorrelation is the lag which is, for instance  $r_2 - r_1$  and looking at it in the Fourier space it should be  $k_2 - k_1$  and not simply  $k$  as is always done, in this work too.

In Chapter Five an analysis for the DAX index financial data was carried out and an important result is the one showing a spectrum of  $-2$ . This result does not say a lot about the process, even the plunge of the 11th of September events does not show on the spectrum, and this is a good reason to look for other methods other than the ones that have been used so far to analyze non-stationary data. This kind of data, the non-stationary, is an important category of data since most of the signals are of this type, like voices, signals on a radar screen, images, ... etc. in short signals which have a beginning and an end. Indeed, the literature is full with such methods like the Short-Time Fourier Transform (STFT) or simply spectrograms, Wigner-Ville spectrum and Wavelets. The results that are produced by the later methods needs more sophisticated filtering techniques to be understood adequately. Another important result in this chapter is that the class of financial data resembled by the DAX index is Markovian, and that using the structure function or the return to analyze these data produces simply random data, as is clearly seen from eq. 5.7, with a flat spectrum and an autocorrelation that drops immediately to zero, and this, the random data, should be dealt with within the framework of thermodynamics. It is worthwhile mentioning that there is still significant scientific literature considering financial time series as a non-Markovian multifractal process (see for instance [137] and [138] but also [140] and the references therein). It is worthwhile checking whether the financial time series is constituted of partly fractal patches and partly multifractal patches. Also more efforts should be invested in exploring wavelets (real and complex) and explore convenient methods to data-mine it. But also use wavelet as a filtering tool and compare its results with the other tools. The same applies for the Wigner-Ville spectrogram.

On the light of chapter five one could also investigate the following

- The statement that the correlation of nonstationary data is long should be scrutinized because the autocorrelation is a tool for stationary and not for nonstationary data.
- The hypothesis of Taylor's frozen turbulence could not be used for nonstationary data.
- The basic cornerstone of the CFD, the Reynolds decomposition, should not be used when the data is nonstationary, which is the actual case in weather

systems, and probably a new formulation based on eqs. (5.5) or (5.6) should be used calculating the trend and the volatility with Markovian analysis.

- Probably one should investigate the possibility of using a higher order structure function and not simply the first order Taylor expansion as in eq. (4.1).

A next stage in this line of research is to answer the question of classifying the modelled and experimental intermittent signals. Most certainly they should be classified according to their dimensions, energy distributions, and indeed how much determinism is embedded into them or are they just random; noticing that in the case of LES the small scales contains some determinism into them and they are not random. It is possible to produce signals with a certain tailor-designed distribution and spectrum using filtering, but it is questionable whether that is enough to get the desired signal for the next step.

Once these questions have been answered we could start experimenting by adding these flary signals to a variety of large scale signals, whether meteorological or financial, and which are a result of either RANS, LES, PCA, or wavelet filtering, or simply signals sampled with low resolution, or probably even to the Lorenz attractor data, and see what do we get. These mixing experiments of gusting signals with large scale signals should continue until one gets signals that are similar to the ones actually registered from the real events, be it turbulence, earthquakes, etc. Probably one would find, that for each type of a large scale one needs a specific type of a flare signal as a seed to reproduce the desired type of a phenomenon. To borrow an analogy from biology probably one would find that to produce a large scale human-being one needs a certain type of seeds, of DNA, to build on it the larger scales and according to the dynamics that are programmed in these gusts (seeds). So a hurricane needs a certain type of a flare signal to reproduce it which is different than the one needed for an earthquake or a brainstorm EEG analysis. A crash in the financial markets needs a certain type of flare signal to reproduce its: dynamics, Markovity or non-Markovity, randomness, self- similarity and multifractality, ... etc or probably just bits and pieces of all lumped together in one time series. So, a deeper look into the mechanisms producing these signals in order to model them is needed. After all, and according to Lorenz, the flap of the wings of a butterfly which produce a bursty small scale signal could cause a Tornado somewhere else [139], or even according to the Arabian proverb the straw that broke the camel's back (which brings in the whole field of avalanches and self-organized criticality (SOC) and the talk about analyzing the mechanisms and modelling them and not only analyzing the signals). This search for this intermittent signal should not stop upon finding the piece of straw that breaks the back or in which place of the back, and brings an Avalanche, where the system goes into the state of equilibrium, but rather should go on for the hyper-intermittent signals (if one could use such a term) which brings the

system back from equilibrium to non-equilibrium, from causality to non-causality, from stationarity to non-stationarity, from Markovity to non-Markovity, ... etc.

# Appendix A

## Exponential Time Differencing

These methods are used for solving partial differential equations (PDEs) by spectral methods. Many PDEs contain linear and nonlinear terms as we have seen with the NSE, Burgers eq., KSE ...etc. added to that the resulting ordinary differential equations (ODEs) upon discretization are stiff. Thus these methods have been recently developed to get accurate solutions (since they are spectral) for mixed linear and nonlinear stiff equations. [109] and [110].

A discretised general form for such equations looks like

$$u_t = L u + N(u, t) \quad , \quad (\text{A.1})$$

where  $L$  and  $N$  are the linear and nonlinear terms. An integrating factor (IF) for the above eq. is  $v = u \exp(-L t)$ , differentiating the IF we get

$$v_t = -L u e^{-L t} + u_t e^{-L t} \quad . \quad (\text{A.2})$$

Multiplying eq.(A.1) by the IF we obtain

$$-L u e^{-L t} + u_t e^{-L t} = e^{-L t} N(u) \quad . \quad (\text{A.3})$$

Substituting the LHS of eq.(A.3) with eq.(A.2)

$$v_t = e^{-L t} N(v e^{L t}) \quad . \quad (\text{A.4})$$

The last step is differentiating the last equation by the forth order Runge-Kutta method.

# Appendix B

## Various declarations

The necessity for this extra appendix has arisen to shed some light on the used programmes, datasets and other essential matters for declaring the responsibilities:

- The Pencil code [32] which was used to produce the graphics of the paper [33] was completely developed by Prof. Dr. Axel Brandenburg from Nordita Institute and Dr. Wolfgang Dobler from Kiepenheuer Institute for Solar Physics. All the programming work for this figure was done by Prof. Dr. Brandenburg. The code itself is written in Fortran and is a high-order finite difference code for compressible hydrodynamic flows with magnetic fields (MHD). Working on this code has inspired the programs that were used for chapter 2 which one should be able to develop them for higher dimensions.
- All the graphics that exist in chapters 2-5 have been programmed by the author of this thesis in Matlab v.7 (installed on the Oldenburg University computers) except for one program in chapter 2 which is slightly modified and is in Mathematica v.5.1 (students addition) [44]. The toolbox Wavelab v.850 was partially used after modifying it in the last chapter.
- The experimental data, that were used in fig.3.1 and later on are a possession Of the following persons and their affiliated working groups: Prof. Dr. M. Reza Rahimi Tabar [117], Dr. Christoph Renner [118], Prof. Dr. Joachim Peinke ([105] and [122]), and the pulsar GRO see [120].
- In all the used figures starting from chapter 2-5 the colours distribution convention that has been used is the same and is the RGB colourspace. The colours are used such that red is given to the highest amplitudes and blue for the lowest.

# Appendix C

## Curriculum Vitae

Family Name	Mohammed
First Name	Amjed
Date of Birth	05.05.1960
Place of Birth	Iraq - Baghdad
1965-1978	Primary, Intermediate and Secondary school in Baghdad (Baghdad College) with a General Education Certificate.
1978-1984	Studying Physics in Baghdad University - Iraq with a B.Sc. in Physics.
1997-2002	Studying Physics in Oldenburg University with a Physics Diploma equivalent to Master (rating: Good). The title of the thesis was (Numerical Simulations of Turbulence and Stochastic Analysis).
01, July, 2002	Started with the Ph.D in Oldenburg University with Prof. J. Peinke.
April, 2004	The first publication (Non-Fickian diffusion and tau approximation from numerical turbulence) in (Physics of Fluids) Vol. 16, No. 4, April 2004.

# Appendix D

## Erklärung

Ich erkläre hiermit, daß ich die vorliegende Arbeit selbst verfasst und nur die im Literaturverzeichnis angegebenen Quellen und Hilfsmittel verwendet habe.

Oldenburg, den

.....

Amjed Mohammed

# Bibliography

- [1] J.L. Lumley as editor, *Research Trends in Fluid Dynamics* (American Institute for Physics Press, 1996). v, 11
- [2] H. Tennekes, J.L. Lumley, *A First Course in Turbulence*, (MIT Press 1992). 4, 5, 12, 60, 63, 69, 70
- [3] Katepalli R. Sreenivasan, "Fluid turbulence", *Rev. Mod. Phys.* **71**, 383, (1999).
- [4] W.D. McComb, *The Physics of Fluid Turbulence*, (Oxford Science Publications, 1990).
- [5] M.B. Abbott, D.R. Basco, *Computational Fluid Dynamics*, (Longman 1990). 2, 13, 15
- [6] J.H. Ferziger, M. Perić, *Computational Methods for Fluid Dynamics*, (Springer 1997). 3, 5, 10
- [7] M.B. Abbott, A. McCowan, I.R. Warren, *Numerical modelling of free-surface flows that are two-dimensional in plane*, H.B. Fischer (ed.), "Transport models for inland and coastal waters" (Academic Press 1981). 15
- [8] R.A. Clark, J.H. Ferziger, W.C. Reynolds, "Evaluation of subgrid turbulence models using a fully-simulated turbulent flow" *Rep.no. TF-9, Dept. of Mech. Eng., Stanford University*, (1977). 15
- [9] Amjed Mohammed, *Numerical simulations of turbulence and stochastic analysis*, Diplomarbeit, Oldenburg University, 2002. 2, 33
- [10] A. Brandenburg, P. Käpyla, A. Mohammed, "Passive scalar diffusion as a damped wave", *Progress in Turbulence*, J. Peinke, A. Kittel, S. Barth, M. Oberlack, Eds., (Springer 2005). 33
- [11] D.R.Chapman, "Computational aerodynamics development and outlooks", *AIAA Journal* **17**, Dec. (1979). 12

- [12] S.B. Pope, *Turbulent Flows*, (Cambridge University Press, 2000). 7, 9, 18
- [13] P. Moin, J. Kim, "Tackling turbulence with supercomputers", *Scientific American*, Jan. (1997). 13
- [14] H.K.Versteeg and W.Malalasekera, *Computational Fluid Dynamics: The Finite Volume Method*, (Longman 1999). 9, 10
- [15] P. Sagaut, *Large Eddy Simulation for Compressible Flows*, (Springer 2001). 13, 14, 15, 16
- [16] J.D. Murphy, "Turbulence Modelling", *Encyclopedia of Fluid Mechanics*, Vol. 6, N.P.Cheremisinoff, Ed., (Gulf Publishing Company 1987). 9
- [17] D.C. Leslie, G.L. Quarini, "The application of turbulence theory to the formulation of subgrid modelling procedures", *JFM* **97**, 65, (1979). 15
- [18] A. Yoshikazawa, "Large eddy simulation of turbulent flows", *Encyclopedia of Fluid Mechanics*, Vol. 6, N.P.Cheremisinoff, Ed. (Gulf Publishing Company 1987). 16
- [19] T. Dubois, F. Jauberteau, R. Temam: *Dynamic multilevel methods and the Numerical Simulation of Turbulence*, (Cambridge University Press 1999). 16, 17
- [20] D.C. Wilcox, *Turbulence Modelling for CFD*, (DCW Industries, 2000). 5
- [21] J.D.Anderson, *Computational Fluid Dynamics*, (McGraw-Hill, 1995). 11
- [22] T. Kobayashi, M. Kano, "Numerical prediction of turbulent plane couette flow by large eddy simulation", *Direct and large Eddy Simulation of Turbulence*, Proceedings of the EUROMECH Colloquium No. 199, München, Ulrich Schumann, Rainer Friedrich, Eds., Friedr. Vieweg and Sohn, (1985). 15
- [23] C. Canuto, M.Y. Hussaini, *Spectral Methods in Fluid Dynamics*, (Springer 1988). 10
- [24] K.D. Squires, J.R. Forsythe, P.R. Spalart, "Detached-eddy simulation of the separated flow around a forebody cross-section", *Direct and Large-Eddy Simulation Workshop 4 Proceedings*, B.J. Guerts, R. Friedrich, O. Métais, (eds.), Enschede, the Netherlands, July 2001. 18
- [25] M.Lesieur, O.Métais, "New trends in large-eddy simulations of turbulence", *Annu.Rev.Fluid Mech.* ,**28**, 45, (1996). 17

- [26] G.T. Csanady, *Turbulent Diffusion in the Environment*, (Reidel, Dordrecht, 1973). 20
- [27] Z.U.A. Warsi, *Fluid Dynamics theoretical and computational approaches*, (CRC Press, 1998). 4, 8, 20, 58
- [28] A.K. Das, "A non-Fickian diffusion equation", J. Appl. Phys. **70**, 1355, (1991). 24, 28
- [29] E.G. Blackman, G. B. Field, "A new approach to turbulent transport of a mean scalar", Phys. Fluids **15**, L73, (2003). 23, 24
- [30] A. Brandenburg, "Computational aspects of astrophysical MHD and turbulence", arXiv:astro-ph/0109497 . 5, 21
- [31] All the movies are found on <http://www.nordita.org/brandenb/movies/p-scalar> . 5
- [32] See the website <http://www.nordita.org/software/pencil-code/> 91
- [33] A. Brandenburg, P. Käpylä, A. Mohammed, "Non-Fickian diffusion and tau approximation from numerical simulations", Phys. Fluids **16**, 1020, (2004). x, 5, 6, 23, 24, 91
- [34] <http://www.nordita.org/software/pencil-code/> . 5
- [35] G.H. Weiss, "First passage times for correlated random walks and some generalizations", J. Stat. Phys. **37**, 325 (2005). 26
- [36] B.H. Lavenda, "Classical variational derivation and physical interpretation of Dirac's equation", Foundations of Physics **17**, 221, (1987). 26
- [37] L.N. Trefethen, *Spectral Methods in Matlab*, (SIAM 2000). 21, 30
- [38] Aly-Khan Kassam, L.N. Trefethen, "Fourth-Order Time-Stepping for Stiff PDEs", SIAM J. Sci. Comput. **26**, 1214, (2005). 30
- [39] H. Haken, *Synergetics, an introduction*, (Springer 1977). 25
- [40] H. Risken, *The Fokker-Planck Equation*, (Springer 1996). 26, 28
- [41] N.G. van Kampen, *Stochastic processes in physics and chemistry*, (Elsevier B.V. 2006). 26, 29
- [42] C.W. Gardiner, *Handbook of Stochastic Methods*, (Springer 2004). 26
- [43] Till D. Frank, *Nonlinear Fokker-Planck Equations*, (Springer 2005). 28, 29

- [44] Michael Trott, *The Mathematica GuideBook*, (Springer 2006). 28, 91
- [45] W.E. Schiesser, *The Numerical Method of Lines*, (Academic Press 1991). 28
- [46] M.A. Manna, A. Neveu, "A singular integrable equation from short capillary-gravity waves", 2003, arXiv: physics/0303085. 32
- [47] R.S. Johnson, *A Modern Introduction to the Mathematical Theory of Water Waves*, (Cambridge University Press 1997). 32
- [48] J.D. Murray, *Mathematical Biology*, (Springer 1989). 33
- [49] M.C. Cross, P.C. Hohenberg, "Pattern formation outside of equilibrium", Rev. Mod. Phys. **65**, 851, (1993). 33
- [50] A.J. Koch, H. Meinhardt, "Biological pattern formation: from basic mechanisms to complex structures", Rev. Mod. Phys. **66**, 1481, (1994). 33
- [51] M. Al-Ghoul, B. Chan Eu, "Hyperbolic reaction-diffusion equations, patterns, and phase speeds for the brusselator", J. Phys. Chem. **100**, 18900, (1996). 33
- [52] R. FitzHugh, "Impulses and physiological states in theoretical models of nerve-membrane", Biophys. J. **1**, 445 (1961). 33
- [53] S. Barland et al., "Experimental evidence of van der Pol - Fitzhugh - Nagumo dynamics in semiconductor optical amplifiers", Phys. Rev. E **68**, 036209 (2003). 33
- [54] C. Cattaneo, "Sulla conduzione del calore", Atti Sem. Mat. Fis. Univ. Modena **3**, 83 (1948). 34
- [55] D.D. Joseph, L. Preziosi, "Heat Waves", Rev. Mod. Phys. **61**, 41 (1989). 34
- [56] K. R. Naqvi, S. Waldenstrøm, "Brownian Motion Description of Heat Conduction by Phonons", Phys. Rev. Lett. **95**, 065901 (2005).
- [57] Gang Chen, "Ballistic-Diffusive Equations for Transient Heat Conduction From Nano to Macroscales", Journal of Heat Transfer **124**, 320, (2002). 35
- [58] M.A. Aziz and S. Gavin, "Causal diffusion and the survival of charge fluctuations in nuclear collisions", Phys. Rev. C **70**, 034905 (2004). 35
- [59] R.W. Davies, "The Connection between the Smoluchowski Equation and the Kramers-Chandrasekhar Equation", Phys. Rev. **93**, 1169, (1954). 34
- [60] M. Kac, Rocky Mountain J. Math. **4**, 497 (1974), based on 1956 notes from the Magnolia Petroleum Company colloquium lectures. 34

- [61] B. Gaveau et al, "Relativistic Extension of the Analogy between Quantum Mechanics and Brownian Motion", *Phys. Rev. Lett.* **5**, 419, (1984). [34](#)
- [62] T. Ogasawara, S. Toh, "A new model of turbulent relative dispersion: a self-similar telegraph equation based on persistently separating motions", [nlin.CD/0510053](#), (2005). [34](#)
- [63] Richardson, L. F. *Weather Prediction by Numerical Process*, (Cambridge Univ. Press, 1922). [52](#)
- [64] P. Kechagia, Y.C. Yortsos, P. Lichtner, "Nonlocal Kardar-Parisi-Zhang equation to model interface growth", *Phys. Rev. E* **64**, 016315, (2001). [30](#)
- [65] A.R. Kerstein, Wm.T. Ashurst, "Propagation rate of growing interfaces in stirred fluids", *Phys. Rev. Lett.* **68**, 934, (1992). [30](#)
- [66] A.N. Kolmogorov, "The local structure of turbulence in incompressible viscous fluid for very large Reynolds numbers", *Dokl. Akad. Nauk. SSSR* **30**, 301, (1941). [54](#)
- [67] T. Nagatsuma, K. Enpuku, K. Sueoka, K. Yoshida, F. Irie, "Flux-flow-type Josephson oscillator for millimeter and submillimeter wave region. III. Oscillation stability", *Journal of Applied Physics* **58**, 441, (1985). [35](#)
- [68] A.V. Ustinov, T. Doderer, R.P. Huebener, N.F. Pedersen, B. Mayer, V.A. Oboznov, "Dynamics of sine-Gordon solitons in the annular Josephson junction", *Phys. Rev. Lett.* **69**, 1815, (1992). [35](#)
- [69] I.V. Vernik, S. Keil, N. Thyssen, T. Doderer, A.V. Ustinov, H. Kohlstedt, R.P. Huebener, "Fluxon pinning in annular Josephson junctions by an external magnetic field", *Journal of Applied Physics* **81**, 1335, (1997). [35](#)
- [70] A. Mohammed, E.D. Leonel, "On the dynamical properties of a flare map", to be published in the *Journal of Statistical Mechanics*. [37](#)
- [71] S.F. Edwards, D.R. Wilkinson, "The Surface Statistics of a Granular Aggregate", *Proc. Roy. Soc. (Lond.) A* **381**, 17, (1982). [30](#)
- [72] G. Pruessner, "Drift Causes Anomalous Exponents in Growth Processes", *Phys. Rev. Lett.* **92**, 246101 (2004). [31](#)
- [73] M. Waechter, F. Riess, H. Kantz, J. Peinke, "Stochastic analysis of road surface roughness", [arXiv:physics/0203068](#), 2002. [31](#)
- [74] T. Bohr, M. Jensen, G. Paladin, A. Vulpiani, *Dynamical Systems Approach to Turbulence*, (Cambridge University Press 1998). [30](#), [31](#)

- [75] H.A. Panofsky, J.A. Dutton, *Atmospheric Turbulence*, (Wiley 1984). 53
- [76] H.G. Schuster, *Deterministic Chaos*, (VCH Verlagsgesellschaft mbH. 1988). 36, 39, 41, 46
- [77] M. Lakshmanan, S. Rajasekar, *Nonlinear Dynamics*, (Springer 2003). 46
- [78] E.N. Lorenz, "Deterministic nonperiodic flow", J. Atmos. Sci. **20**, 130, (1963). 38, 39, 85
- [79] M. Berezowski, "Effect of delay time on the generation of chaos in continuous systems", Chaos, Solitons and Fractals **12**, 83, (2001). 40
- [80] O.E. Rössler, "An equation for continuous chaos", Phys. Lett. A **57**, 397, (1976).
- [81] G. Hartmann, O. Rössler, "Coupled flare attractors- a discrete prototype for economic modelling", Discrete Dynamics in Nature and Society, **3**, no. 1, 25, (1999).
- [82] Y. Pomeau, P. Manneville, "Intermittent transition to turbulence in dissipative dynamical systems" , Commun. Math. Phys. **74**, 189, (1980). 40
- [83] J.F. Heagy, N. Platt, S.M. Hammel, "Characterization of on-off intermittency", Phys. Rev. E **49**, 1140, (1994). 40
- [84] H.O. Peitgen, P.H. Richter, Eds., *The beauty of fractals*, (Springer-Verlag 1986). 43
- [85] E. Covas, R. Tavakol, P. Ashwin, A. Tworkowski, J.M. Brooke, "In-out intermittency in partial differential equation and ordinary differential models", Chaos **11** no.2, 404, (2001). 40
- [86] G. Hartmann, "Attraktoren mit Flare-Dynamik in Systemen fern vom Gleichgewicht", Ph.D. thesis, Tübingen University, 2002.
- [87] N. Blamforth, A. Provenzale, E. Spiegel, M. Martens, C. Tresser, C.W. Wu, "Red spectra from white and blue noise", Proc. R. Soc. Lond. B **266**, 311, (1999). 41
- [88] T. Sauer, C. Grebogi, J.A. Yorke, "How long do numerical chaotic solutions remain valid?", Phys. Rev. Lett. **79** no.1, 59, (1997). 39
- [89] H. Nusse, J.A. Yorke, "Is every approximate trajectory of some process near an exact trajectory of a nearby process?", Commun. Math. Phys. **114**, 363, (1988). 39

- [90] C. Meneveau, K.R. Sreenivasan, "Simple multifractal cascade model for fully developed turbulence", *Phys. Rev. Lett.* **59** no.13, 1424, (1987). [45](#)
- [91] D. Schertzer, S. Lovejoy, "Physical modelling and analysis of rain and clouds by anisotropic scaling multiplicative processes", *J. Geophysical Research* **92**, no. D8, 9693, (1987). [45](#)
- [92] P. Grassberger, I. Procaccia, "Characterization of strange attractors", *Phys. Rev. Lett.* **50**, 346, (1983). [45](#), [46](#)
- [93] Steven H. Strogatz, *Nonlinear dynamics and chaos*, (Perseus Publishing 1994). [46](#)
- [94] D. Kaplan, L. Glass, *Understanding nonlinear dynamics*, (Springer Verlag 1995). [46](#), [48](#)
- [95] H. Kantz, T. Schreiber, *Nonlinear times analysis*, (Cambridge University Press 2004). [45](#), [48](#), [50](#)
- [96] F. Takens, "Detecting strange attractors in turbulence", in *Dynamical systems and turbulence*, Eds. D.A. Rand, L.S. Young, *Lect Notes Math.* **898** (Springer Verlag), 336, (1981). [48](#)
- [97] I.T. Jolliffe, *Principal Component Analysis*, (Springer 2004). [49](#)
- [98] A. Hyvärinen, J. Karhunen, E. Oja, *Independent component analysis*, (Wiley 2001). [49](#), [77](#)
- [99] D. Broomhead, G.P. King, "Extracting qualitative data dynamics from experimental data", *Physica D* **20**, (1986). [50](#)
- [100] C.D. Meyer *Matrix analysis and applied linear algebra*, (SIAM 2000). [51](#)
- [101] U. Frisch, *Turbulence, the Legacy of A.N. Kolmogorov*, (Cambridge University Press 1998). [11](#), [56](#), [64](#), [68](#), [70](#)
- [102] G.I. Taylor, "Statistical Theory of Turbulence", *Proc. R. Soc. London A* **151**, 421, (1935). [62](#), [66](#)
- [103] G.I. Taylor, "Diffusion by continuous movements", *Proc. London Math. Soc.* **20**, 196, (1921). [62](#)
- [104] M. Lesieur, *Turbulence in fluids*, (Kluwer Academic Press 1990). [61](#)
- [105] O. Chanal, B. Chabaud, B. Castaing, B. Hebral, "Intermittency in a turbulent low temperature gaseous helium jet", *Eur. Phys. J. B.* **17**, 309, (2000). [xiii](#), [xiv](#), [61](#), [62](#), [67](#), [69](#), [70](#), [71](#), [91](#)

- [106] G.K. Batchelor, *The theory of homogeneous turbulence*, (Cambridge University Press 1993). 58, 66
- [107] A. Vincent, M. Meneguzzi, "The spatial structure and statistical properties of homogeneous turbulence", *J.F.M.* **225**, 1, 1991. 64
- [108] Prof. Dr. Joachim Peinke, private communication. 33
- [109] S.M. Cox, P.C. Mathews, "Exponential time differencing for stiff systems", *J. Comput. Phys.* **176**, 430, (2002). 90
- [110] A.K. Kassam, L.N. Trefethen, "Fourth-order time stepping for stiff PDEs", *SIAM J. Sci. Comput.* **26**, 1214, (2005). 90
- [111] J.C.R. Hunt, J.C. Vassilicos, "Kolmogorov's contributions to the physical and geometrical understanding of small-scale turbulence and recent developments", *Proceedings: Mathematical and Physical Sciences*, **434**, No. 1890, (Turbulence and Stochastic Process: Kolmogorov's Ideas 50 Years On), 183, (1991). 65
- [112] H. Tennekes, J.C. Wyngaard, "The intermittent small-scale structure of turbulence: data-processing hazards", *J. Fluid Mech.* **55**, 93, (1972). 65
- [113] R. Benzi, S. Ciliberto, R. Tripicciono, C. Baudet, F. Massaioli, S. Succi, "Extended self-similarity in turbulent flows", *Phys. Rev. E* **48**, R29, (1993). 64
- [114] A.N. Kolmogorov, "Dissipation of energy in locally isotropic turbulence", *Dokl. Akad. Nauk. SSSR* **32**, 16, (1941). 65
- [115] R.A. Antonia, E.J. Hopfinger, Y. Gagne, and F. Anselmet, "Temperature structure functions in turbulent shear flows", *Phys. Rev. A* **30**, 2704, (1984). 66
- [116] F. Anselmet, Y. Gagne, E.J. Hopfinger and R.A. Antonia, "High-order velocity structure functions in turbulent shear flows", *JFM* **140**, 63, (1984). 65
- [117] The earthquake data was supplied by M. Reza Rahimi Tabar. 38, 91
- [118] C. Renner, J. Peinke, R. Friedrich, "Experimental indications for Markov properties of small-scale turbulence", *J. Fluid Mech.* **433**, 383 (2001). xii, xiii, xiv, 38, 49, 51, 61, 62, 67, 70, 91
- [119] M. Nelkin, "Intermittency in Fully Developed Turbulence as a Consequence of the Navier-Stokes Equations", *Phys. Rev. Lett.* **30** no. 21, 1029, (1973). 68
- [120] XTE TOO observation of GRO J1744-28 on week 021 (June 21-27, 1996 or day 173-179). 38, 91

- [121] K.R. Sreenivasan, R.A. Antonia, "The phenomenology of small-scale turbulence", *Annu. Rev. fluid Mech.* **29**, 435, (1997). [68](#)
- [122] The source of the financial data is Karlsruher Kapitalmarktdatenbank (KKMDB) and is a property of Oldenburg University. [xiv](#), [74](#), [91](#)
- [123] Jürgen Franke, Wolfgang Härdle, Christian Hafner, *Einführung in die Statistik der Finanzmärkte*, (Springer 2004). [76](#), [77](#)
- [124] J. Voit, *The statistical mechanics of financial markets*, (Springer 2003). [75](#)
- [125] Ruey S. Tsay, *Analysis of Financial Time Series*, (Wiley Interscience 2005). [75](#)
- [126] Alfred Mertins, *Signal Analysis*, (Wiley, 1999). [81](#), [82](#)
- [127] Noel Cressie, "Kriging nonstationary data", *JSTOR* **81** no. 395, 625, (1986). [78](#)
- [128] D. Gabor, "Theory of communication", *Journal of the IEE*, **93**, 429, 1946.
- [129] P. Flandrin, *Time-frequency, Time-scale analysis (wavelet analysis and its applications)*, (Academic Press, 1999). [79](#)
- [130] Eberhard Hüsler, *Statistische Signale*, (Springer 2001). [79](#)
- [131] P. Goupillaud, A. Grossman, J. Morlet, "Cycle-Octave and Related Transforms in Seismic Signal Analysis", **23**, 85, (1984). [82](#)
- [132] Leon Cohen, *Time-frequency analysis*, (Prentice Hall 1995). [79](#)
- [133] R. Carmona, Wen-L. Hwang, B. Torresani, *Practical time-frequency analysis*, (Academic Press 1998). [81](#), [82](#)
- [134] M. Pelc, J. Marciak-Kolzowska, M. Kozłowski, "The modified Klein Gordon equation for neolithic population migration", *arXiv:physics/0703120*. [85](#)
- [135] F.G. Mertens, E. Arévalo, A.R. Bishop, "Nondissipative diffusion of lattice solitons out of thermal equilibrium", *Phys. Rev. E* **72**, 036617 (2005). [85](#)
- [136] L. Pecora, L. Moniz, J. Nichols, T.L. Carroll, "A unified approach to attractor reconstruction", *Chaos* **17**, 013110 (2007). [86](#)
- [137] F. Schmitt, D. Schertzer, S. Lovejoy, "Multifractal fluctuations in Finance", *arXiv:cond-mat/0102369*. [87](#)

- [138] A. Turiel, C.J.P. Vicente "Role of multifractal sources in the analysis of stock market time series", *Phys.A*, **355**, 475 (2005). [87](#)
- [139] E.N. Lorenz, "Predictability: Does the Flap of a Butterfly's Wings in Brazil set off a Tornado in Texas?", a talk, 1972. [88](#)
- [140] Z.Q. Jiang, W.X. Zhou, "Multifractality in stock indexes: Fact or fiction?", arXiv:0706.2140. [87](#)

# Index

- $\beta$ -model, 64
- $\tau$  approximation, 23
- Fokker-Planck eq.
  - nonlinear, 29
- autocorrelation function (ACF), 58, 74
- autoregressive moving average (ARMA), 78
- bifurcation, 40
  - route of, 42
- bivariate joint distribution, 28
- Black-Scholes equation, 77, 85
- box-counting dimension, 43, 45
- Brownian motion, geometrical (GBM), 77
- Burgers eq., 29
- capacity dimension, 43
- causality violation, 33
- closure problem, 5, 7, 23
- compressibility, 2
- continuity equation, 1, 21
- convolution, 3, 13, 58
- correlation, 2, 5, 56, 58
- correlation dimension (CD), 45, 46, 48
- correlation integral, 45
- correlations
  - double, 23
  - triple, 23
- covariance matrix, 50
- damped harmonic oscillator, 24
- diffusion advection eq., 21
- diffusion constant, 20, 25
- dissipation, 5, 55, 60, 64, 68
  - Kolmogorov scale, 12
  - numerical, 33
  - range, 60
  - rate, 65
  - spectrum, 67, 68
  - structure function, 68
- eddy turnover time, 11
- Eden model, 30
- Edwards-Wilkinson eq. (EWE), 30
- embedding dimension, 43
- ergodic, 54
- ETD4RK, 30
- extended self-similarity (ESS), 65, 68
- Fick's law, 20, 21, 33
- Fickian diffusion, 21, 25
- Fisher's equation, 33
- flatness (F), 71
- flux, 20
- Fokker-Planck eq., 26
  - bivariate quasilinear, 29
  - non-Fickian, 27
- Fourier's equation, 20
- fractal, 43, 45
  - dimension, 45
- Gabor, 79
- global warming trend, 53
- Hausdorff dimension, 43
- heat equation, 20
- heteroscedastic process, 74
- histogram equalization, 86

- homoscedastic process, 73
- increment, 52
- independent component analysis (ICA), 50
- inertial subrange, 54, 56, 60, 65, 67
- intermittency, 36, 40, 64, 71
  - route to chaos, 42
- isotropy, 20, 23, 25
- Itô's
  - process, 77
  - lemma, 77
- iterated function system (IFS), 43
- Kármán street, 48
- Kardar-Parisi-Zhang eq. (KPZ), 30, 31
- Karhunen-Lòve transform, 49, 77
- Klein-Gordon equation, 35
- Koch curve, 43
- Kolmogorov equation, 26
- Kolmogorov's dimension, 43
- Kolmogorov's universal equilibrium theory, 65, 68
- Kuramoto-Sivashinsky eq. (KSE), 31
- Langevin eq., 30
- log-Poisson model, 64
- logistic map, 33, 40
- lognormal distribution, 77
- lognormal model, 64
- Markovian process, 75
- master equation, 25
- Maxwell-Cattaneo's eq., 34
- mean, 54
- molecular diffusion, 19
- moments, 69, 70
- multifractal, 54
- Navier-Stokes equation, 1, 64
- non-Fickian diffusion, 24, 27, 33, 35
- non-Fickian equation, 24
- non-stationary process, 73
- Pareto distribution, 36
- power law, 43
- principal component analysis (PCA), 49
- probability density function (PDF), 69, 75
- random region, 60
- return, 75, 78
- Reynolds decomposition, 2
- Reynolds number, 60
- Reynolds tensor, 2, 23, 50
- Reynolds-Averaged Navier-Stoke (RANS), 3
- scalograms, 82
- Schwarz inequality, 58
- self-similar, 54
- self-similarity, 43
- shadowing, 39
- Short-Time Fourier Transform (STFT), 79
- sine-Gordon eq., 35
- singular spectrum analysis (SSA), 50, 77
- singular value decomposition (SVD), 50, 51
- spectrograms, 82
- spectrum, 55, 74
- structure function, 43, 52, 75
- Taylor microscale, 61
- Taylor's Hypothesis of frozen turbulence, 53
- Telegrapher's eq., 34
- variance, 70
- volatility, 73
- wave equation, 24
- white noise, 75
- Wiener process, 74
- Wiener process, generalized, 75
- Wigner-distribution, 81
- Wigner-Ville spectrum (WV), 81